The application of traveltime inverse in linearly inhomogeneous and elliptically anisotropic media

by

© **Izabela Kudela**

A thesis submitted to the School of Graduate Studies in partial fulfillment of the requirements for the degree of Master of Science.

Department of Earth Sciences

Memorial University

September 2019

St. John's, Newfoundland and Labrador, Canada

Abstract

We use ray methods for seismological investigations that allow us to address a variety of problems by applying several mathematical tools.

With the assumption of elliptical anisotropy and linear inhomogeneity, it results in simplifications of the equations; thereby, it allows us to obtain analytic expressions for the trajectories of seismic signals, as well as their traveltimes. Traveltimes are essential for processing and velocity determination from VSP surveys.

To solve the inverse problem, we minimize the difference between the traveltimes calculated from the model and traveltimes from the dataset. We ensure that for a single medium, the inverse is stable and gives unique solutions. For the more complex problems with many parameters, we examine the stability of the inversion.

Herein, we investigate one particular case of eight symmetry classes that material described by a Hookean solid can possess. We consider a particular case of the transversely isotropic (TI) medium. An accurate enough analogy of a seismic performance with a model of a TI Hookean solid is consistent with parallel layers that serve as an analogy for the behaviour of waves in a sedimentary basin.

For such medium, we use the Backus average of a stack of isotropic layers that results in a TI medium.

We investigate whether we may encounter the issue with numerical considerations of the Backus (1962) product approximation. For isotropic media, despite the stability conditions, it may lead to an issue within the Backus average. In the context of global seismology, we examine whether this issue may occur.

Furthermore, we discuss several physical constraints imposed on elasticity parameters of a TI tensor. Using the assumption of the equal level of increasing velocity of P- and S-waves and the same anisotropy from $ab\chi$ model and TI medium, we obtain two

out of five elasticity parameters of a TI tensor.

For different elasticity parameters, we show several numerical examples to examine how these restrictions affect a TI tensor with known values of certain elasticity constants that are acquired from the vertical or horizontal measurements.

Keywords: VSP, Metropolis-Hastings, Inversion, MATLAB, Backus average, TI tensor

Acknowledgements

I would like to express my highest gratitude to my supervisor Prof. Michael A. Slawinski for the fruitful comments, remarks, and engagement through the learning process of this master thesis.

Furthermore, I would like to thank my co-supervisor Dr. Tomasz Danek, for his valuable conversations. The special acknowledgments are to Filip Adamus, Ayiaz Kaderali, and Theodore Stanoev whose collaboration was instrumental for this master thesis. I wish to acknowledge the group of people who helped me to proceed with the thesis as well as the discussions and editorial support of Theodore Stanoev, David Dalton, and Filip Adamus. I would like to thank Alison Malcom for her insightful comments that improved the final version of the thesis. Also, I wish to acknowledge the graphical support of Elena Patarini. This research was performed in the context of The Geomechanics Project supported by Husky Energy.

Last, but not least, I would like to give the special thank to my husband for his understanding, mental support and fruitful conversations that gave me the strength to go through the whole process of writing the thesis.

Table of contents

List of figures

List of tables

List of symbols

a	vertical velocity
b	velocity gradient
χ	ellipticity parameter
p	ray parameter
Z	depth
X	offset
t	traveltime
t_m	traveltime from measurement
$t_{ab\chi}$	traveltime from $ab\chi$ model
θ	ray angle
v	velocity
v_h	horizontal velocity
v_v	vertical velocity
P	probability
σ	standard deviation
ε	noise
$\bar{\varepsilon}$	difference between traveltime from model and $t_{ab\chi}$
X_c	location of the last source at which the signal reaches the receiver on its way down
c_{ijkl}	elasticity tensor
c^{TI}_{ijkl}	transversely isotropic elasticity tensor
$c^{\overline{\mathrm{TI}}}_{ijkl}$	transversely isotropic elasticity tensor after Backus average
$\chi_{\overline{\mathrm{TI}},b}$	anisotropy parameter in Backus model
x_k	vector
w_k	weight

u	displacement vector
σ_{ij}	stress
ε_{kl}	strain
ν	Poisson's ratio
λ, μ	Lamé parameters
ρ	density
λ_i	eigenvalues
v_P	velocity of P-wave
v_S	velocity of S-wave
qP	quasi-P wave
qS	quasi-S wave
I_i	invariant

List of abbreviations

VSP	Vertical Seismic Profiling
TI	Transversely Isotropic
PREM	Preliminary Reference Earth Model

Chapter 1

Introduction

Using ray methods, we are equipped to apply the equations for seismological studies. In the context of ray theory, we can achieve the trajectories of seismic signals and their traveltimes.

Herein, we study a particular case of a ray traveling in the medium with both an elliptical velocity dependence with direction and a linear velocity dependence with depth. These assumptions allow us to obtain analytic expressions for rays and traveltimes. Traveltimes are essential for processing and velocity determination from vertical seismic profiling (VSP) (Slawinski et al., 2004).

More specifically, parameters a and b describe a change of velocity with depth, and χ describes the anisotropy. To obtain a, b, and χ, we perform the inversion to match the traveltimes from the dataset. In the first case, for a single-medium model, we use the Metropolis-Hastings algorithm (Hastings, 1970), based on Monte Carlo methods. In the second case, we use the minimization function, *fminsearch*, in MATLAB for multi-layer media.

In this thesis, we examine the two cases of the dataset: the predicted and field data.

The predicted data are obtained from the established model of a, b, and χ; the field data are obtained from Kaderali (2009). Additionally, in the case of predicted data, for both methods, we ensure the correctness of the method and also investigate different noise levels added to the traveltimes.

For the case with *fminsearch* function (Lagarias et al., 1998), we present the cases of one, two, three, and four parallel layers, where we determine a, b, and χ for each layer. The more information about the algorithm one can find in Mathews and Frank (2004).

We set the depths of the layers. The inversion involves optimization of the ray paths, based on the velocity model; their shape is elliptical. The fourth layer case is added to examine the extent to which the number of layers affects the estimate, including its uniqueness and stability. Also, in each case, we interpret the accuracy of the results using computed residuals. As the two inversions are based on the same dataset, we compare the results and confirm the correctness of the two methods.

We also investigate the materials that possess certain symmetries (Bos et al., 2004). In the context of our studies, this means that we can measure a property of a material in several different orientations of the coordinate system and obtain the same result each time. In an accurately chosen coordinate system, the form of the elasticity matrix allows us to recognize the symmetry of this continuum. Herein, we consider a particular case of the transversely isotropic medium, which is consistent with parallel layers.

We consider a model used in applied seismology as a stack of parallel layers. Each layer possesses elastic properties. For the averaging purposes and to obtain one set of parameters for a single equivalent medium, we use Backus (1962) average that is commonly used in applied seismology. The behavior of such a medium is analogous to

the response of a stack of layers to a signal whose wavelength is much greater than the thickness of individual layers (Bos et al., 2017a). For isotropic thin layers, the thick layer is transversely isotropic (Postma, 1955). Such single think layer can be good representation of the whole medium and allows us to compare results from previous search with a, b, and χ.

As a consequence of averaging, the anisotropy might serve as an accurate-enough analogy within the realm of continuum mechanics. Thus, for example, the same continuum with its anisotropy might serve as an analogy for the behaviour of waves in a sedimentary basin (Helbig, 1994).

Bos et al. (2017a) examine the mathematical foundations of the Backus approach such as the approximation of the average of a product as the product of the averages, which underlies the averaging process. We estimate the difference between them and find whether the possibility of the issue with product approximation may occur. Using the stability conditions of the isotropic stress-strain relations, we investigate the physical possibility of the issue with approximation to arise.

Applying the Preliminary Reference Earth Model (PREM) of Dziewoński and Anderson (1981), we examine whether Backus average fails within the context of seismology at a regional scale. Including density, ρ, P- and S- wave speeds, we compute Lamé and elasticity parameters and determine the relative error of the Backus average.

In Section 9.2, we consider transversely isotropic (TI) elasticity tensor with a symmetry axis that coincides with a vertical x_3-axis of a coordinate system that refers to depth. A TI tensor has five independent elasticity parameters; determining their values via seismic measurements may be challenging. For example, one may perform vertical seismic profiling at offsets close to zero, to obtain vertical speeds of quasi-P and quasi-S waves. This way, five unknown parameters are reduced to only three.

Most often, we do not have an opportunity of knowing the values of all five parameters, but we still might want to use a TI tensor to describe the properties of a medium. Consequently, it is useful to restrict the range of the possible values of the remaining elasticity parameters that are unknown. In other words, putting several restrictions on these parameters enables us to predict better or estimate their values.

We apply formulae, derived by Sayed and Stanoev (2019), to calculate the two elasticity parameters of a TI elasticity tensor using the values of a, b, and χ. It is possible with parameterization of a TI medium resulting from the Backus average of thin, homogeneous, isotropic layers and also with assumption that the medium is linearly inhomogeneous, which means that the velocity changes linearly with depth and b is the level of such change. Consequently, we put more specific constraints on the other three elasticity parameters. It is possible with the assumption of the equal parameter b, for P- and S-waves. Derived relations allow us to compare results from different measurements and computational methods. We assume that the level of anisotropy, from the $ab\chi$ model and anisotropy from TI medium with the assumption of the same b parameter, $\chi_{\overline{\mathrm{TI}},b}$, are equal. We make such assumptions, to be able to compute P- and S- waves speeds and then to compare their ratio with $\sqrt{3}$.

Additionally, in Chapter 13, we show numerical examples based on four distinct TI tensors with the values of elasticity parameters from the Green-river shale obtained from Thomsen (1986). In each case, we know the values of a different set of elasticity parameters. Their known values might correspond to the real cases of acquiring the data from, respectively: vertical and horizontal seismic measurements of the quasi-P (qP) wave, vertical measurements of quasi-P and quasi-S (qS) waves, horizontal measurements of quasi-P and quasi-S waves, and vertical and horizontal measurements of quasi-P and quasi-S waves.

Chapter 2

Velocity model

[1] We restrict ourselves to a study of a particular case of wave propagation that is correlated with both an elliptical velocity dependence with direction and a linear velocity dependence with depth. This assumption enables to achieve analytic expressions for rays and traveltimes (Slawinski, 2015). We wish to show the limitations of one traveltime expression with the explanation and present an alternative more complex one. To characterize this, we define a velocity model in which the signal propagates in linearly inhomogeneous and elliptically anisotropic medium (Slawinski et al., 2004),

$$v(\theta, Z) = (a + bZ)\sqrt{\frac{1 + 2\chi}{1 + 2\chi \cos^2 \theta}}\,, \tag{2.1}$$

where

$$\chi = \frac{v_h^2 - v_v^2}{2v_v^2}\,,$$

with v_h and v_v being magnitudes of horizontal and vertical velocities, respectively. θ is the ray angle measured with respect to the vertical axis. χ is a dimensionless quantity;

[1] Chapters 2-8 are the results of the work with Ayiaz Kaderali on unpublished papers Kaderali and Kudela (2019a) and Kaderali and Kudela (2019b).

if v_h and v_v are equal, then $\chi = 0$ and the medium is isotropic. In expression (2.1), parameter a is the velocity of the signal at the surface in $\frac{m}{s}$, Z is depth and b is the velocity gradient in $\frac{1}{s}$. The rays in such a medium are arcs of ellipses (Epstein and Slawinski, 1999). The traveltime of a signal between a source and a receiver is (Slawinski et al., 2004)

$$t = \frac{1}{b} \ln \left(\frac{a + bZ}{a} \frac{1 + \sqrt{1 - a^2 p^2 (1 + 2\chi)}}{1 + \sqrt{1 - (a + bZ)^2 p^2 (1 + 2\chi)}} \right), \tag{2.2}$$

where

$$p = \frac{2X}{\sqrt{(X^2 + (1 + 2\chi) Z^2)[(2a + bZ)^2 (1 + 2\chi) + b^2 X^2]}} .$$

The source is located at $(0, 0)$ and the receiver at (X, Z); p is a ray parameter that is constant along the ray, due to lateral homogeneity.

Expression (2.2) is valid for a downgoing ray only. For such a study, we aim to know the point for which the signal starts to reach the receiver on its way up. The location of the last source at which the signal reaches the receiver from above is (Slawinski, 2015, p. 537)

$$X_c = \sqrt{\frac{1 + 2\chi}{b} (2a + bZ) Z} . \tag{2.3}$$

In expression (2.2) the traveltime corresponding to the part where the signal travels upward is subtracted due to the prior integration along the z-axis performed to obtain traveltime. To avoid this, we use the traveltime expression as given by Rogister and Slawinski (2005),

$$t = \frac{\tanh^{-1} \left[pbX - \sqrt{1 - p^2 a^2 (1 + 2\chi)} \right] + \tanh^{-1} \left[\sqrt{1 - p^2 a^2 (1 + 2\chi)} \right]}{b}. \tag{2.4}$$

The traveltime from expression (2.4) is valid for the entire ray, the downgoing and

upgoing segments, due to traveltime integral between the source at $(0, 0)$ and the receiver at (X, Z) with respect to Z-axis.

Chapter 3

Methods

3.1 Metropolis-Hastings method

We use the Metropolis-Hastings algorithm—based on Metropolis and Ulam (1949) and Hastings (1970)—works to generate a sequence of values of a, b, and χ in such a way that each set of these three parameters aims to achieve a smaller misfit between traveltimes from calculation and the dataset.

The algorithm is based on Markov-Chain Monte Carlo method. It generates a random set of samples that we use to obtain the numerical results; thus, we consider it a Monte Carlo sequence. These sets of samples are produced iteratively; the distribution of the next samples is dependent only on the current set of samples, which is a property of a Markov-Chain. Specifically, at each iteration, the algorithm picks candidates for the next set of samples based on the current set, comparing their probabilities, namely,

$$P(a_{n+1}, b_{n+1}, \chi_{n+1} | a_n, b_n, \chi_n) \,,$$

where

$$P = \exp\left(-\left\|\frac{t_{ab\chi} - t}{\sigma}\right\|^2\right),$$

and where t stands for the traveltimes obtained from the dataset, $t_{ab\chi}$ represents traveltimes obtained using expression (2.4); σ is a limit of the acceptable misfit between the samples; $\|\|$ stands for norm.

Either candidates are accepted—in which case the candidate values are used in the next iteration, or candidates are rejected—so that the candidate values are discarded and the new candidate is sampled for the next iteration.

Herein, we present pseudocode to illustrate used algorithm:

Define number of iterations n, standard deviation σ

Draw initial a, b, χ*–random numbers from the set range*

Compute t_0 *and* P_i

Draw new a, b, χ *with the set step*

Compute t_{i+1} *and* P_{i+1}

start loop for $i = 2 : n$

if $[0, 1] < min\left(1, \frac{P_{i+1}(t_n)}{P_i(t_i - 1)}\right)$

$t_i = t_{i+1}$

else

$t_i = t_{i-1}$

end loop

Examples of the codes are show in Appendices B–D.

Initially, the algorithm draws a random set of samples from the range, $a \in [1000; 5000]$, $b \in [0; 1]$, and $\chi \in [0; 0.1]$. The step for each parameter for the next iteration is random from the range $a \in [-10; 10]$, $b \in [-0.01; 0.01]$ and $\chi \in [-0.001; 0.001]$. Figure 3.1 shows the results of a single chain for parameter a. Whether we execute the algorithm

multiple times, each time first 10% of the samples are far from the values accepted at further iterations. The goal is to present data as histograms and read from one peak the result. For imaging purposes, we wish to show only the values that are close to the result. As we draw the samples from a sufficiently wide range for each parameter, the values from the first iterations are far from the correct results. After running the code and observing the results, we decide to save the results from the iteration and cut only first 10% of samples.

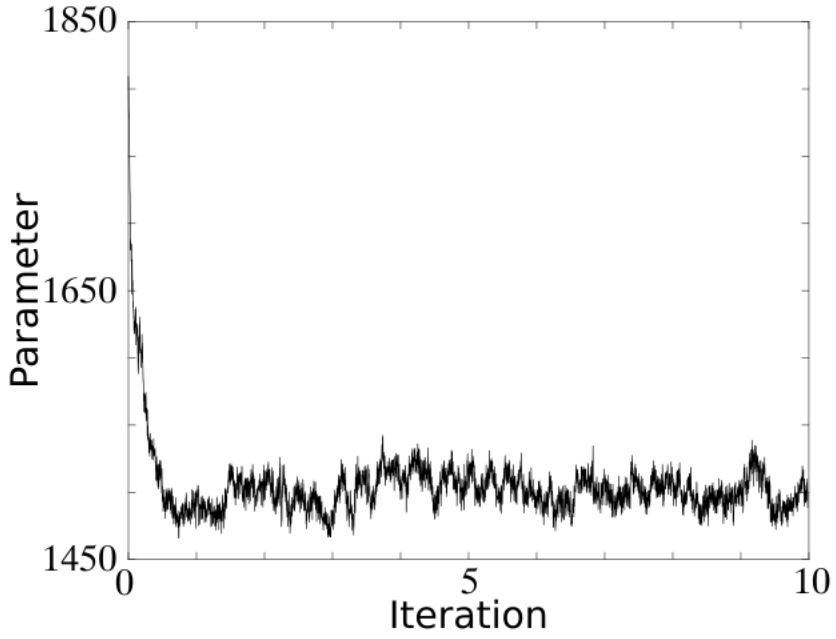

Figure 3.1: The value of the calculated parameter a at each iteration; $a = 1500$. To eliminate the influence of the starting values, we cut the first 10% of the iterations. The number of the iterations on the horizontal axis is multiplied by 10^4.

If we present the values of a, b, and χ, which meet the conditions of the Metropolis-Hastings algorithm (Raushan, 2011), on histograms, we are able to read the results from these plots. The highest peak of each histogram indicates the most probable value for each parameter.

3.2 fminsearch

For multi-layer media, the method of finding the parameters has two parts. Firstly, we find the points where the signal crosses the boundaries. As the model is elliptically anisotropic, seismic rays are elliptic-shaped curves. Herein, we use Fermat's principle, which is that the path taken between two points by a ray is the path that can be traversed in the stationary time (Bona and Slawinski, 2003). To find the coordinates of the points where ray crosses boundaries, we minimize traveltime for each ray separately. Commonly depths of the layers may be determined by well-log interpretation. As a consequence, we set the boundaries of the layers, also to reduce the number of unknowns in the algorithm. Secondly, the optimization of the velocity model is performed for all sources together to obtain one set of parameters for the entire layer. Along with the entire offsets, we encounter almost vertical rays that consist of information only about vertical velocity, which is insufficient for determination of χ. As the values for each parameter may differ significantly for each separate ray, we make the whole computation along the source line. The objective function is the sum of the squared differences between the measured (t_m) and calculated ($t_{ab\chi}$) traveltimes,

$$\sum_{i=1}^{n}(t_m^i - t_{ab\chi}^i)^2 \to \min\,,$$

where n is a number of traveltimes.

For the inversion purposes, to obtain the traveltime, we use expression (2.4) in all calculations. Both minimizations are carried out with *fminsearch*; a built-in optimization function in MATLAB. *fminsearch* attempts to find a local minimum of the target function. The optimization function uses the Nelder-Mead algorithm—described thoroughly in Lagarias et al. (1998)—which requires the startup values.

For a single-medium case, the results are unique and after proceeding with greater amount of layers we are able to propose and then set startup values for further computations. With the knowledge about common values for each parameter, after running code with chosen values, we get an insight from the results about startup values for the final computation.

Chapter 4

Synthetic data tests

We conduct synthetic data tests to ensure the correctness of the algorithms with simple models and also to examine the effect of the noise added to the traveltimes in both cases.

4.1 Dataset

Herein, the dataset consists of predicted traveltimes. To obtain such traveltimes, we calculate the traveltime of a signal between a source and a receiver propagating through a single medium using expression (2.2), with $a = 1500$, $b = 0.8$, $\chi = 0.02$. The resulting traveltime with respect to offset is illustrated in Figure 4.1. The geometry is based on VSP measurements. The source line consists of two-hundred and fifty locations with an interval of 20 m; the maximum offset is 5000 m, whereas the depth of the one receiver is 2500 m. With such geometry, having a dataset with two-hundred and fifty traveltimes, even with one receiver, we possess enough data to determine desired parameters accurately.

For far offsets in such geometry, we find the last source for which the signal reaches the receiver on its way down. The location of this source is calculated from expression (2.3). In our model, $X_c = 4031\,\mathrm{m}$, which corresponds to the cusp from Figure 4.1. After the cusp, the receiver is reached by an upgoing signal. Due to the change of the direction, the traveltime beyond the cusp is calculated with the opposite sign than the traveltime before the cusp. As a consequence, traveltime starts to decrease.

To model the actual traveltime, as opposed to using expression (2.2) along the entire source line, it is necessary to use expression (2.4). The dashed line illustrates such a result in Figure 4.1. Both expressions (2.2) and (2.4) are convenient for the inversion purposes, as it is mathematical curve fitting.

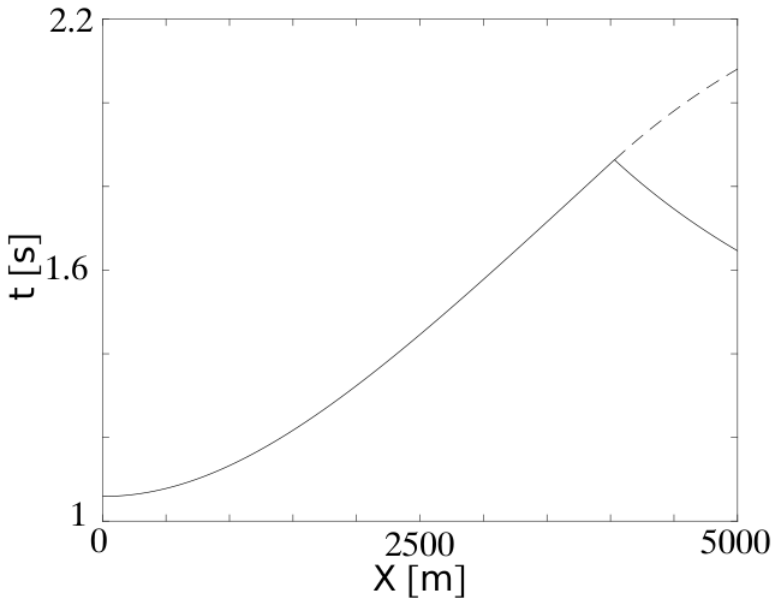

Figure 4.1: Traveltimes with respect to the offset X. The solid line stands for traveltime obtained from expression (2.2). The dashed line stands for the traveltime from expression (2.4).

4.2 Metropolis-Hastings

To examine the stability of the inverse problem we added normally distributed random noise of ± 2 ms and ± 5 ms to the traveltime. To avoid the cusp, shown in Figure 4.1, and for the purpose of inversion, we use expression (2.4), for all subsequent calculations.

One of the goal of this thesis is also to examine the correctness and applicability of Metropolis-Hastings method. Other, less complicated methods like curve-fitting might be enough to obtain satisfactory results, but Monte Carlo methods allow us also to examine the effect of noise added to the data and ambiguity of some results. The algorithm searches for the optimal values of the parameters to obtain the smallest misfit between the predicted and calculated traveltimes. The results are presented in Figures 4.2–4.7. We show two variations of added noise to discuss the influence of its magnitude on calculated parameters. The vertical lines on histograms indicate the values of a, b, and χ used to obtain the dataset. The horizontal axes on the plots show the value of the parameter and the vertical axes represent the number of accepted samples. In other words, the result of each parameter corresponds to the value that is most frequently accepted by the algorithm. The obtained distribution are close to Gaussian. Thanks to that we are able to uniquely read the results from the histograms and also we see that other results from iteration are evenly distributed around the peak.

The values of a, b, and χ chosen to match the predicted traveltimes with ± 2 ms noise are shown in Figures 4.2–4.4.

We read from the histograms the most probable values which are approximately $a = 1500$, $b = 0.8$ and $\chi = 0.02$. The standard deviation of the distributions is 5 ms and is

greater than the noise added to the traveltimes and the accuracy of the measurement, which is also 2 ms. In spite of the noise, the results of the search match the values from the model.

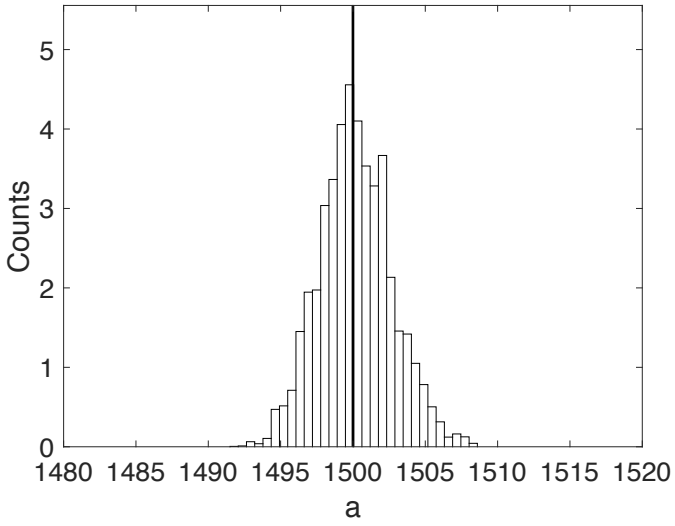

Figure 4.2: Distribution of parameter a for ± 2 ms noise. The values on the vertical axis are multiplied by 10^4.

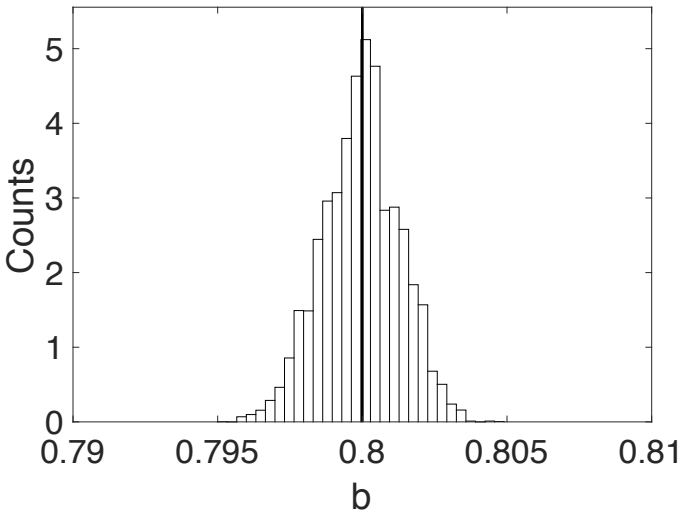

Figure 4.3: Distribution of parameter b for ± 2 ms noise. The values on the vertical axis are multiplied by 10^4.

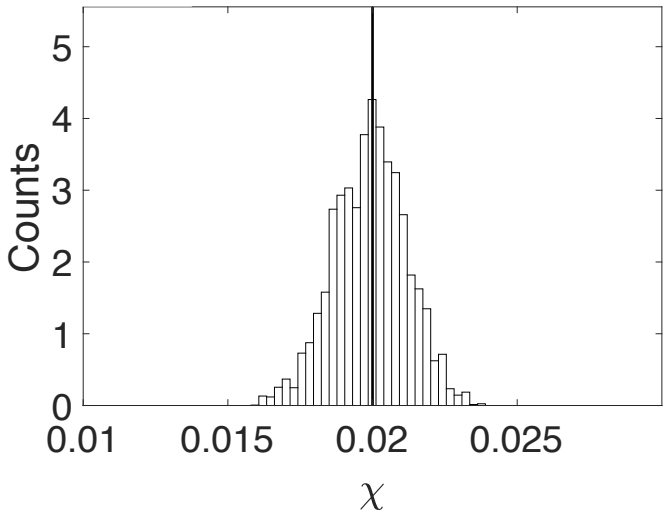

Figure 4.4: Distribution of parameter χ for ± 2 ms noise. The values on the vertical axis are multiplied by 10^4.

The results for the predicted traveltimes with larger noise of ± 5 ms are shown in Figures 4.5–4.7. The vertical line does not coincide with the peak of the histogram, as more values that were accepted by the algorithm are slightly smaller than the values from the model and the bin does not contain that wide range of numbers. The approximate values of the calculated parameters are also consistent with the values from the dataset. The advantage of using Metropolis-Hastings algorithm, over some other minimization methods, is the opportunity to examine the influence of noise in the data. It is also possible with linear methods as the data presented as histograms reveal Gaussian distribution. Greater noise does not significantly affect the results of inversion; the histograms still show nearly exact results of the search. However, the histograms are broader, because we increase the value of σ which is the acceptable difference between calculated and measured traveltimes. As for the noise traveltimes it is possible that this difference may increase, to move to the next iteration, the acceptable misfit needs to raise.

For that case, the standard deviation is 10 ms that is greater than the noise and also the accuracy of the measurement. As a consequence, the algorithm accepts more samples.

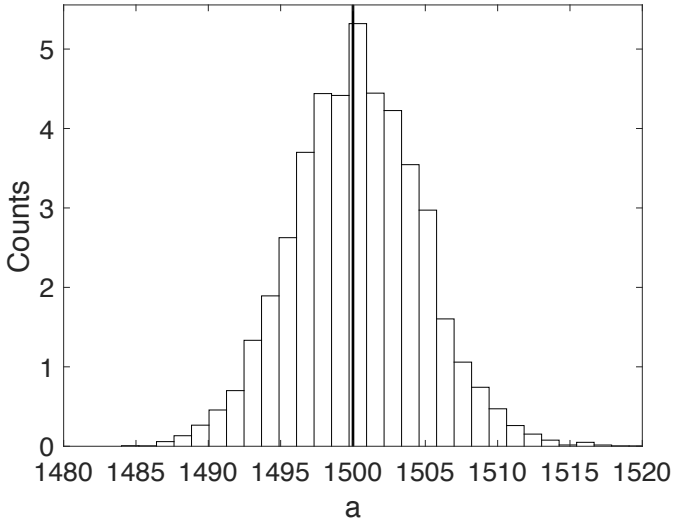

Figure 4.5: Distribution of parameter a for ± 5 ms noise. The values on the vertical axis are multiplied by 10^4.

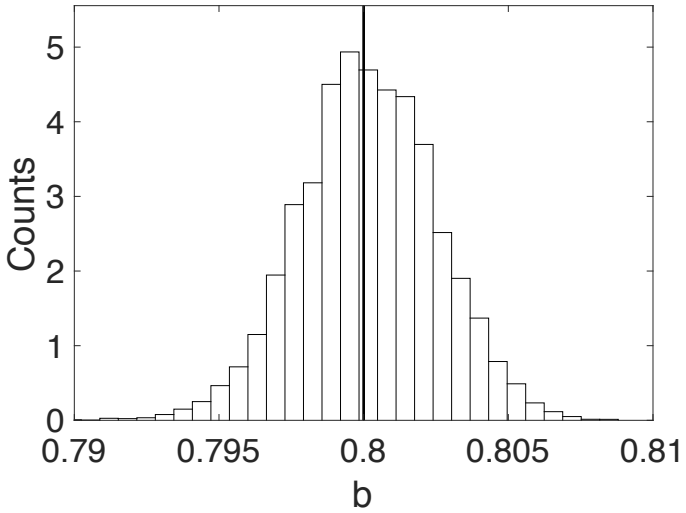

Figure 4.6: Distribution of parameter b for ± 5 ms noise. The values on the vertical axis are multiplied by 10^4.

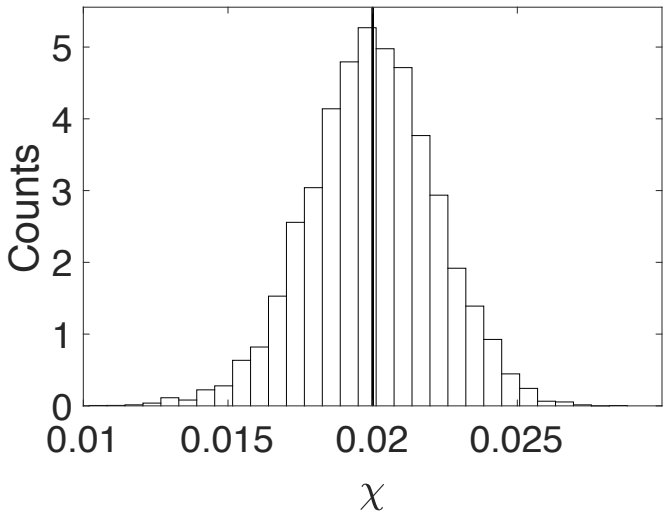

Figure 4.7: Distribution of parameter χ for $\pm 5\,\mathrm{ms}$ noise. The values on the vertical axis are multiplied by 10^4.

Each time the algorithm is executed, despite random initialization of used seed values and noise, the resultant values of a, b, and χ are the same. However, at a new execution, the shape of the histograms is not the same, yet the highest peak corresponds to the same values of a, b, and χ. The distributions suggest that we find the global minimum as the histogram consists of only one peak. The single-mode distributions of a, b, and χ suggest a uniqueness of the solution. The advantage of the Metropolis-Hastings algorithm is that it does not require any information about the target distributions, and the results do not depend on the startup values.

4.3 fminsearch

We conduct synthetic tests to show the reliability of the results based on measured traveltimes in three model variations and also examine the influence of noise added to the traveltimes. The predicted traveltimes are modelled from the values presented in Section 4.1.

4.3.1 The impact of white noise

We conduct the synthetic data test by adding random noise to the traveltimes to examine the effect of the perturbation on the resultant traveltimes. We show four examples of different noise levels; ± 0.01 ms, ± 2 ms, ± 5 ms, ± 10 ms. The case of ± 0.01 ms is added to ensure the correctness of the method. For each of the cases, we run the algorithm one-hundred times to examine the impact of the noise added to the traveltimes. As the random noise is added from a uniform distribution, it is enough to obtain a satisfactory examination of the noise from only one-hundred runs. The number of the runs does not need to be as big as the number of the runs for Metropolis-Hastings algorithm. We calculate the standard deviation for each parameter to investigate how the parameters change at each run.

We present two cases: first with a single-medium model and second with three-layer medium; the boundaries of the layers are 700 m and 1400 m. The values of corresponding a, b, and χ are given in Table 4.1 and 4.2.

We obtain synthetic traveltimes, t_m, from expression (2.4) for given a, b, and χ. Consequently, we add uniformly distributed random noise, ε, scaled by some number in each case. We conduct the inversion on t_m^e and obtain a, b, and χ. Therefore, we

calculate traveltime, $t_{ab\chi}$, based on the resultant parameters.

$$t_m \xrightarrow{+\varepsilon} t_m^e \xrightarrow{\text{inverse } (a,\, b,\, \chi)} t_{ab\chi}$$

In Table 4.1 and 4.2 we show the results of examination for single-medium model and three-layer medium, respectively. We present results for a, b, and χ with the different noise levels, where $\bar{\varepsilon}$ is the difference between traveltime from the model, t_m, and traveltime based on the parameters from the inversion, $t_{ab\chi}$. Residuals are the average differences between perturbed traveltimes, t_m^e, and the resultant traveltimes, $t_{ab\chi}$. Average noise is the difference between traveltime without noise t_m and perturbed traveltimes t_m^e.

$$\bar{\varepsilon} = t_m - t_{ab\chi},$$

$$\text{Residuals} = t_m^e - t_{ab\chi},$$

$$\text{Average noise} = t_m - t_m^e.$$

ε	No noise	± 0.01 ms	± 2 ms	± 5 ms	± 10 ms
a	1500	1500 (0.04)	1496.58 (9.71)	1491.24 (27.01)	1482.90 (55.70)
b	0.8	0.8 (0.00005)	0.8042 (0.0123)	0.8109 (0.0325)	0.8215 (0.0614)
χ	0.02	0.02 (0.00001)	0.01856 (0.027)	0.01640 (0.01173)	0.01287 (0.01650)
$\bar{\varepsilon}$ [ms]	0	0	0.1661	0.3991	0.8041
Res [ms]	0	0.0046	0.9173	2.2934	4.5867
Av. noise [ms]	0	0.0046	0.9283	2.3208	4.6416

Table 4.1: The example of a, b, and χ with standard deviation in parenthesis for each parameter; with the residuals, average noise and $\bar{\varepsilon}$ in the case of a single-medium model.

ε	No noise	± 0.01 ms	± 2 ms	± 5 ms	± 10 ms
a_1	1500	1498.09 (7.15)	1559.94 (122.85)	1367.25 (150.10)	1433.16 (221.85)
b_1	0.4	0.4021 (0.0099)	0.2797 (0.2812)	0.5529 (0.2501)	0.4686 (0.3101)
χ_1	0.01	0.01077 (0.00117)	0.00712 (0.01150)	0.00052 (0.06786)	0.00093 (0.20529)
a_2	1800	1800.96 (5.50)	1750.22(146.88)	1849.06 (178.56)	1704.32 (277.35)
b_2	0.3	0.3028 (0.0062)	0.3456 (0.2732)	0.4088 (0.2937)	0.6240 (0.3177)
χ_2	0.015	0.01405 (0.00152)	0.00474 (0.02581)	0.04699 (0.04172)	0.02189 (0.08071)
a_3	2000	1999.75 (2.32)	2072.44 (66.66)	2006.94 (180.62)	2084.42 (243.22)
b_3	0.2	0.2000(0.0057)	0.0785 (0.0912)	0.2459 (0.2083)	0.1242 (0.2378)
χ_3	0.035	0.03507 (0.00126)	0.04255 (0.01538)	0.01037 (0.01863)	0.02099 (0.02249)
$\bar{\varepsilon}$[ms]	0	0.0006	0.1056	0.2909	0.5623
Res[ms]	0	0.0045	0.9166	2.2920	4.5839
Av. noise [ms]	0	0.0046	0.9283	2.3208	4.6416

Table 4.2: The example of a, b, and χ with standard deviation in parenthesis for each parameter; with the residuals, average noise and $\bar{\varepsilon}$ in the case of three-layer medium.

The noise, ε, is sampled from the uniform distribution, the average noise is around twice smaller than ε. To examine the effect of noise on the traveltimes, we compare the level of noise, ε, or the average noise with $\bar{\varepsilon}$. As the value of $\bar{\varepsilon}$ is smaller than ε, we conclude that the effect of the noise does not have a significant impact on the traveltimes, although the values of parameters a, b, and χ are gradually different from the model with greater noise.

Herein, we present the example of the search with ± 5 ms of added noise for a single-medium model as histograms to compare with the results from Section 4.2. The histograms show that the results do not present the dominant value around the values that are set in the model as it is for the Metropolis-Hastings method.

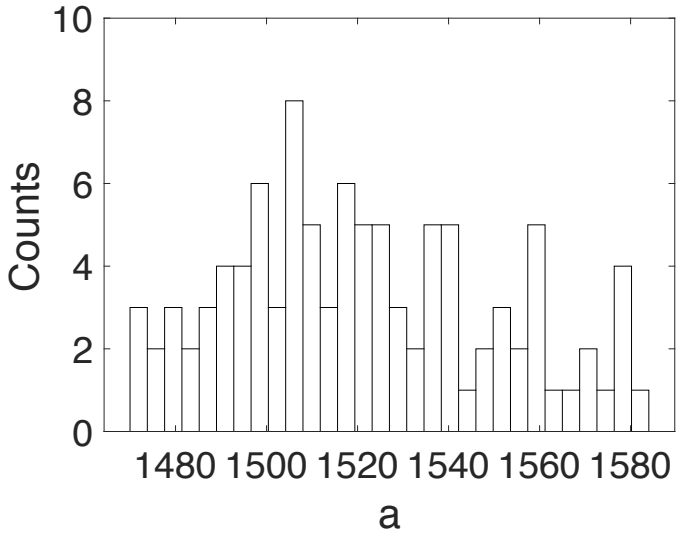

Figure 4.8: Distribution of parameter a for ± 5 ms noise.

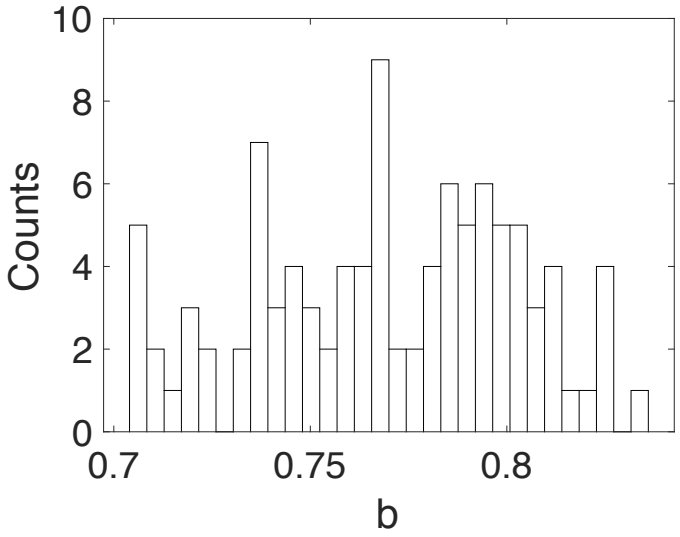

Figure 4.9: Distribution of parameter b for ± 5 ms noise.

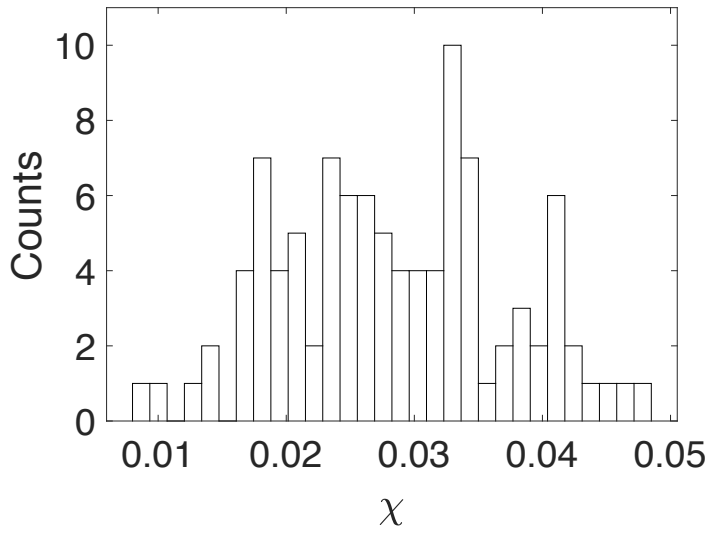

Figure 4.10: Distribution of parameter χ for ± 5 ms noise.

As shown in Chapter 7, the small change in traveltime affects the value of χ most. In other words, the value of χ changes significantly, but it does not affect the traveltime. In the case with 10 ms noise in a single medium, χ has a very low value, but the residuals are still in the range of acceptance. Consequently, the perturbation in traveltime has the least impact on a as it changes minimally. Additionally, we show

that the residuals are also smaller than the average noise.

4.3.2 Single-medium case

In this section we show a case of a single medium for the traveltimes obtained from the values for a, b, and χ from Section 4.1. The model, startup values, and results are shown in Table 4.3.

Model	Startup values	Results
$a = 1500$	$a = 2000$	$a = 1500$
$b = 0.8$	$b = 0.1$	$b = 0.8$
$\chi = 0.02$	$\chi = 0.001$	$\chi = 0.02$

Table 4.3: a, b, and χ after optimization for a single medium.

For a single-medium case the results do not depend on startup values. Whether the startup values are different the results remain the same. The results confirm the uniqueness of the solution for a three parameter model. The calculation carried out on the synthetic data shows that the method of velocity model optimization gives results consistent with the expected model.

4.3.3 Two-layer case

We show the nonuniqueness of the problem for the medium divided into two layers. Section 4.1 presents the geometry of the medium. The boundary of the layer is at 1000 m. In Table 4.4 we show the case with the startup values and layer of the boundary being the same as values from the model. The results are consistent with the values from the model.

Model	Startup values	Results
$a_1 = 1500$	$a_1 = 1500$	$a_1 = 1500$
$b_1 = 0.5$	$b_1 = 0.5$	$b_1 = 0.5$
$\chi_1 = 0.04$	$\chi_1 = 0.04$	$\chi_1 = 0.04$
$a_2 = 1800$	$a_2 = 1800$	$a_2 = 1800$
$b_2 = 0.3$	$b_2 = 0.3$	$b_2 = 0.3$
$\chi_2 = 0.015$	$\chi_2 = 0.015$	$\chi_2 = 0.015$

Table 4.4: a, b, and χ after optimization. Startup values are the same as the values from the model.

As in the case with field data, the values of the parameters are not known, in Table 4.5 we show the case with the startup values that are different from the model.

Model	Startup values	Results
$a_1 = 1500$	$a_1 = 1400$	$a_1 = 1384.29$
$b_1 = 0.5$	$b_1 = 0.6$	$b_1 = 0.7274$
$\chi_1 = 0.04$	$\chi_1 = 0.014$	$\chi_1 = 0.04264$
$a_2 = 1800$	$a_2 = 2000$	$a_2 = 1767.37$
$b_2 = 0.3$	$b_2 = 0.1$	$b_2 = 0.3884$
$\chi_2 = 0.015$	$\chi_2 = 0.05$	$\chi_2 = 0.00664$

Table 4.5: a, b, and χ after optimization with different startup values.

The average residuals are 0.024 ms and the standard deviation is 0.028 ms. The results do not match with the model values, but the averaged residuals and the standard deviation are satisfactory. The low residuals suggest that the resultant values give the traveltime that is very similar to the traveltime from the model.

4.3.4 Three-layer case

We show the inexactness of the problem for the medium divided into three layers. The boundaries of the first and second layer is at 700 m and 1400 m, respectively.

In Table 4.6 we show the case with the startup values and the depth of the boundaries being the same as the values from the model. The results are exactly the same.

Model	Startup values	Results
$a_1 = 1500$	$a_1 = 1500$	$a_1 = 1500$
$b_1 = 0.4$	$b_1 = 0.4$	$b_1 = 0.4$
$\chi_1 = 0.01$	$\chi_1 = 0.01$	$\chi_1 = 0.01$
$a_2 = 1800$	$a_2 = 1800$	$a_2 = 1800$
$b_2 = 0.3$	$b_2 = 0.3$	$b_2 = 0.3$
$\chi_2 = 0.015$	$\chi_2 = 0.015$	$\chi_2 = 0.015$
$a_3 = 2000$	$a_3 = 2000$	$a_3 = 2000$
$b_3 = 0.2$	$b_3 = 0.2$	$b_3 = 0.2$
$\chi_3 = 0.035$	$\chi_3 = 0.035$	$\chi_3 = 0.035$

Table 4.6: a, b, and χ after optimization. The layers in the calculations are exactly the same as layers from the model. The startup values are equal to the values from the model.

Table 4.7 presents the case with different startup values.

Model	Startup values	Results
$a_1 = 1500$	$a_1 = 1400$	$a_1 = 1486.99$
$b_1 = 0.4$	$b_1 = 0.3$	$b_1 = 0.3238$
$\chi_1 = 0.01$	$\chi_1 = 0.02$	$\chi_1 = 0.03740$
$a_2 = 1800$	$a_2 = 2000$	$a_2 = 1835.71$
$b_2 = 0.3$	$b_2 = 0.25$	$b_2 = 0.2629$
$\chi_2 = 0.015$	$\chi_2 = 0.01$	$\chi_2 = 0.01314$
$a_3 = 2000$	$a_3 = 2200$	$a_3 = 2039.39$
$b_3 = 0.2$	$b_3 = 0.1$	$b_3 = 0.1704$
$\chi_3 = 0.035$	$\chi_3 = 0.05$	$\chi_3 = 0.02681$

Table 4.7: a, b, and χ after optimization with different startup values.

The average residuals are 2.6 ms and the standard deviation is 1.8 ms.

The introduction of the third layer confirms the instability of the problem. The synthetic tests confirm that the more parameters we provide, the more unreliable the results are.

The tests of the inverse performed on the synthetic dataset ensure that the inverse is stable and gives the solutions that match the predicted data. In the case of the Metropolis-Hastings method, we have shown that the different levels of noise added to the predicted traveltimes neither affect its stability, nor change the solutions, but affect the shape of the histograms. In the case of *fminsearch* method, with the increasing noise, the results are gradually different from the values from the model. However, the resultant traveltimes perform the residuals lower than the averaged noise. Both tests confirm the correctness of the method.

Chapter 5

Field data

5.1 Geometry

The field data traveltimes and the geometry are obtained from Kaderali (2009). A walkaway VSP was acquired over a five-level array of receivers. The receiver array covered a vertical depth range from 1973 m to 2013 m with 10 m separation between receivers. The source line was positioned to be centred over the receiver array depth range. The source line consisted of two-hundred source locations with an interval between sources of approximately 25 m, with maximum source-receiver offsets from the centre of the receiver array of 4000 m and 1000 m, in opposite directions.

Herein, we wish to find the location of the last source at which the signal reaches the receiver from above. We calculate the X_c from expression (2.3) and find the furthest source for which the signal travels on its way down. Firstly, we conduct the calculation for a single-medium model, which contains only one layer, based on all traveltimes; the results are following: $a = 1347$, $b = 0.89$ and $\chi = 0.057$. Secondly, we calculate X_c from expression (2.3) for each receiver. The results are shown in Table 5.1.

Receiver	X_c [m]
1	3317
2	3328
3	3340
4	3351
5	3363

Table 5.1: The furthest offset for each receiver for which the signal travels only downward.

For the inversion purposes and to avoid the cusp shown in Figure 4.1, we use expression (2.4) for all subsequent calculations. The last twenty-one traveltimes from the first and second receiver are noisy, so to increase the accuracy of inversion, we truncate them from the dataset. The dataset consists of the traveltimes from one-hundred and seventy-nine sources from each of the first and second receiver, two-hundred sources from each of the last three receivers. The optimization is based on nine-hundred and fifty-eight traveltimes.

5.2 Metropolis-Hastings

In this section, for the purpose of inversion, we consider the entire dataset that consists of nine-hundred and fifty-eight traveltimes. The offsets are far enough so that the traveltimes are obtained from various incident angles. As the rays are not only vertical, we are able to uniquely determine the level of anisotropy, χ. As the value of χ determines the difference between vertical and horizontal velocity, we expect to have a wide range of offsets in the data to have information also from horizontal components. In Section 6.1.1, we show that for almost vertical rays the value of χ is nonunique. Herein, we present the results of the inversion using the Metropolis-Hastings method. Figures 5.1–5.3 present the histograms with the results of the inversion for each parameter.

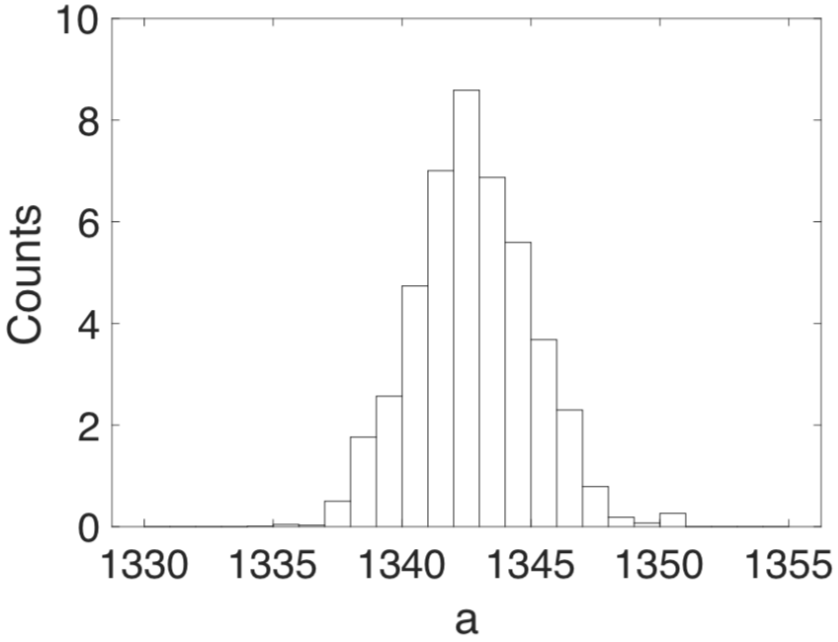

Figure 5.1: Distribution of parameter a for all dataset. The values on the vertical axis are multiplied by 10^4.

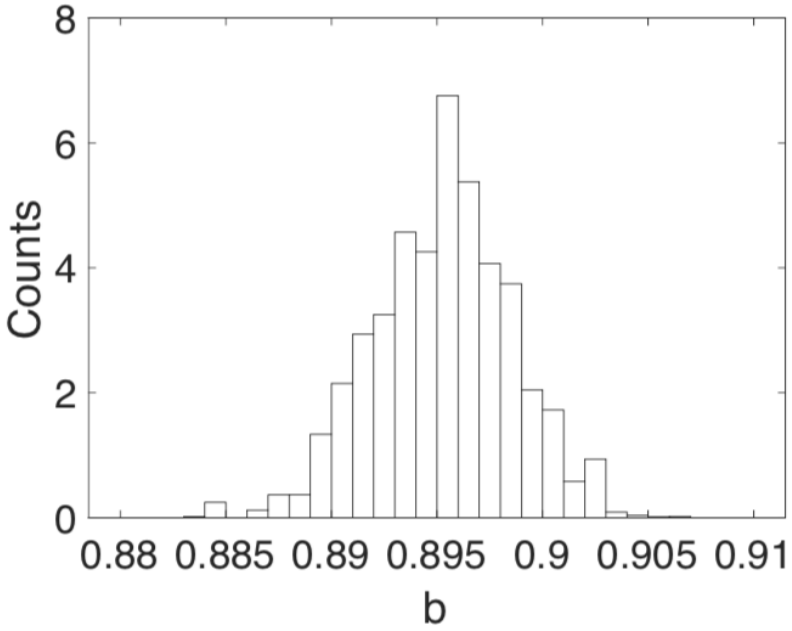

Figure 5.2: Distribution of parameter b for all dataset. The values on the vertical axis are multiplied by 10^4.

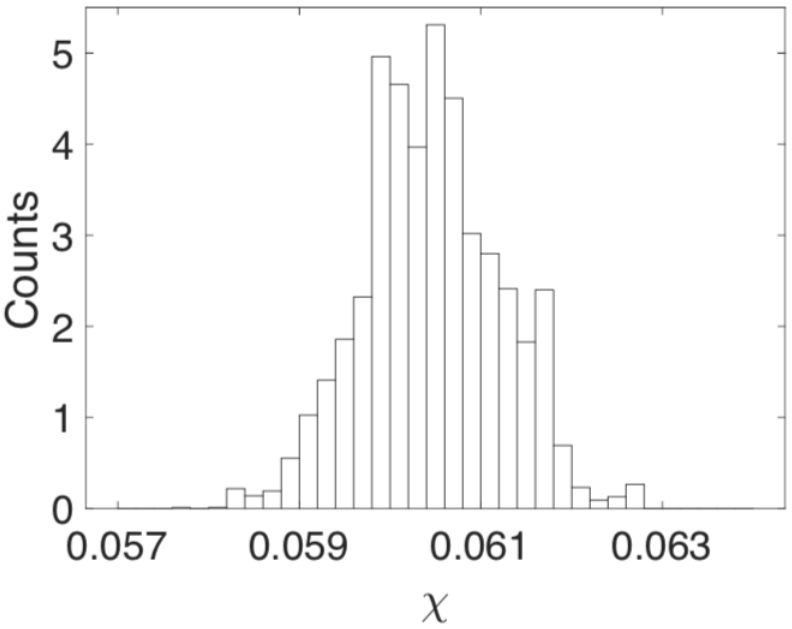

Figure 5.3: Distribution of parameter χ for all dataset. The values on the vertical axis are multiplied by 10^4.

To determine the exact value for each parameter, we decide to choose the middle value of the highest bin in each histogram. The other possible way of determining the exact value is to calculate the average or the mode of the values that the bin consists of. We read from the histograms the most optimal values, which are $a = 1342.4$, $b = 0.897$, and $\chi = 0.0606$. The averaged residuals are 1.72 ms. Each time we execute the algorithm, the shape of the histogram is slightly different. Furthermore, the location of the highest bin can differ. In Table 5.2, we present the middle value of the highest bin, five runs for each parameter.

Run	a	b	χ	Residuals [ms]
1	1342.5	0.897	0.0604	1.72
2	1342.5	0.893	0.0606	1.90
3	1342.5	0.896	0.0608	1.64
4	1342.5	0.897	0.0606	1.72
5	1342.5	0.896	0.0604	1.62

Table 5.2: The values for each parameter after five runs with the corresponding residuals.

As the above table shows, the results do not reveal significant differences. Unsurprisingly, the residuals are very similar to the values for each parameter do not change rapidly.

We notice an essential feature of the Metropolis-Hastings method—that for a single medium, the solution does not depend on the values of the set of initial samples. They are generated randomly, and at each run, the calculated most probable values of a, b, and χ are almost the same. Moreover, the single-mode distributions of a, b, and χ allow us to infer that for a single medium, the local minimum is also the global minimum.

5.3 fminsearch

In this section, we present the results of the inversion using *fminsearch* method. We consider four cases of different model variations; a single medium, two-layer, three-layer, and four-layer medium. We calculate a set of a, b, and χ for each of the layer. We examine whether the greater number of the layers affects the stability of the calculation.

5.3.1 Single-medium case

Herein, we consider a single-medium model that consists of only three parameters a, b, and χ. Figure 5.4 presents the examples of the elliptical shape of the rays that travel through the single-medium from the source to the receiver.

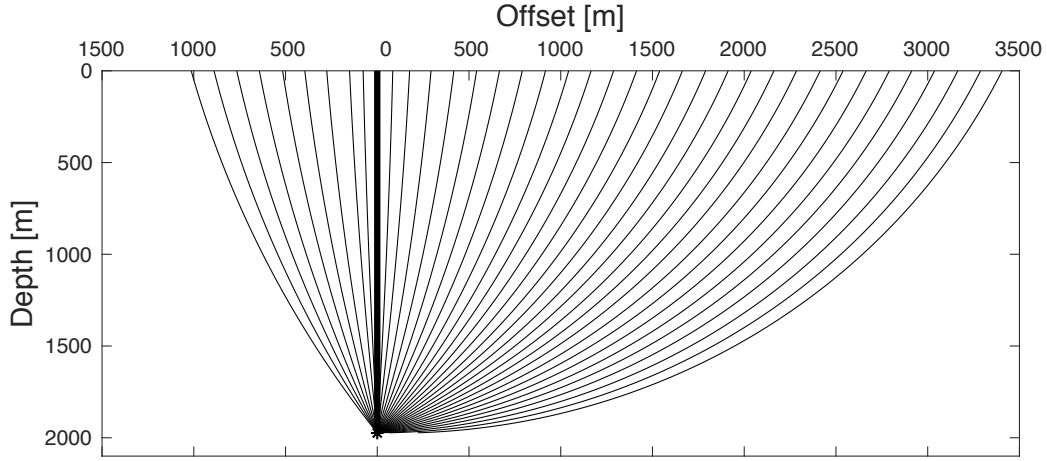

Figure 5.4: The examples of the rays that travel through the single-medium from the sources to the receivers.

To obtain a, b, and χ we minimize the difference between traveltimes from the measurements and the traveltimes from calculations. The results of the inversion are presented in Table 5.3.

Results
$a_1 = 1342.7$
$b_1 = 0.895$
$\chi_1 = 0.0604$

Table 5.3: Resultant a, b, and χ for a single-medium model.

The average residuals are up to 1.62 ms and the standard deviation is 1.19 ms. Figure 5.5a shows the residuum for each traveltime from the entire dataset. Figure 5.5b presents the histogram of residuals.

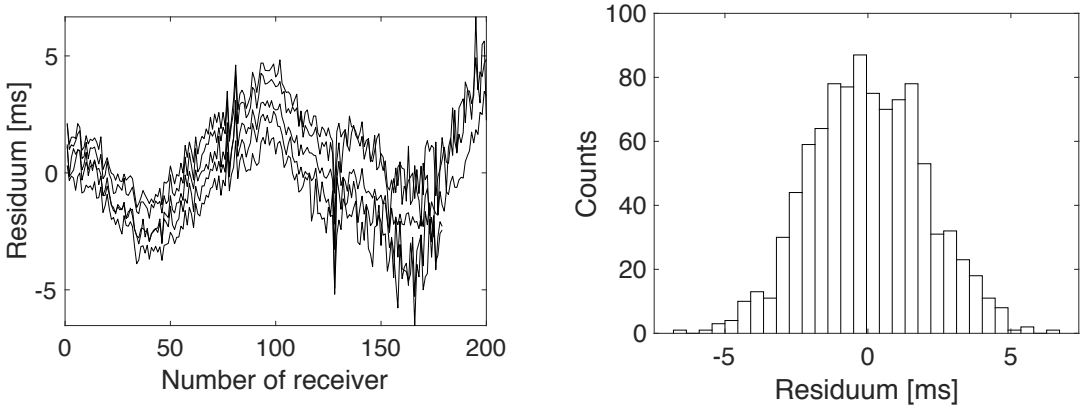

(a) Residuals

(b) Histogram of residuals

Figure 5.5: Differences in traveltimes for each source and receiver in a single-medium case.

The results do not depend on startup values. It suggests that for a single-medium model with three parameters, we find the global minimum. A single-medium model, due to its large thickness of 2013 m is a significant generalization. To find a better fit and smaller residuals, we divide the medium into more layers. Consequently, we aim to find the different set of parameters for each layer, which—however—results in certain differences and limitations of the inverse process, to be discussed below.

5.3.2 Two-layer case

Herein, we consider the medium devided into two layers that consists of six parameters, including a set of a, b, and χ for each layer. The boundary of the layer is at 1000 m. The points, where the ray paths cross subsequent boundaries, are calculated for each pair of sources and receivers, conserving Fermat's principle. Figure 5.6 presents the examples of the rays that travel through the two-layer medium from the source to the receiver.

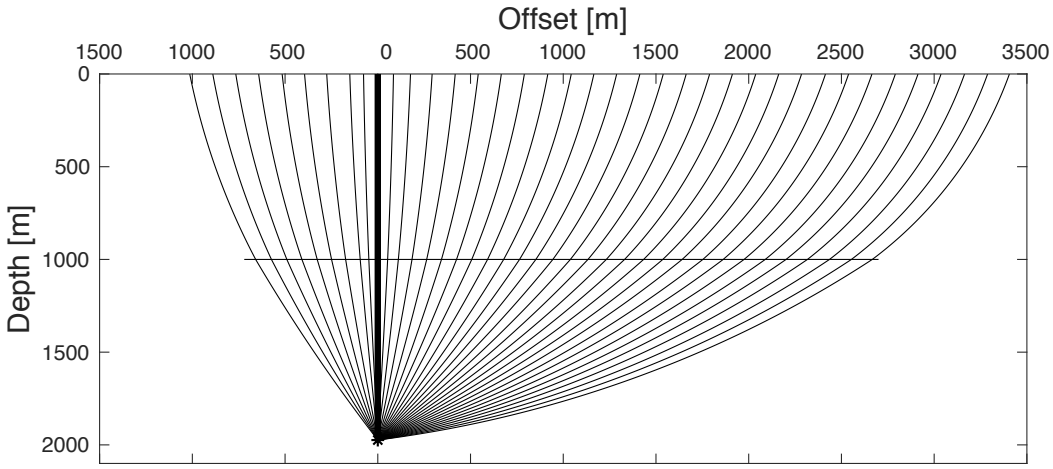

Figure 5.6: The examples of the rays that travel through the two-layer medium from the source to the receiver. The depth of the boundary is 1000 m

The parameters corresponding to the least difference between measured and modelled traveltimes are presented in Table 5.4. To show the dependence of each parameter on the startup values we perform two sets of calculations.

First case		Second case	
Startup values	Results	Startup values	Results
$a_1 = 1400$	$a_1 = 1100.99$	$a_1 = 1100$	$a_1 = 942.05$
$b_1 = 0.8$	$b_1 = 1.4933$	$b_1 = 1$	$b_1 = 1.6224$
$\chi_1 = 0.05$	$\chi_1 = 0.0021$	$\chi_1 = 0.01$	$\chi_1 = 0.0009$
$a_2 = 2100$	$a_2 = 2422.22$	$a_2 = 2400$	$a_2 = 3015.97$
$b_2 = 0.6$	$b_2 = 0.5481$	$b_2 = 0.5$	$b_2 = 0.0673$
$\chi_2 = 0.01$	$\chi_2 = 0.0993$	$\chi_2 = 0.01$	$\chi_2 = 0.0039$
Average residuals	1.1 ms	Average residuals	0.8 ms
Standard deviation	1.4 ms	Standard deviation	1 ms

Table 5.4: a, b, and χ of two layers and their dependence on startup values.

Figure 5.7 presents the differences between the modelled and measured traveltimes for both cases. Figure 5.8 shows the histograms of residuals.

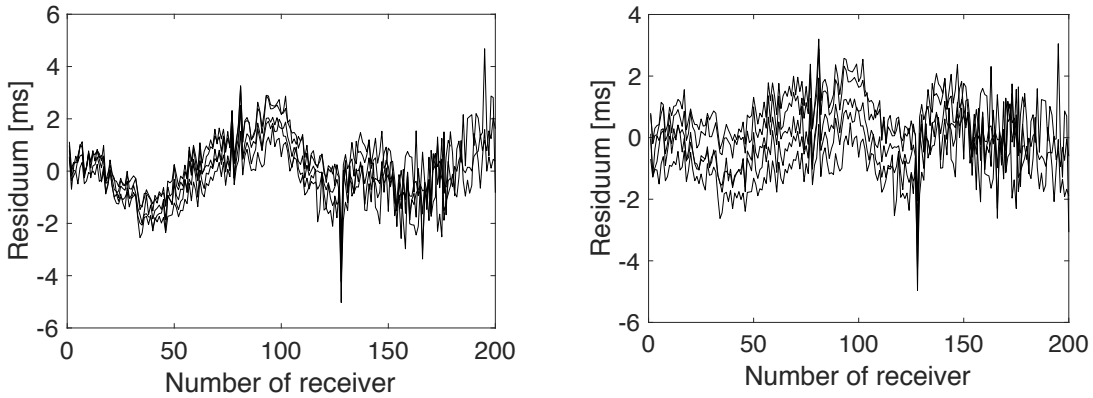

(a) First case **(b)** Second case

Figure 5.7: Differences in traveltimes for each source and receiver in two cases.

In two-layer case, the results of the inversion with six unknowns depend on startup values. Table 5.4 shows that the change of the startup values affects the results, but

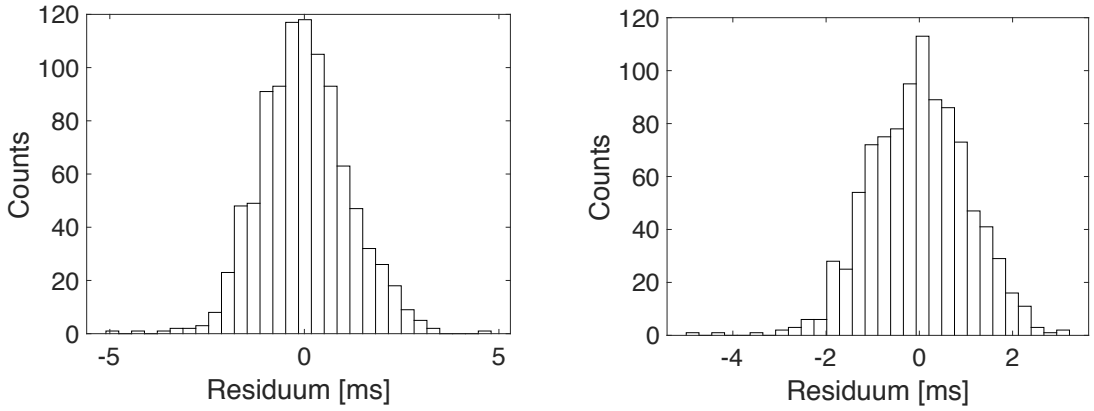

(a) First case **(b)** Second case

Figure 5.8: Histograms of residuals.

does not affect the residuals significantly.

In Chapter 7, we show how the change of values of a, b, and χ affects the modelled traveltimes. For the two-layered case with six parameters the problem is nonunique. This means that we find various local minima and there are many combinations of a, b, and χ that allow us to fit the measured traveltimes with low residuals. The empirical accuracy is excellent if the purpose of the inversion is imaging the traveltimes; however, if we aim to define the mechanical properties of rocks, it is not reliable.

5.3.3 Three-layer case

In this section, we consider three-layer velocity model. In terms of the previous considerations, we add one more layer and examine the stability. We divide the medium into three layers. The boundaries of the first and second layer are 500 m and 1000 m, respectively. Figure 5.9 shows the examples of the rays that travel through the three-layer medium from the source to the receiver. As the results of the inversion, we obtain nine parameters, consisting of a, b, and χ for each layer.

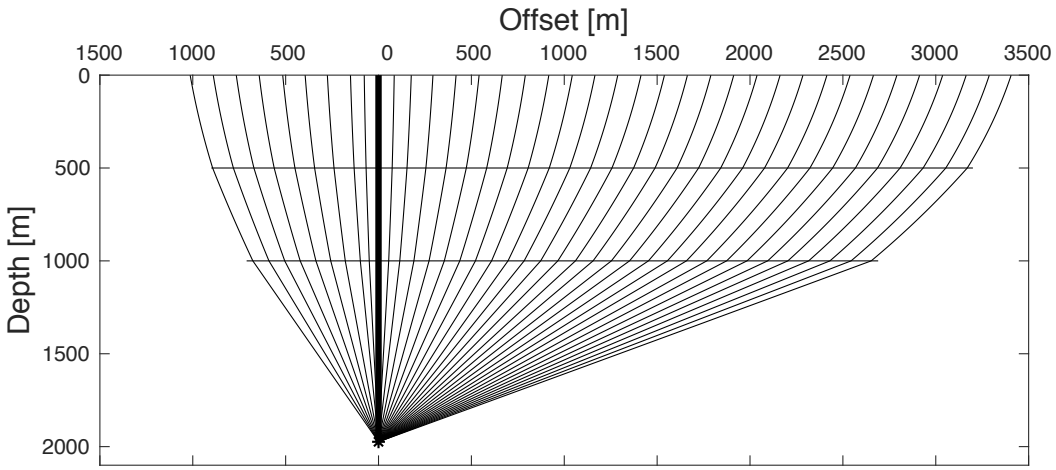

Figure 5.9: The examples of the rays that travel through the three-layer medium from the source to the receiver.

To show the dependance of parameters on the startup values, we perform two cases of different seed values for each parameter. The resultant values of a, b, and χ are presented in Table 5.5.

First case		Second case	
Startup values	Results	Startup values	Results
$a_1 = 1400$	$a_1 = 1088.97$	$a_1 = 1000$	$a_1 = 1329.65$
$b_1 = 0.8$	$b_1 = 1.5078$	$b_1 = 1.2$	$b_1 = 0.0836$
$\chi_1 = 0.05$	$\chi_1 = 0.0032$	$\chi_1 = 0.01$	$\chi_1 = 0.0247$
$a_2 = 1800$	$a_2 = 2308.38$	$a_2 = 2000$	$a_2 = 2934.07$
$b_2 = 0.6$	$b_2 = 0.7159$	$b_2 = 1$	$b_2 = 1.1897$
$\chi_2 = 0.01$	$\chi_2 = 0.0002$	$\chi_2 = 0.01$	$\chi_2 = 0.0040$
$a_3 = 2200$	$a_3 = 2696.54$	$a_3 = 3000$	$a_3 = 2756.11$
$b_3 = 0.3$	$b_3 = 0.0069$	$b_3 = 0.3$	$b_3 = 0.0376$
$\chi_3 = 0.05$	$\chi_3 = 0.1903$	$\chi_3 = 0.05$	$\chi_3 = 0.1606$
Average residuals	0.9 ms	Average residuals	0.8 ms
Standard deviation	1.2 ms	Standard deviation	1.1 ms

Table 5.5: a, b, and χ of three layers and their dependence on startup values.

Figure 5.13 presents the values of the differences between modelled and measured traveltimes for both cases. Figure 5.14 shows the histograms of residuals.

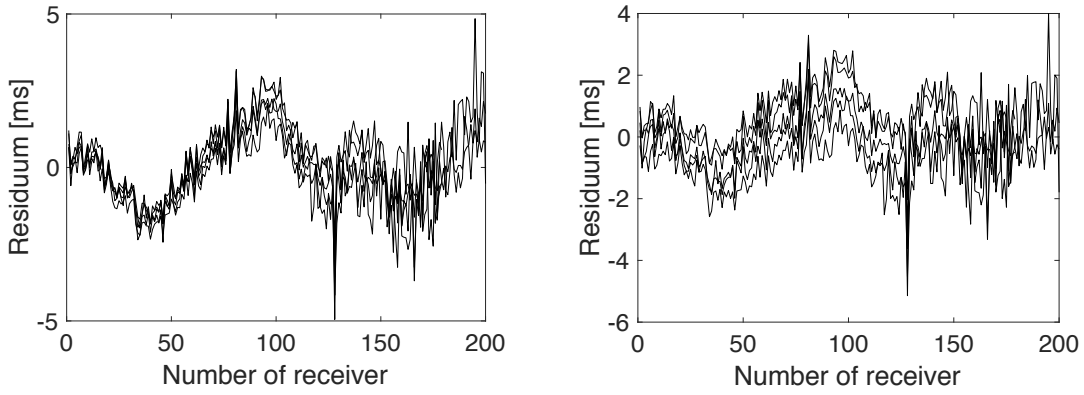

(a) First case **(b)** Second case

Figure 5.10: Differences in traveltimes for each source and receiver.

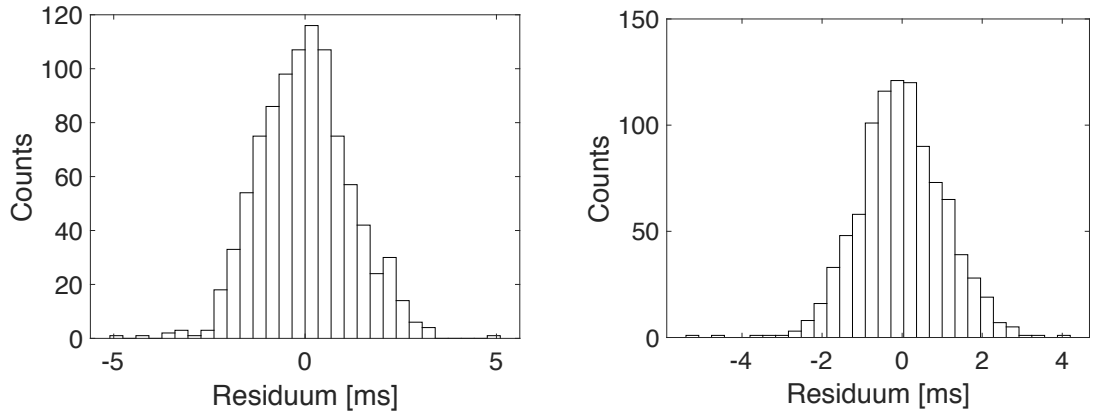

(a) First case **(b)** Second case

Figure 5.11: Histograms of residuals.

For a three-layer model with nine parameters, the values depend on startup values; each time the startup values change the results are different. The division into more layers results in the lower residuals, but does not necessarily provide the real geological properties of the medium. Lower residuals confirm that the division of the medium into more layers allows us to fit traveltimes with better accuracy. However, the unreliability of each parameter is greater as the change of the startup value of one parameter can change the results significantly. In the first case, we notice that, for the first and second layer, the results suggest the weak anisotropy of the medium as the value of χ is very low. Additionally, for the third layer, low parameter b indicates the homogeneity of this layer.

5.3.4 Four-layer case

In this section, we consider four-layer velocity model. In terms of the previous considerations, we add one more layer and examine the stability. We divide the medium into four layers. The boundaries of the first, second, and third layer are 500 m, 1000 m, and 1500 m, respectively. Figure 5.12 shows the examples of the rays that travel through

the four-layer medium from the source to the receiver. We obtain twelve parameters, consisting of a, b, and χ for each layer.

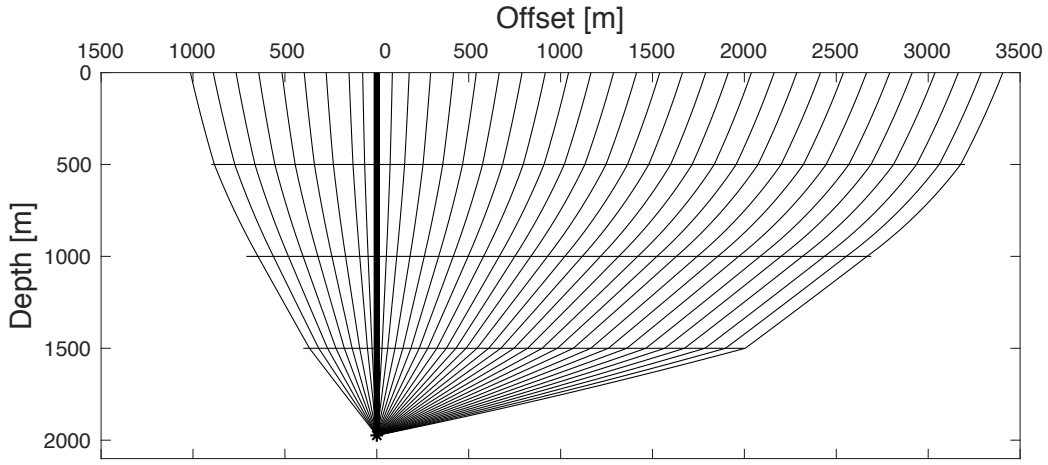

Figure 5.12: The examples of the rays that travel through the four-layer medium from the source to the receiver.

To show the dependance of parameters on the startup values, we perform two cases of different seed values for each parameter. The resultant values of a, b, and χ are presented in Table 5.6.

First case		Second case	
Startup values	Results	Startup values	Results
$a_1 = 1000$	$a_1 = 1185.23$	$a_1 = 1100$	$a_1 = 941.23$
$b_1 = 1$	$b_1 = 0.6659$	$b_1 = 1.2$	$b_1 = 1.0861$
$\chi_1 = 0.01$	$\chi_1 = 0.0063$	$\chi_1 = 0.01$	$\chi_1 = 0.0010$
$a_2 = 1400$	$a_2 = 1984.08$	$a_2 = 1400$	$a_2 = 2601.68$
$b_2 = 0.8$	$b_2 = 1.3216$	$b_2 = 0.9$	$b_2 = 0.4816$
$\chi_2 = 0.01$	$\chi_2 = 0.00001$	$\chi_2 = 0.01$	$\chi_2 = 0.0059$
$a_3 = 1800$	$a_3 = 2505.73$	$a_3 = 1900$	$a_3 = 2507.14$
$b_3 = 0.6$	$b_3 = 0.5956$	$b_3 = 0.5$	$b_3 = 1.4573$
$\chi_3 = 0.01$	$\chi_3 = 0.0288$	$\chi_3 = 0.01$	$\chi_3 = 0.0007$
$a_4 = 2400$	$a_4 = 2956.12$	$a_4 = 2300$	$a_4 = 2989.22$
$b_4 = 0.3$	$b_4 = 0.0986$	$b_4 = 0.2$	$b_4 = 0.0138$
$\chi_4 = 0.01$	$\chi_4 = 0.0681$	$\chi_4 = 0.05$	$\chi_4 = 0.0496$
Average residuals	0.9 ms	Average residuals	0.8 ms
Standard deviation	1.2 ms	Standard deviation	1 ms

Table 5.6: a, b, and χ of four layers and their dependence on startup values.

Figure 5.13 presents the values of the differences between modelled and measured traveltimes for both cases. Figure 5.14 shows the histograms of residuals.

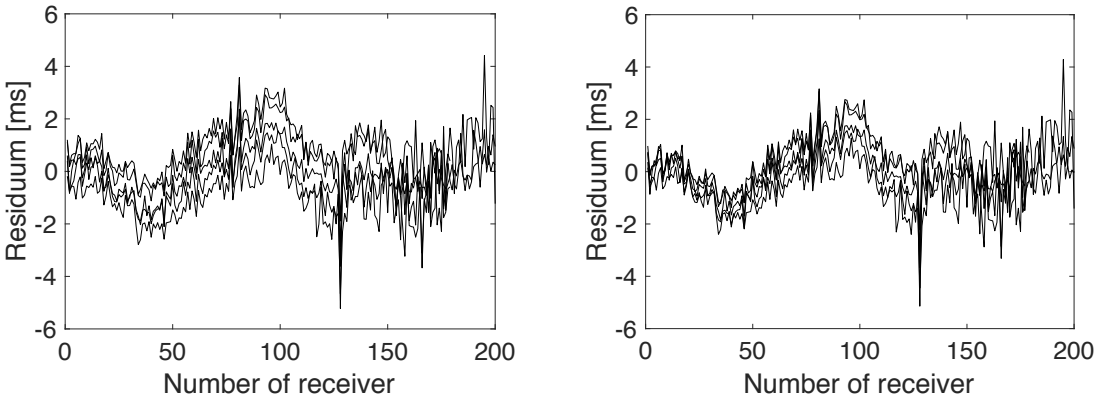

(a) First case **(b)** Second case

Figure 5.13: Differences in traveltimes for each source and receiver.

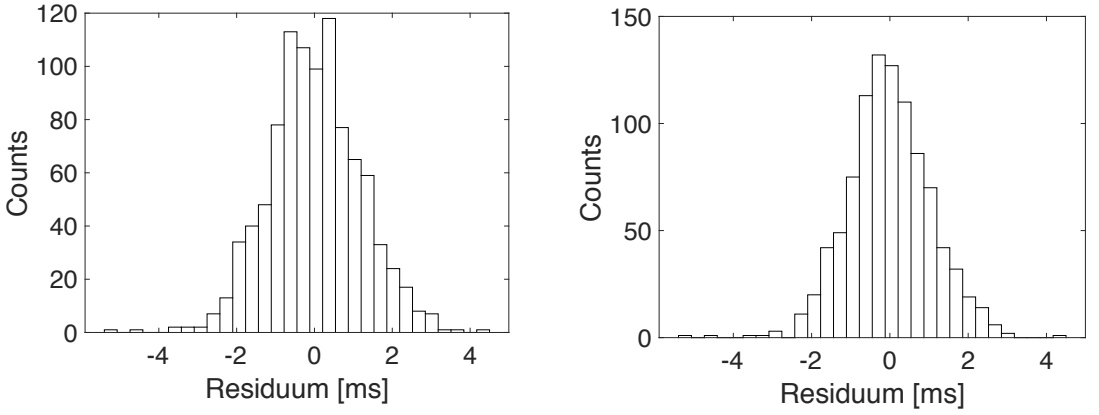

(a) First case **(b)** Second case

Figure 5.14: Histograms of residuals.

For a four-layer model with twelve parameters, the values also depend on startup values. For each of four models, the residuals suggest that the model is too simple and do not provide the significantly better residuals. Additionally, as the accuracy of the measurement is around 2 ms, from the plots that show the differences between traveltimes, we notice that standard deviation is smaller than 2 ms. It means that we are not able to find a satisfying fit with more reliable results as the residuals are smaller than the precision of the data acquisition.

However, the unreliability of each parameter is greater as the change of the startup value of one parameter can change the results significantly. We notice that, for the first and second layer, the results suggest the weak anisotropy of the medium as the value of χ is very low.

The method is error-laden because it numerically searches for the values that present the least-square difference between the traveltimes. If the medium is divided into more layers, we obtain more unknowns in the target function. Consequently, we achieve a better fit. Even if the residuals of this search are satisfactory, the respective values differ from each other. Since it is a mathematical curve fitting, the algorithm finds the best match, but the results do not necessarily represent the mechanical properties that describe the medium. We obtain unique results only in a single-medium model—however, a model of 2000 m depth with only three parameters is a significant generalization. For the two-, three-, and four-layer cases, we encounter the instability problem; the function that requires the startup values, the results depend on their values performing similarly low residuals.

5.4 Comparison of two methods

In this section, we compare the results from the Metropolis-Hastings algorithm and *fminsearch* method for a single-medium case. For the comparison purposes, both methods perform an investigation on the entire dataset, described in Section 5.1.

The comparison of the parameters obtained from Metropolis-Hastings and from *fminsearch* function is shown in Table 5.7.

Metropolis-Hastings	*fminsearch*
$a = 1342$	$a = 1343$
$b = 0.9$	$b = 0.9$
$\chi = 0.0606$	$\chi = 0.0604$
Residuals= 2.27 ms	Residuals= 2.62 ms

Table 5.7: The comparison of a, b, and χ using two different methods for a single-medium model.

The Metropolis-Hastings algorithm does not provide the optimal results, but we obtain the distribution of each parameter. Although the two methods are different, the peak values from histograms from Section 5.2 and the results from Section 5.3.1 match and suggest the correctness of both methods. Also, the results do not depend on the initial values.

In conclusion, the results of the two different methods does not reveal the great differences. The same values of the parameters also confirm that in the problem of a single medium we are able to find the unique solutions.

Chapter 6

Different cases of determining anisotropy and inhomogeneity parameters

In this section, we present the investigation of the level of increasing velocity with depth $(a + bz)$ using the rays that reach the receiver with the incident angle smaller than 10° and also with the assumption of isotropy. Moreover, fixing the values of a and b from the previous search, we obtain the anisotropy parameter, χ, for the entire dataset.

6.1 Metropolis-Hastings

6.1.1 Low-incident angle

Herein, for the purpose of the inversion, we consider only part of the dataset, namely, the traveltimes obtained from the rays that reach the receiver with the small incident angle. We calculate the incident angles for all walkaway data to obtain traveltimes from rays that go nearly vertically. The dataset consists of one-hundred and forty traveltimes from walkaway for the rays that travel to the receiver with the incident angle smaller than 10° which are twenty-eight traveltimes from each of receiver.

For the short-offset data, it is impossible to obtain information about anisotropy since all rays are nearly parallel to each other (Danek and Slawinski, 2012). We confirm that χ can have any value in near offsets as the algorithm accepts each sampled value for χ. Each time we execute the algorithm, the shape of the histogram is different and does not present the major peak with the same value.

The results of the Metropolis-Hastings algorithm are presented in Figures 6.1–6.3.

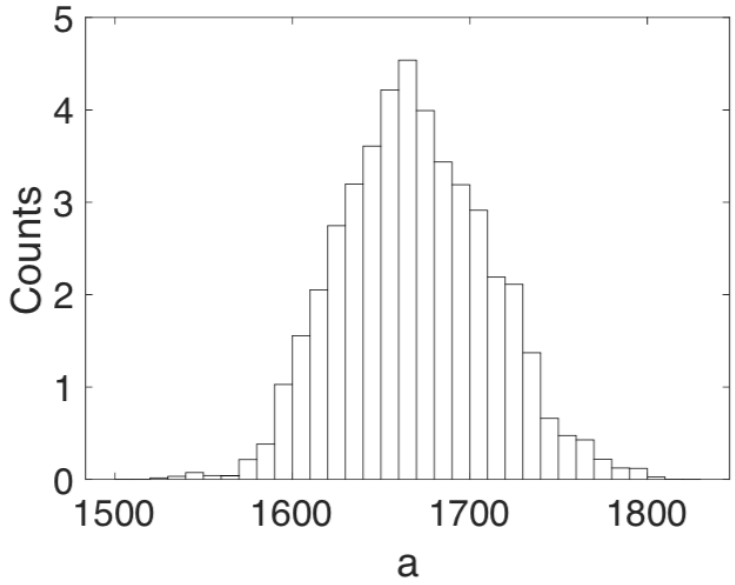

Figure 6.1: Distribution of parameter a for the case of low incident angle. The values on the vertical axis are multiplied by 10^4.

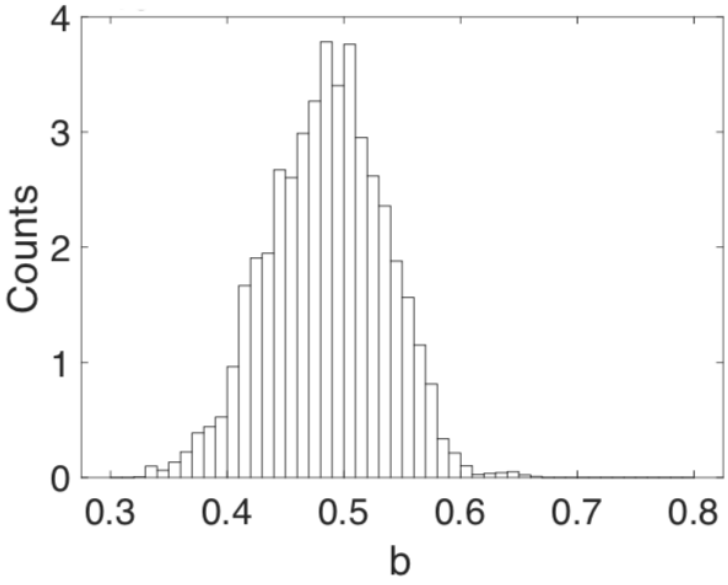

Figure 6.2: Distribution of parameter b for the case of low incident angle. The values on the vertical axis are multiplied by 10^4.

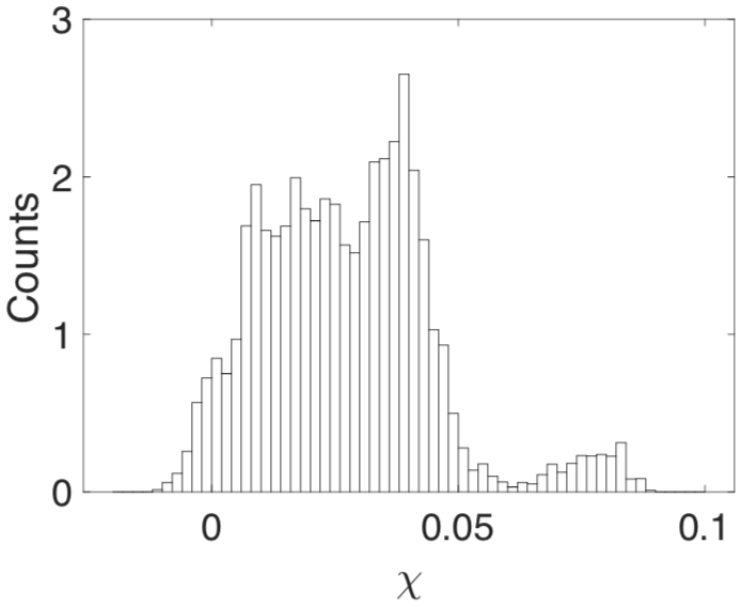

Figure 6.3: Distribution of parameter χ for the case of low incident angle. The values on the vertical axis are multiplied by 10^4.

From histograms we read the most probable values of $a = 1680$ and $b = 0.47$; the value of χ is nonunique. In Figure 6.3, we notice the flattened and broader histogram with a wide range of values for χ. Additionally, each time we run the code, the shape of the histogram for χ is different. We also encounter the cases of the negative values of χ accepted by the algorithm. Danek and Slawinski (2012) state that negative value of χ is physically acceptable, since it obeys the conservation of energy, which requires the elasticity tensor to be positive-definite and entails $\chi \in (-0.5; \infty)$. Even though the near-offset data are insufficient to consider the effects of anisotropy, they provide the information about a and b. In turn, the fixed values of a and b may be used in the far-offset case to better estimate the anisotropy parameter χ. Such an example is shown in Section 6.1.3.

6.1.2 Low-incident angle and isotropic case

For the rays that travel almost vertically, the elliptical anisotropy is hard to justify. Using the same dataset as in Section 6.1.1, we consider the isotropic medium ($\chi = 0$) and evaluate only the level of inhomogeneity. The results of the inversion are shown in Figures 6.4 and 6.5.

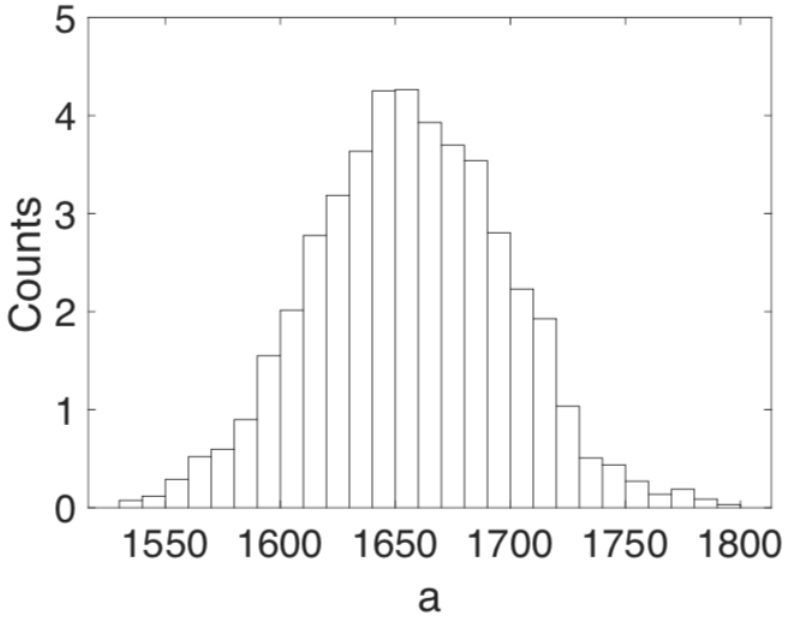

Figure 6.4: Distribution of parameter a for low incident angle and isotropic case. The values on the vertical axis are multiplied by 10^4.

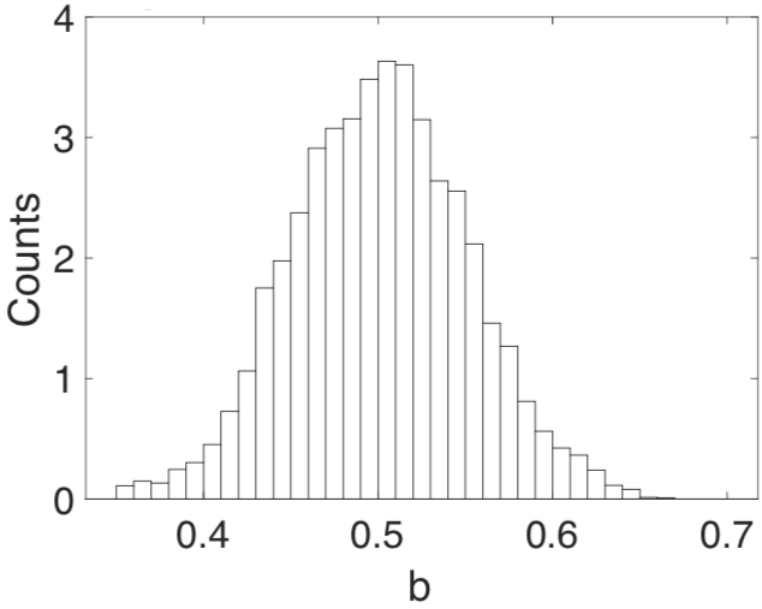

Figure 6.5: Distribution of parameter b for low incident angle and isotropic case. The values on the vertical axis are multiplied by 10^4.

The most probable values of the parameters are: $a = 1655.5$, $b = 0.51$. The averaged residuals range up to 2.9 ms. The results of the search match the results from Section 6.1.1.

6.1.3 Entire dataset with a and b fixed

For the entire dataset consisting of all one-thousand-six traveltimes, we calculate the value of χ with the values of $a = 1655$, $b = 0.5$, taken from Section 6.1.2, which are fixed. Herein, we examine the level of anisotropy for far offsets. The result of the inversion is presented in Figure 6.6.

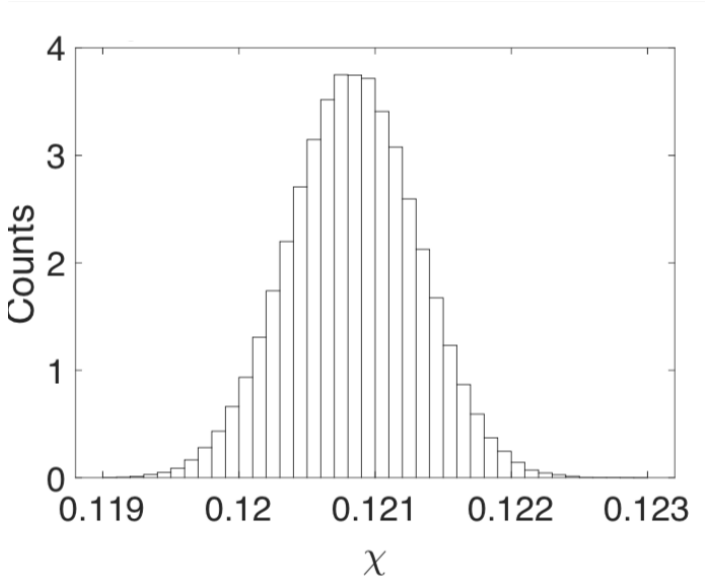

Figure 6.6: Distribution of parameter χ for all data for $a = 1655$ and $b = 0.5$. The values on the vertical axis are multiplied by 10^4.

The value of $\chi = 0.121$, while the averaged residuals are up to 6.8 ms. Larger residuals indicate the fact that values of a and b are fixed and taken from the near–offset data. In this case, the resultant value of χ suggests a high level of anisotropy in the entire medium.

The study conducted on the data that consists of only the traveltimes obtained from the incident angle lower than 10° ensure the inability of finding the level of anisotropy as the rays are vertical and nearly parallel to each other. χ represents the difference in horizontal and vertical velocities. If we possess information only from vertical rays that carry any information about vertical velocity, the horizontal velocity is missing, and as a consequence χ is unconstrained. We notice that for the case of near and far offsets, the histograms do not contain the case of $\chi = 0$, which indicated the anisotropy of the medium. By analogous argument, the case of $b = 0$ is also rejected. In other words, the algorithm never accepts the case of the medium being homogeneous or isotropic.

6.2 fminsearch

In this section, we calculate linear inhomogeneity parameters for the case of low-incident angles with the assumption of isotropy for the whole medium. Consequently, with the values of a and b fixed from previous calculation, we obtain the level of anisotropy from the entire dataset.

6.2.1 Single-medium case

For the case with low-incident angle and without the assumption of isotropy we obtain a very low level of anisotropy. The resultant value of χ is different with a new run. As shown in Section 6.1.1, we cannot infer the elliptical anisotropy from vertical rays. Therefore, we proceed with the calculation directly with the assumption of isotropy.

6.2.1.1.0 Low-incident angle and isotropic case

Herein, for the purpose of the inversion, we consider only part of the dataset, namely, the traveltimes obtained from the rays that reach the receiver with 10° incident angle. We consider the isotropic medium, where $\chi = 0$ and calculate a and b. The least misfit between the calculated and measured traveltimes is presented in Table 6.1.

Results
$a_1 = 1658.08$
$b_1 = 0.4988$
$\chi_1 = 0$

Table 6.1: a and b for a single-medium model—low-incident angle and isotropic case.

The average residuals are up to 0.34 ms and the value of standard deviation is 0.23 ms. Figure 6.7a shows the residuals and Figure 6.7b presents the histogram with value of each difference between measured and calculated traveltime.

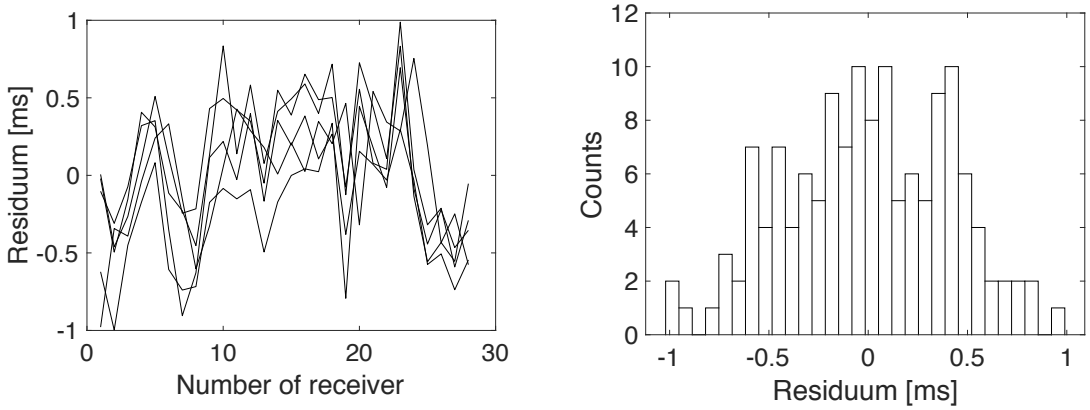

(a) Residuals **(b)** Histogram of residuals

Figure 6.7: Difference in traveltimes for each source and receiver.

6.2.1.2.0 Determining anisotropy

We fix the values of $a = 1658$ and $b = 0.5$ from Section 6.2.1.1 and calculate χ for the whole dataset. $\chi = 0.1178$ gives the least misfit between the measured and modelled traveltimes. The average residuals are up to 7.5 ms and the standard deviation is 4.9 ms. Figure 6.8a shows the value of difference between the calculated and measured traveltimes and Figure 6.8b presents the histogram of the residuals.

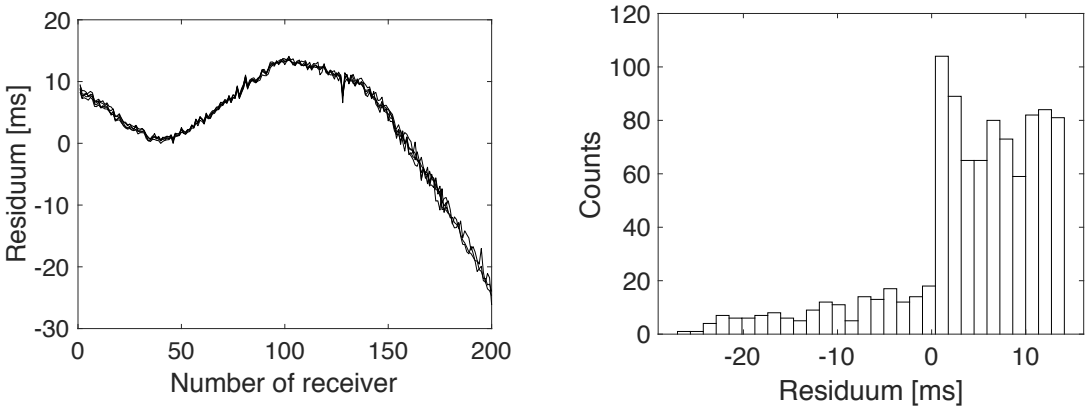

(a) Residuals

(b) Histogram of residuals

Figure 6.8: Difference in traveltimes for each source and receiver.

The high residuals indicate the fact that the values of a and b are from the different medium of the offset around 350 m. From the plots that show residuals, we notice that the further the receiver, the higher the misfit between the traveltimes. We conclude that the values obtained from the search are more applicable for near offset rather than far offsets.

6.2.2 Two-layer case

6.2.2.1.0 Low-incident angle and isotropic case

Herein, we divide a medium into two layers. The depth of the boundary is 1000 m. The dataset consists of the traveltimes of the rays that are nearly parallel to each other. The calculation is based on one-hundred and forty traveltimes, twenty-eight from each receiver. We achieve four parameters, a and b for each of the two isotropic ($\chi = 0$) layers. The results of the inverse are in Table 6.2.

Startup values	Results
$a_1 = 1100$	$a_1 = 1420.82$
$b_1 = 1$	$b_1 = 0.7651$
$\chi_1 = 0$	
$a_2 = 2400$	$a_2 = 2591.71$
$b_2 = 0.5$	$b_2 = 0.0604$
$\chi_2 = 0$	

Table 6.2: a and b for each of the two isotropic layers with startup values—low-incident angle.

The average residuals are up to 0.3 ms and the standard deviation is 0.3 ms. Figure 6.9a shows the difference between calculated and measured traveltimes and Figure 6.9b presents the histogram of the residuals.

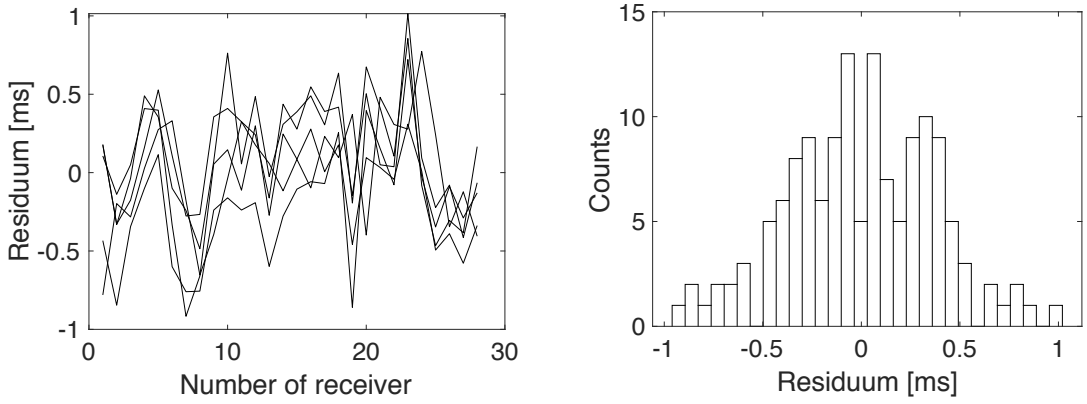

(a) Residuals

(b) Histogram of residuals

Figure 6.9: Difference in traveltimes for each source and receiver.

The results depend on startup values. Low residuals show that the introduction of two more parameters allows to obtain a better fit to the traveltimes. Nevertheless, we obtain an unstable problem with unreliable results.

6.2.2.2.0 Determining anisotropy

We fix the values of a and b from Section 6.2.2.1 and determine the level of anisotropy for the entire dataset. The results are presented in Table 6.3.

Startup values	Results
$a_1 = 1421$	
$b_1 = 0.77$	
$\chi_1 = 0.01$	$\chi_1 = 1 \times 10^{-9}$
$a_2 = 2592$	
$b_2 = 0.06$	
$\chi_2 = 0.01$	$\chi_2 = 0.1248$

Table 6.3: χ for each layer with startup values. a and b are fixed from Section 6.2.2.1

The average residuals are up to 3.8 ms and the standard deviation is 3.7 ms. Figure 6.10a shows the residuals and Figure 6.10b presents the histogram with the values of each difference between measured and calculated traveltime.

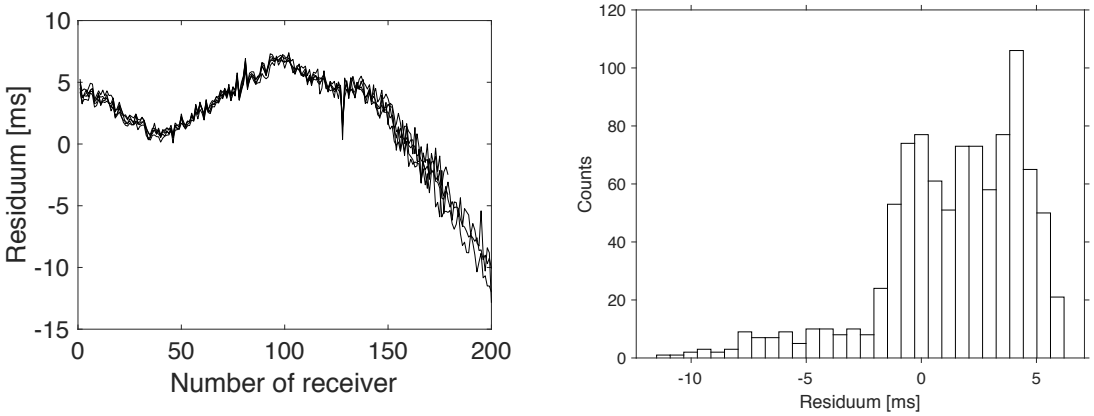

(a) Residuals

(b) Histogram of residuals

Figure 6.10: Difference in traveltimes for each source and receiver.

6.2.3 Three-layer case

6.2.3.1.0 Low-incident angle and isotropic case

We divide the medium into three isotropic layers. The boundaries of layers are the following: 500 m and 1000 m. Herein, we consider only the rays that travel from the source to the receiver with less than 10° incident angle. The calculation is based on one-hundred and forty traveltimes from five receivers. The results are shown in Table 6.4.

Startup values	Results
$a_1 = 1400$	$a_1 = 1390.47$
$b_1 = 0.8$	$b_1 = 0.0343$
$\chi_1 = 0$	
$a_2 = 1800$	$a_2 = 2296.54$
$b_2 = 0.6$	$b_2 = 0.4679$
$\chi_2 = 0$	
$a_3 = 2200$	$a_3 = 2618.16$
$b_3 = 0.4$	$b_3 = 0.0296$
$\chi_3 = 0$	

Table 6.4: a and b for each layer with startup values—low-incident angle and isotropic case.

The average residuals are up to 0.28 ms and the value of standard deviation is 0.36 ms. Figure 6.11a shows the residuals for each traveltime and Figure 6.11b presents the histogram of residuals.

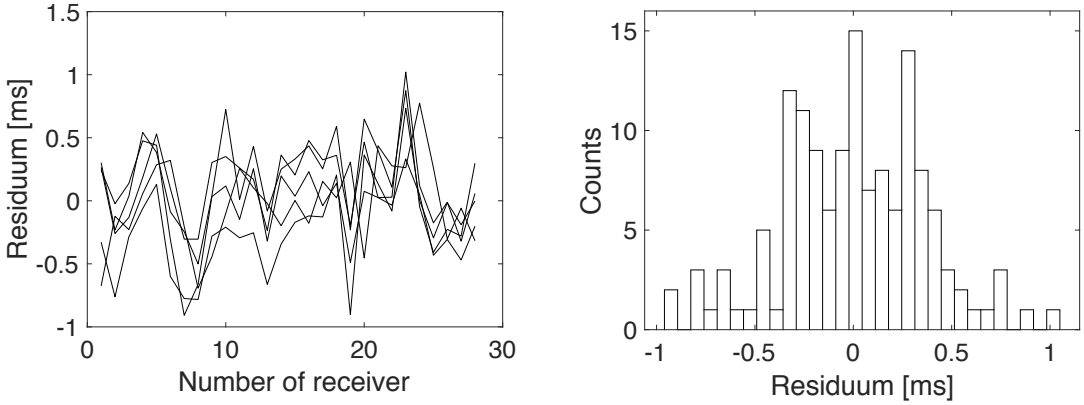

(a) Residuals **(b)** Histogram of residuals

Figure 6.11: Difference in traveltimes for each source and receiver.

6.2.3.2.0 Determining anisotropy

For the entire dataset consisting of all nine-hundred and eight traveltimes, we determine the anisotropy. We fix the values of a and b from Section 6.2.3.1 and calculate only χ for each layer from the entire dataset. The results are presented in Table 6.5.

Startup values	Results
$a_1 = 1390$	
$b_1 = 0.03$	
$\chi_1 = 0.01$	$\chi_1 = 1 \times 10^{-10}$
$a_2 = 2297$	
$b_2 = 0.47$	
$\chi_2 = 0.01$	$\chi_2 = 0.186$
$a_3 = 2618$	
$b_3 = 0.03$	
$\chi_3 = 0.01$	$\chi_3 = 1 \times 10^{-10}$

Table 6.5: The values of χ for each layer with startup values. a and b are fixed from Section 6.2.3.1

The average residuals are up to 3.1 ms and the value of standard deviation is 3.6 ms. Figure 6.12a shows the residuals for each traveltime and Figure 6.12b shows the histogram with the value of each difference between measured and calculated traveltime. The results suggest the isotropy of the first and the third layer.

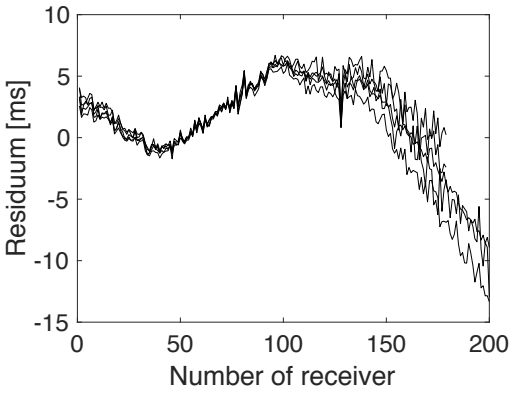

(a) Residuals

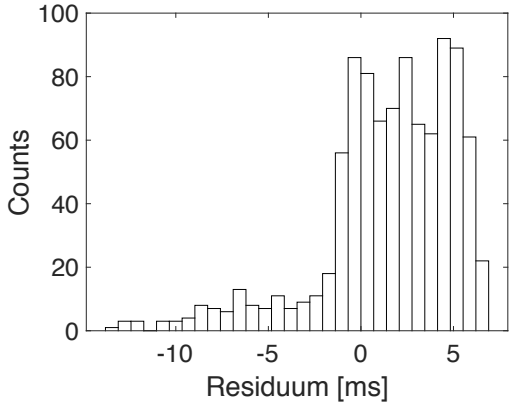

(b) Histogram of residuals

Figure 6.12: Difference in traveltimes for each source and receiver.

6.3 Comparison of two methods

Herein, in Table 6.6, we compare the results of the search for the case with 10° of the incident angle in isotropic medium.

Metropolis-Hastings	*fminsearch*
$a = 1658$	$a = 1655$
$b = 0.5$	$b = 0.5$

Table 6.6: The comparison of a, b in the isotropic case for low incident angle using two different methods.

The results are also in agreement with one another.

Moreover, in Table 6.7, we compare the results of the search of the level of anisotropy for the entire dataset. The values of χ are not significantly different. The little difference is caused by the slightly different values of a and b being fixed for both methods. If the values of a and b are the same for both calculations, the results are consistent with one another.

Metropolis-Hastings	*fminsearch*
$\chi = 0.121$	$\chi = 0.118$

Table 6.7: The comparison of χ for the entire dataset with a and b fixed, using two different methods.

Chapter 7

Change of traveltimes with respect to each parameter

To examine the reliability of a, b, and χ, we show the change of the traveltime with respect to the change of each parameter.

Figure 7.1 presents the traveltimes calculated for a single medium with $a \in [1000, 3000]$, $b = 0.6$, and $\chi = 0.01$. Figure 7.2 presents the traveltimes calculated for $a = 2000$, $b \in [0, 1]$, and $\chi = 0.01$. Figure 7.3 presents the traveltimes calculated for $a = 2000$, $b = 0.6$, and $\chi \in [0, 0.5]$. The depth of the receiver is 2500m and the offset is 3000m.

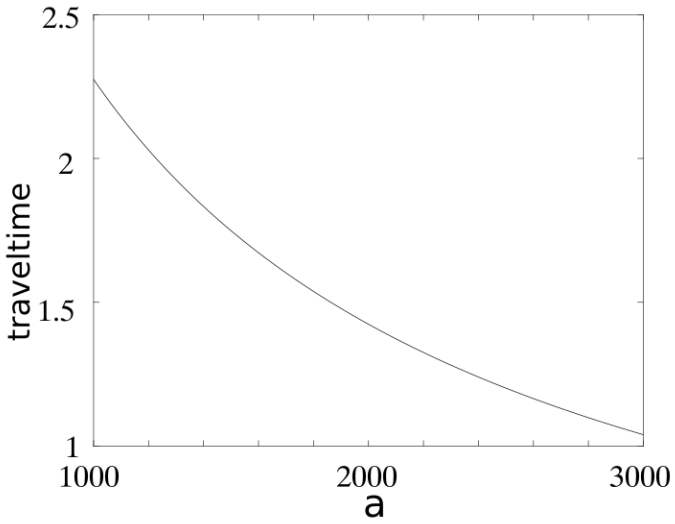

Figure 7.1: Traveltime with respect to parameter a

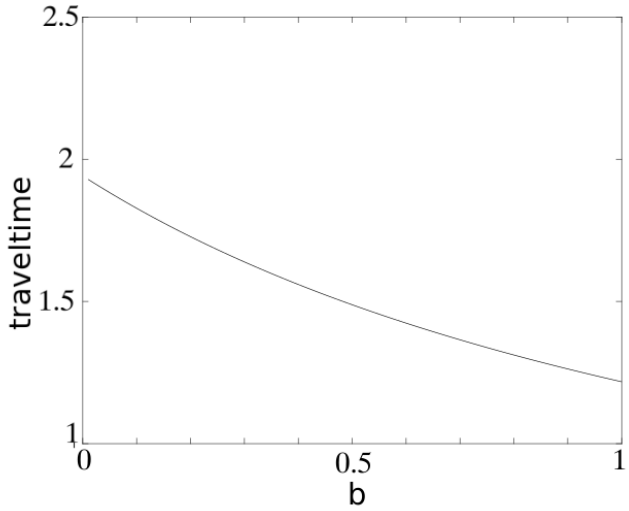

Figure 7.2: Traveltime with respect to parameter b

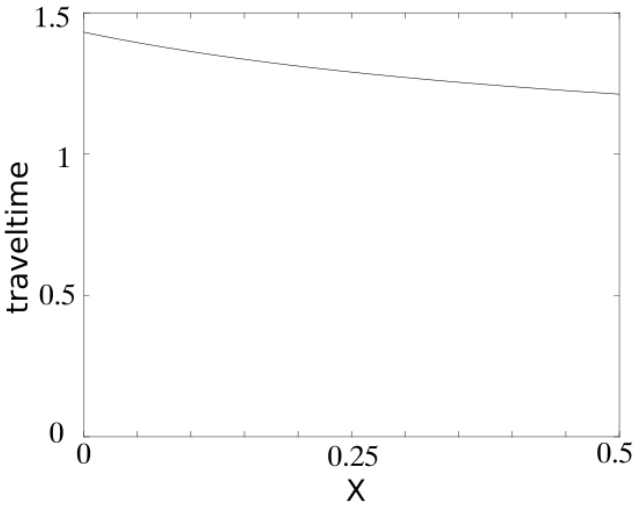

Figure 7.3: Traveltime with respect to parameter χ

The plots indicate how the change of a parameter affects the traveltime, *ceteris paribus*. We conclude that the change of a affects the traveltime most. The change of χ has weak impact on traveltime. This means that small perturbations in traveltime change significantly the value of χ. The resultant values of χ can vary and still fit the traveltime with low residuals. We cannot infer physical properties from χ and gain information about the anisotropy from the optimization, but the introduction of this parameter into the model enables us to fit the curve of traveltime more accurately.

To examine the change of each parameter with respect to the offset, we evaluate partial derivative of traveltime from expression (2.2) and (2.4) with respect to each parameter,

$$\frac{\partial t}{\partial a}\Big|_{a,b,\chi,Z,X}, \qquad \frac{\partial t}{\partial b}\Big|_{a,b,\chi,Z,X}, \qquad \frac{\partial t}{\partial \chi}\Big|_{a,b,\chi,Z,X}.$$

To present the numerical example of derivations, we choose the typical values for the parameters and the constant depth. We calculate the equations numerically for such parameters where $a = 2000$, $b = 0.6$, $\chi = 0.01$, and $Z = 2500$. Figure 7.4 shows the values of derivatives for each parameter with respect to offset.

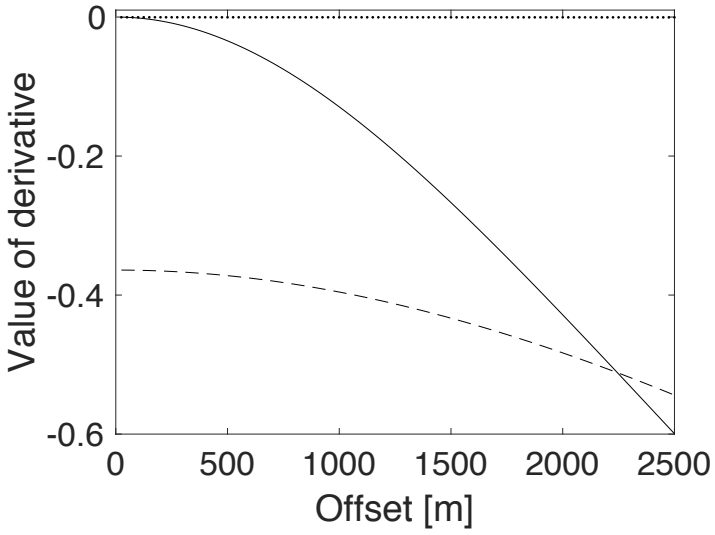

Figure 7.4: The values of partial derivatives for each parameter; dotted line represents parameter a, dashed line parameter b, solid line parameter χ.

The derivatives of expressions (2.2) and (2.4) give the same results. We conclude that χ is the most sensitive to a change of startup values as the slope of the function is the largest with increasing depth. Since χ changes the most, it is the least reliable. The value of the partial derivative of traveltime with respect to a does not change rapidly with the change of the startup values.

We show that as the values of χ change significantly, giving the same low residuals, we do not infer the level of anisotropy from this model. However, the introduction of this parameter enables to obtain the better fit the traveltime from the measurements; a and b are more reliable than χ and do not change rapidly with the change of traveltime. Also, a small perturbation in traveltime changes a value of χ most significantly. If we aim to find the information about lithology, we only consider the level of inhomogeneity.

Chapter 8

Change of depth of boundary

Herein, we consider three cases of two-layer media with different depth of the boundary between the layers. To investigate the cases above, we choose the same set of starting values for the first layer. For the calculations, we use the *fminseach* method. Each second layer, however, has different startup values. Specifically, the initial values of a differ, while initial values of b and χ remain the same. The results are shown in Table 8.1.

As the value of a changes with depth, to compare them we need to calculate the parameter for the common depths. We project the value of a from each case to the surface. For the depth of 800. m, we get $a = 2911.81$. For the depth of 1000 m, we get $a = 2948.67$. For the depth of 1200 m, we get $a = 2686.06$.

In varying the interface depth, it is better to compare parameter b, than a, since the latter corresponds to the value at the interface, which changes. In Figures 8.1—8.3, we present the linear increase of velocity with depth for each of three cases. As parameter b is the vertical gradient, in the plot, we notice that the slope of the parts that correspond to the second layer are different.

Depth at 800 m		Depth at 1000 m		Depth at 1200 m	
Startup values	Results	Startup values	Results	Startup values	Results
$a_1 = 1100$	$a_1 = 1330.89$	$a_1 = 1100$	$a_1 = 942.05$	$a_1 = 1100$	$a_1 = 911.77$
$b_1 = 1$	$b_1 = 0.3972$	$b_1 = 1$	$b_1 = 1.6224$	$b_1 = 1$	$b_1 = 1.7364$
$\chi_1 = 0.01$	$\chi_1 = 0.0114$	$\chi_1 = 0.01$	$\chi_1 = 0.0008$	$\chi_1 = 0.01$	$\chi_1 = 0.0014$
$a_2 = 2000$	$a_2 = 2935.89$	$a_2 = 2200$	$a_2 = 3015.97$	$a_2 = 2600$	$a_2 = 2977.54$
$b_2 = 0.5$	$b_2 = 0.0301$	$b_2 = 0.5$	$b_2 = 0.0673$	$b_2 = 0.5$	$b_2 = 0.2429$
$\chi_2 = 0.01$	$\chi_2 = 0.0231$	$\chi_2 = 0.01$	$\chi_2 = 0.0039$	$\chi_2 = 0.01$	$\chi_2 = 0.0072$
Average residuals	0.9 ms	Average residuals	0.8 ms	Average residuals	0.9 ms
Standard deviation	0.9 ms	Standard deviation	1 ms	Standard deviation	1.2 ms

Table 8.1: a, b, and χ for each layer with different depths and with startup values.

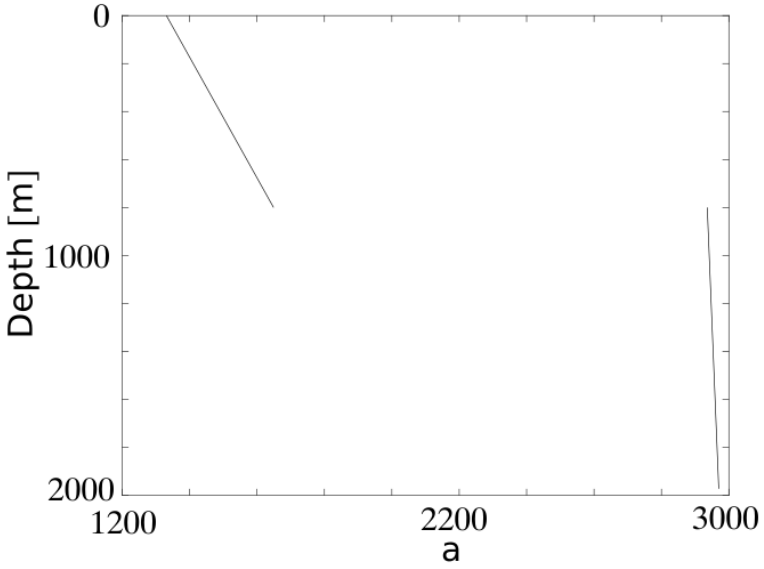

Figure 8.1: The linear increase of velocity with depth, the depth of the layer is 800 m

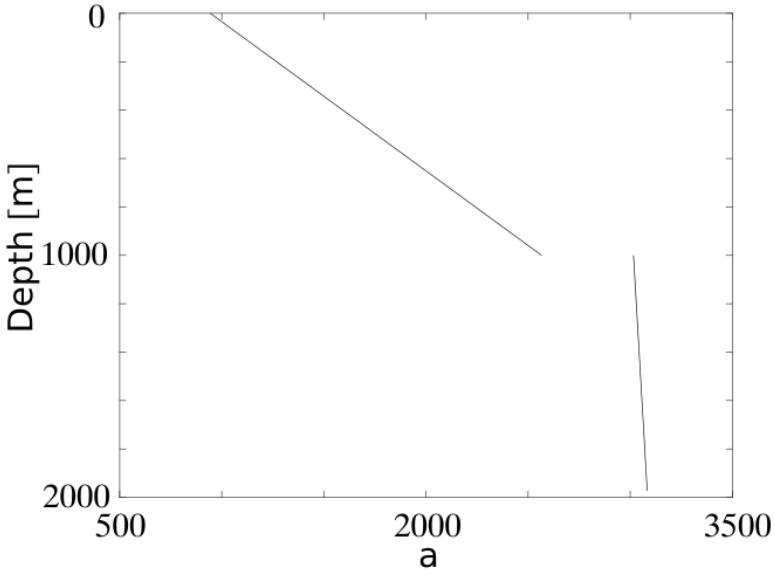

Figure 8.2: The linear increase of velocity with depth, the depth of the layer is 1000 m

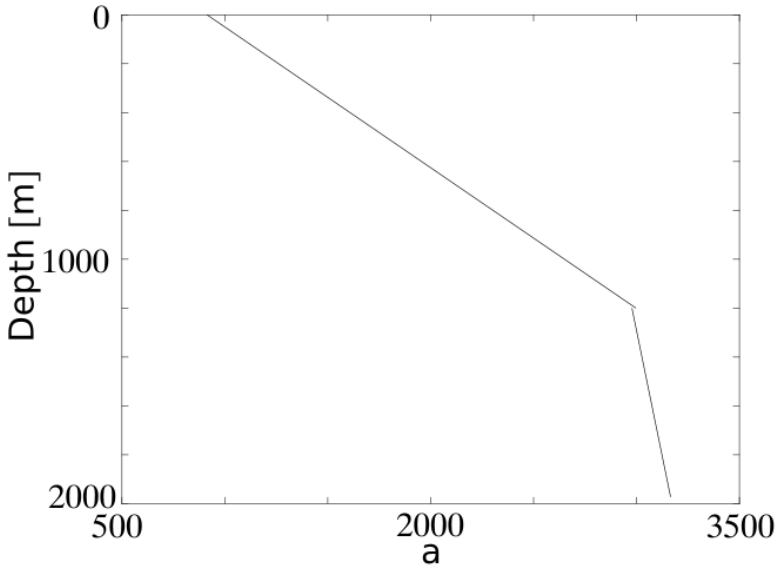

Figure 8.3: The linear increase of velocity with depth, the depth of the layer is 1200 m

The projected values of a to the common surface differ from each other, because the resultant values of b, which is the velocity gradient, are not consistent with one another. The change of the depth of the layer for the inversion affects the results significantly.

Chapter 9

Linear elasticity

[2] In this section, we introduce the notion of the elasticity tensor. We use the components of the aforementioned tensor in Chapters 10-13. Specifically, we consider the isotropic and transversely isotropic elasticity tensors. They are necessary for the development of Chapters 10 and 11. Further, we invoke the physical restrictions imposed on these tensors. The restrictions are essential for Chapters 12 and 13, respectively.

The forces applied to a single point are, in the theory of linear elasticity, expressed in terms of a stress tensor and their resultant deformations in terms of a strain tensor. The strain tensor for infinitesimal displacements in three dimensions, by the definition, is

$$\varepsilon_{ij} := \frac{1}{2}\left(\frac{\partial u_i}{\partial x_j} + \frac{\partial u_j}{\partial x_i}\right) \qquad i,j = 1,2,3\,, \tag{9.1}$$

where, subscripts i and j, denote Cartesian coordinates, and u_i are the components of the displacement vector describing the deformations in the i-th direction. The Hooke's

[2] Chapters 9-10 are the modified versions of the work with Theodore Stanoev (Kudela and Stanoev, 2018)

law provides the constitutive equation that relates stresses and strains, namely,

$$\sigma_{ij} = \sum_{k=1}^{3} \sum_{\ell=1}^{3} c_{ijk\ell} \varepsilon_{k\ell} \qquad i, j = 1, 2, 3\,, \tag{9.2}$$

which states that the applied load at a point is linearly related to the deformation by elasticity tensor, $c_{ijk\ell}$. Equation (9.2) is the fundamental equation of linear elasticity; solids that obey this equation are called Hookean solids. The Hooke's law for the general anisotropy in matrix notation is

$$\begin{bmatrix} \sigma_{11} \\ \sigma_{22} \\ \sigma_{33} \\ \sigma_{23} \\ \sigma_{13} \\ \sigma_{12} \end{bmatrix} = \begin{bmatrix} c_{1111} & c_{1122} & c_{1133} & c_{1123} & c_{1113} & c_{1112} \\ c_{2211} & c_{2222} & c_{2233} & c_{2223} & c_{2213} & c_{2212} \\ c_{3311} & c_{3322} & c_{3333} & c_{3323} & c_{3313} & c_{3312} \\ c_{2311} & c_{2322} & c_{2333} & c_{2323} & c_{2313} & c_{2312} \\ c_{1311} & c_{1322} & c_{1333} & c_{1323} & c_{1313} & c_{1312} \\ c_{1211} & c_{1222} & c_{1233} & c_{1223} & c_{1213} & c_{1212} \end{bmatrix} \begin{bmatrix} \varepsilon_{11} \\ \varepsilon_{22} \\ \varepsilon_{33} \\ 2\varepsilon_{23} \\ 2\varepsilon_{13} \\ 2\varepsilon_{12} \end{bmatrix}.$$

The elasticity tensor for general anisotropy contains 36 different components.

For an isotropic medium, Hooke's law may be rewritten conveniently in a matrix notation as

$$\begin{bmatrix} \sigma_{11} \\ \sigma_{22} \\ \sigma_{33} \\ \sigma_{23} \\ \sigma_{13} \\ \sigma_{12} \end{bmatrix} = \begin{bmatrix} c_{1111} & c_{1111} - 2c_{2323} & c_{1111} - 2c_{2323} & 0 & 0 & 0 \\ c_{1111} - 2c_{2323} & c_{1111} & c_{1111} - 2c_{2323} & 0 & 0 & 0 \\ c_{1111} - 2c_{2323} & c_{1111} - 2c_{2323} & c_{1111} & 0 & 0 & 0 \\ 0 & 0 & 0 & c_{2323} & 0 & 0 \\ 0 & 0 & 0 & 0 & c_{2323} & 0 \\ 0 & 0 & 0 & 0 & 0 & c_{2323} \end{bmatrix} \begin{bmatrix} \varepsilon_{11} \\ \varepsilon_{22} \\ \varepsilon_{33} \\ 2\varepsilon_{23} \\ 2\varepsilon_{13} \\ 2\varepsilon_{12} \end{bmatrix},$$

which also may be expressed in terms of Lamé parameters

$$\begin{cases} \lambda := c_{1111} - 2c_{2323} \\ \mu := c_{2323} \end{cases}.$$

In isotropy the elasticity tensor contains only two independent components, c_{1111} and c_{2323}.

Herein, we consider the TI medium—a medium composed of parallel isotropic layers, whose rotation symmetry axis coincides with x_3-axis, that is normal to a plane of isotropy. The plane of each layer is the plane of isotropy, and the vertical axis is the axis of symmetry. This transverse plane has infinite planes of symmetry, and thus, within this plane, the material properties are the same in all directions. Transverse isotropy is observed in sedimentary rocks, for example, shales or schists. Each layer has the same properties in-plane, but properties through the thickness are different. The components of the TI tensor remain unchanged with the rotation about any angle along the symmetry axis. The TI tensor may be expressed in a matrix form using Kelvin's notation as

$$C^{\mathrm{TI}} = \begin{bmatrix} c_{1111} & c_{1122} & c_{1133} & 0 & 0 & 0 \\ c_{1122} & c_{1111} & c_{1133} & 0 & 0 & 0 \\ c_{1133} & c_{1133} & c_{3333} & 0 & 0 & 0 \\ 0 & 0 & 0 & 2c_{2323} & 0 & 0 \\ 0 & 0 & 0 & 0 & 2c_{2323} & 0 \\ 0 & 0 & 0 & 0 & 0 & 2c_{1212} \end{bmatrix}, \tag{9.3}$$

where $c_{1122} = c_{1111} - 2c_{1212}$. The TI tensor contains five independent components.

9.1 Stability conditions—Isotropic case

Fundamental physical restrictions imposed on a elasticity tensor are the stability conditions. They express the fact that it is necessary to expend energy to deform a material (e.g. Slawinski, 2015, Section 4.3). These conditions mean that every elasticity tensor must be positive-definite, wherein a tensor is positive-definite if and only if all eigenvalues of its symmetric-matrix representation are positive. For any isotropic elasticity tensor, the inequalities

$$c_{1111} \geq \tfrac{4}{3}\, c_{2323} \geq 0 \ ,$$

or, in a different notation, using Lamé parameters,

$$\lambda \geq -\tfrac{2}{3}\,\mu \qquad \text{and} \qquad \mu \geq 0$$

ensure that all eigenvalues are positive, thus the stability conditions are satisfied.

9.2 Stability conditions—Transversely isotropic case

[3] Herein, we consider the transversely isotropic elasticity tensor and aim to find the stability conditions for all components. The elasticity tensor from expression (9.3) has five independent parameters. Its eigenvalues are

$$\lambda_1 = \lambda_2 = 2c_{1212}\,, \qquad \lambda_3 = \lambda_4 = 2c_{2323}\,,$$

[3]Section 9.2 and Chapter 13 are based on the work with Filip Adamus (Adamus and Kudela, 2019).

$$\lambda_5 = \frac{1}{2}\left(2c_{1111} - 2c_{1212} + c_{3333} + \sqrt{(2c_{1111} - 2c_{1212} - c_{3333})^2 + 8(c_{1133})^2}\right),$$

$$\lambda_6 = \frac{1}{2}\left(2c_{1111} - 2c_{1212} + c_{3333} - \sqrt{(2c_{1111} - 2c_{1212} - c_{3333})^2 + 8(c_{1133})^2}\right).$$

To satisfy the stability conditions the eigenvalues must be positive, after algebraic manipulation, we obtain

$$\begin{gathered} c_{1212} > 0\,, \quad c_{2323} > 0\,, \quad c_{3333} > 0\,, \quad c_{1111} - c_{1212} > 0\,, \\ (c_{1111} - c_{1212})\, c_{3333} > (c_{1133})^2\,, \end{gathered} \tag{9.4}$$

which are the fundamental constraints imposed on a TI tensor.

9.2.1 Common considerations

Let us consider the speeds of qP, quasi-transverse (SV), and transverse (SH) waves in a TI medium in both vertical (vrt) and horizontal (hor) directions of propagation.

$$V_{qP}(\text{vrt}) = \sqrt{\frac{c_{3333}}{\rho}}\,, \qquad V_{SV}(\text{vrt}) = \sqrt{\frac{c_{2323}}{\rho}}\,, \qquad V_{SH}(\text{vrt}) = \sqrt{\frac{c_{2323}}{\rho}}\,,$$

$$V_{qP}(\text{hor}) = \sqrt{\frac{c_{1111}}{\rho}}\,, \qquad V_{SV}(\text{hor}) = \sqrt{\frac{c_{2323}}{\rho}}\,, \qquad V_{SH}(\text{hor}) = \sqrt{\frac{c_{1212}}{\rho}}\,,$$

where ρ denotes density. Commonly, seismic waves propagate faster in the horizontal direction than vertical one. Thus, we may introduce two constraints,

$$c_{1111} > c_{3333} \qquad \text{and} \qquad c_{1212} > c_{2323}\,, \tag{9.5}$$

which come from the speeds of qP and SH waves, respectively. Another assumption we can make is that qP wave propagates faster than SV or SH wave, if they propagate

in the horizontal or in the vertical direction. Hence, we obtain

$$c_{3333} > c_{2323}\,, \qquad c_{1111} > c_{2323}\,, \qquad \text{and} \qquad c_{1111} > c_{1212}\,. \tag{9.6}$$

We notice that the last constraint, coming from the assumption that $V_{qP}(\text{hor}) > V_{SH}(\text{hor})$, is included in the stability conditions from expression (9.4).

Some of the constraints from both expressions (9.5) and (9.6) are related to each other. To show this, let us use the relation $c_{1122} = c_{1111} - 2c_{1212}$, and rewrite the last inequality of expression (9.6), $c_{1111} > c_{1212}$, as,

$$c_{1122} + c_{1212} > 0\,. \tag{9.7}$$

Then, we rewrite middle inequality of expression (9.6), $c_{1111} > c_{2323}$, as,

$$c_{1122} + c_{1212} + c_{1212} > c_{2323}\,,$$

and from inequality (9.7), we see that the sum of the first two terms on the left-hand side is a positive quantity and two other terms represent the last inequality of expression (9.5). In other words, a constraint $c_{1111} > c_{2323} \Leftrightarrow |a| + c_{1212} > c_{2323}$, is obvious from constraint $c_{1212} > c_{2323}$.

To summarize, apart from fundamental constraints, we may add three independent and commonly considered assumptions, namely,

$$c_{1111} - c_{3333} > 0\,, \qquad c_{1212} - c_{2323} > 0\,, \qquad \text{and} \qquad c_{3333} - c_{2323} > 0\,. \tag{9.8}$$

Chapter 10

Backus average

As shown by Backus (1962), a medium composed of parallel isotropic layers, whose individual thicknesses are much smaller than the wavelength, respond—to the wave propagation—as a single, homogeneous, transversely isotropic medium.

The elasticity parameters of such a medium are

$$c_{1111}^{\overline{\mathrm{TI}}} = \overline{\left(\frac{\lambda}{\lambda+2\mu}\right)^2}\,\overline{\left(\frac{1}{\lambda+2\mu}\right)}^{-1} + \overline{\left(\frac{4(\lambda+\mu)\mu}{\lambda+2\mu}\right)}, \tag{10.1}$$

$$c_{1122}^{\overline{\mathrm{TI}}} = \overline{\left(\frac{\lambda}{\lambda+2\mu}\right)^2}\,\overline{\left(\frac{1}{\lambda+2\mu}\right)}^{-1} + \overline{\left(\frac{2\lambda\mu}{\lambda+2\mu}\right)}, \tag{10.2}$$

$$c_{1133}^{\overline{\mathrm{TI}}} = \overline{\left(\frac{\lambda}{\lambda+2\mu}\right)}\,\overline{\left(\frac{1}{\lambda+2\mu}\right)}^{-1}, \tag{10.3}$$

$$c_{3333}^{\overline{\mathrm{TI}}} = \overline{\left(\frac{1}{\lambda+2\mu}\right)}^{-1}, \tag{10.4}$$

$$c_{2323}^{\overline{\mathrm{TI}}} = \overline{\left(\frac{1}{\mu}\right)}^{-1}, \tag{10.5}$$

$$c_{1212}^{\overline{\mathrm{TI}}} = \overline{\mu}\,, \tag{10.6}$$

where $\lambda := c_{1111} - 2c_{2323}$ and $\mu := c_{2323}$ are the Lamé parameters for each layer and the overbar denotes the weighted average. The average is weighted by the layer thickness; herein, since all layers have the same thickness, we use an arithmetic average. A TI medium, whose rotation symmetry axis is parallel to the x_3-axis, is

$$c^{\overline{\mathrm{TI}}} = \begin{bmatrix} c_{1111}^{\overline{\mathrm{TI}}} & c_{1122}^{\overline{\mathrm{TI}}} & c_{1133}^{\overline{\mathrm{TI}}} & 0 & 0 & 0 \\ c_{1122}^{\overline{\mathrm{TI}}} & c_{1111}^{\overline{\mathrm{TI}}} & c_{1133}^{\overline{\mathrm{TI}}} & 0 & 0 & 0 \\ c_{1133}^{\overline{\mathrm{TI}}} & c_{1133}^{\overline{\mathrm{TI}}} & c_{3333}^{\overline{\mathrm{TI}}} & 0 & 0 & 0 \\ 0 & 0 & 0 & c_{2323}^{\overline{\mathrm{TI}}} & 0 & 0 \\ 0 & 0 & 0 & 0 & c_{2323}^{\overline{\mathrm{TI}}} & 0 \\ 0 & 0 & 0 & 0 & 0 & c_{1212}^{\overline{\mathrm{TI}}} \end{bmatrix}, \tag{10.7}$$

where $c_{1122}^{\overline{\mathrm{TI}}} = c_{1111}^{\overline{\mathrm{TI}}} - 2c_{1212}^{\overline{\mathrm{TI}}}$. Consequently, expressions (10.1)–(10.6) consist of five independent parameters.

10.1 Product approximation

Let us consider the product approximation of Backus (1962), which states that

> [t]he only approximation that [he makes] in the present paper is the following: if $f(x_3)$ is nearly constant when x_3 changes by no more than ℓ', while $g(x_3)$ may vary by a large fraction of this distance, then, approximately,
>
> $$\overline{f\,g} \approx \overline{f}\;\overline{g}\,. \tag{10.8}$$

Using the formulation of Bos et al. (2017b), which states that

> the difference between the average of the product and the product of the averages is
>
> $$E\,(f\,,\,g) := \overline{f\,g} - \overline{f}\;\overline{g}\,, \tag{10.9}$$
>
> where, for any vector $\overline{x} \in \mathbb{R}^n$, [they] set
>
> $$\overline{x} := \sum_{k=1}^{n} w_k\,x_k$$

with w as a weight and x as any vector.

The relative error is

$$R\,(f\,,\,g) = \frac{E\,(f\,,\,g)}{\overline{f\,g}} \times 100\%\,. \tag{10.10}$$

It follows that if $\overline{g} = 0$ then $R\,(f\,,\,g) = 100\%$. To examine the consequences of $\overline{g} = 0$, in the context of layers composed of isotropic Hookean solids, expressions for f and g may be obtained from the isotropic stress-strain relations (Bos et al., 2017b, Section 3.6). f corresponds to lateral-strain-tensor components that are assumed to

be nearly constant, whereas

$$g = \frac{c_{1111} - 2\,c_{2323}}{c_{1111}} \tag{10.11}$$

corresponds to elasticity parameters that rapidly vary from layer to layer (Slawinski, 2018) .

By applying the stability conditions from Section 9.1 to expression (10.11), we deduce that g is positive when $c_{1111} > 2\,c_{2323}$ and that g is negative when $\frac{4}{3}c_{2323} < c_{1111} < 2\,c_{2323}$; the range of g is illustrated in Figure 10.1.

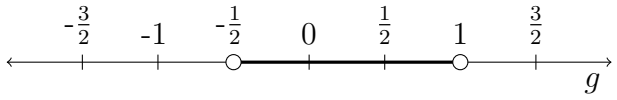

Figure 10.1: The value of g approaches a maximum of 1 when c_{2323} is at a minimum. Conversely, the value of g approaches a minimum of $-\frac{1}{2}$ when c_{2323} is at a maximum; thus, $g \in \left(-\frac{1}{2}\,,\,1\right)$.

Since g can be either negative or positive, and the elasticity parameters—by the stability conditions—are continuous and positive, we conclude that it is possible for g to equal zero.

Considering Slawinski (2018, Exercise 5.13), we might obtain Poisson's ratio in terms of the Lamé parameters,

$$\nu = \frac{\lambda}{2\,(\lambda + \mu)}\,, \tag{10.12}$$

which is the desired expression. Alternatively, we might obtain expression (10.12) by using the relations among Poisson's ratio, Young's modulus and the Lamé parameters (see e.g. Slawinski, 2015, Remark 5.14.7).

For a two-dimensional case, expression (10.12) becomes

$$\nu = \frac{\lambda}{\lambda + 2\,\mu}\,, \tag{10.13}$$

which is equivalent to expression (10.11). Notably, the properties of a transversely isotropic medium are captured by two-dimensional model that contains the rotation-symmetry axis. Expression (10.13) might be useful considering the fact that the Backus average produces a homogeneous transversely isotropic medium that is long-wave equivalent to a stack of thin isotropic layers.

The range of possible values of ν in expression (10.12) are determined by the stability conditions, which are determined from the eigenvalues of the positive-definite elasticity tensor used therein. Thus, the stability conditions for isotropy, in terms of λ and μ, are

$$\lambda > -\frac{2}{3}\mu \quad \text{and} \quad \mu > 0\,. \tag{10.14}$$

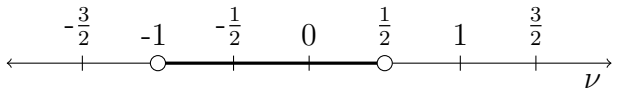

Figure 10.2: The value of ν approaches a maximum of $\frac{1}{2}$ when μ is at a minimum. Conversely, the value of ν approaches a minimum of -1 when μ is at a maximum; thus, $\nu \in \left(-1\,,\,\frac{1}{2}\right)$.

Considering the ranges of values of expressions (10.11) and (10.12), we reckon that if

(a) $g > 0$ then $\nu > 0$,

(b) $g = 0$ then $\nu = 0$,

(c) $g < 0$ then $\nu < 0$.

For naturally occurring solids, $\nu > 0$; the ratio being positive means that the diminishing of a cylinder's length is being accompanied by the extension of its radius (e.g. Slawinski, 2015, p. 203). Hence, the range illustrated in Figure 10.2 reduces to $\nu \in \left(0\,,\,\frac{1}{2}\right)$.

10.2 Preliminary Reference Earth Model

To gain insight into whether or not we might encounter $\overline{g} = 0$, let us consider a seismological example.

The Preliminary Reference Earth Model (PREM) of Dziewoński and Anderson (1981) is a one-dimensional model that presents the properties of the Earth as a function of depth. The PREM is a mathematical analogy that serves as a background model for the planet as a whole; it assumes spherical symmetry in order to subdivide the interior of the Earth into nine principal regions. This model establishes Earth-specific properties that include density, ρ, and P- and S-wave speeds, which are

$$v_P = \sqrt{\frac{\lambda + 2\,\mu}{\rho}} \quad \text{and} \quad v_S = \sqrt{\frac{\mu}{\rho}}\,. \tag{10.15}$$

These nine principal regions are distinguished from one another by a rapid change in speeds of P- and S-waves along interfaces, which indicates a diverse range of elastic properties within the medium. The speeds of the irrotational and equivoluminal waves are functions of the different elasticity parameters and, hence, propagate at different speeds within the model.

Let us consider data from Bormann (2012, Table 1), which lists 84 samples of—among other parameters—v_P, v_S, and ρ as functions of depth ranging from 0 km to 6371 km for an isotropic PREM. In view of the relationship between Lamé and elasticity parameters, we may compute

$$c_{1111} = \rho\, v_P^2 \quad \text{and} \quad c_{2323} = \rho\, v_S^2 \tag{10.16}$$

for each of the 84 samples. Using expressions (10.16), we plot the values of expression (10.11) as a function of depth in Figure 10.3. Therein, the resultant points of discontinuity arise from the rapid change in speed of P- and S-waves across the interfaces of the principal regions.

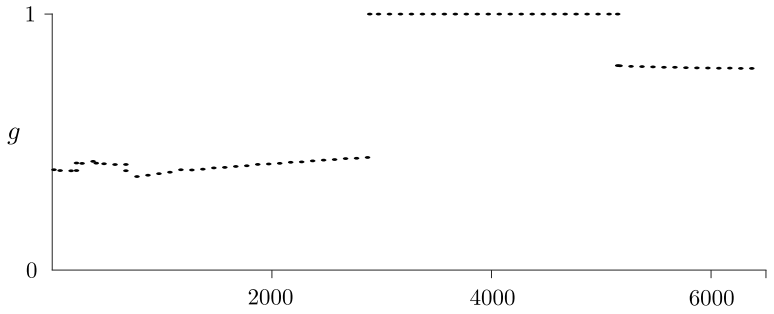

Figure 10.3: g as a function of depth (km)

For samples between 2891 km and 5150 km, $v_S = 0$. Recalling that S-waves do not propagate in liquids, as their resistance to change of shape vanishes (see e.g. Slawinski, 2015, p. 217), we interpret this range of samples to correspond to the outer core. Since the S-wave speed equals zero, $c_{2323} = 0$; consequently, expression (10.11) equals 1.

From Figure 10.3, we observe that $g > 0$ throughout and, thus, deduce that $\overline{g}$ cannot equal zero. Therefore, following the conclusions of Section 10.1, our results support that $g > 0$ for naturally occurring solids within an isotropic PREM. Hence, we may conclude that it is improbable for the relative error of the Backus average approximation to equal 100% for such a model.

Chapter 11

Relation between anisotropy and inhomogeneity

An analytical relation of inhomogeneity and anisotropy parameters is shown in Adamus et al. (2018) for an isotropic medium. Sayed and Stanoev (2019) derive an analytical relation between anisotropy parameter, $\chi_{\overline{\mathrm{TI}},b}$, of the Backus model, and linear inhomogeneity parameter, b, of the $ab\chi$ model for many layers. Further, we assume that our $ab\chi$ model is for isotropic layers and, hence, we recall P- and S-wave velocities:

$$v_P = a_P + b_P Z \quad \text{and} \quad v_S = a_S + b_S Z.$$

Anisotropy of the Backus medium, where

$$v_h = \sqrt{c^{\overline{\mathrm{TI}}}_{1111}} \quad \text{and} \quad v_v = \sqrt{c^{\overline{\mathrm{TI}}}_{3333}}\,,$$

is:

$$\chi_{\overline{\mathrm{TI}},b} := \frac{c^{\overline{\mathrm{TI}}}_{1111} - c^{\overline{\mathrm{TI}}}_{3333}}{2\, c^{\overline{\mathrm{TI}}}_{3333}}.$$

The expressions of following elasticity parameters in terms of increasing velocity and anisotropy are presented by Sayed and Stanoev (2019), namely,

$$\begin{aligned} c^{\overline{\mathrm{TI}}}_{3333} &= \overline{\left(\frac{1}{c_{1111}}\right)}^{-1} = \overline{\left(\frac{1}{v_P^2}\right)}^{-1} \\ &= (a_P + b_P\, h_1)\,(a_P + b_P\, h_2) \end{aligned} \tag{11.1}$$

and

$$\begin{aligned} c^{\overline{\mathrm{TI}}}_{1111} &= \overline{\left(\frac{c_{1111} - 2\, c_{2323}}{c_{1111}}\right)^2}\ \overline{\left(\frac{1}{c_{1111}}\right)}^{-1} + \overline{\left(\frac{4\,(c_{1111} - c_{2323})\, c_{2323}}{c_{1111}}\right)} \\ &= \left(1 - \frac{2\, I_1}{h_2 - h_1}\right)^2 c^{\overline{\mathrm{TI}}}_{3333} + \frac{4\, I_2}{h_2 - h_1} - \frac{4\, I_3}{h_2 - h_1}\,, \end{aligned} \tag{11.2}$$

where

$$\begin{aligned} I_1 = {} & \frac{h_2\, {b_S}^2}{{b_P}^2} - \frac{h_1\, {b_S}^2}{{b_P}^2} \\ & + \frac{\ln\left(a_P + h_1\, b_P\right)\left(2\, a_P\, {b_S}^2 - 2\, a_S\, b_P\, b_S\right)}{{b_P}^3} - \frac{\ln\left(a_P + h_2\, b_P\right)\left(2\, a_P\, {b_S}^2 - 2\, a_S\, b_P\, b_S\right)}{{b_P}^3} \\ & + \frac{{a_P}^2\, {b_S}^2 - 2\, a_P\, a_S\, b_P\, b_S + {a_S}^2\, {b_P}^2}{b_P\left(h_1\, {b_P}^3 + a_p\, {b_P}^2\right)} - \frac{{a_P}^2\, {b_S}^2 - 2\, a_P\, a_S\, b_P\, b_S + {a_S}^2\, {b_P}^2}{b_P\left(h_2\, {b_P}^3 + a_P\, {b_P}^2\right)}\,, \end{aligned}$$

$$I_2 = -\frac{{h_1}^3\, {b_S}^2}{3} - {h_1}^2\, a_S\, b_S - h_1\, {a_S}^2 + \frac{{h_2}^3\, {b_S}^2}{3} + {h_2}^2\, a_S\, b_S + h_2\, {a_S}^2\,,$$

$$
\begin{aligned}
I_3 = {} & h_2 \left(\frac{2\,a_P \left(\frac{2\,a_P\,{b_S}^4}{{b_P}^3} - \frac{4\,a_S\,{b_S}^3}{{b_P}^2} \right)}{b_P} - \frac{{a_P}^2\,{b_S}^4}{{b_P}^4} + \frac{6\,{a_S}^2\,{b_S}^2}{{b_P}^2} \right) \\
& - h_1 \left(\frac{2\,a_P \left(\frac{2\,a_P\,{b_S}^4}{{b_P}^3} - \frac{4\,a_S\,{b_S}^3}{{b_P}^2} \right)}{b_P} - \frac{{a_P}^2\,{b_S}^4}{{b_P}^4} + \frac{6\,{a_S}^2\,{b_S}^2}{{b_P}^2} \right) \\
& + {h_1}^2 \left(\frac{a_P\,{b_S}^4}{{b_P}^3} - \frac{2\,a_S\,{b_S}^3}{{b_P}^2} \right) - {h_2}^2 \left(\frac{a_P\,{b_S}^4}{{b_P}^3} - \frac{2\,a_S\,{b_S}^3}{{b_P}^2} \right) \\
& + \frac{\ln\left(a_P + h_1\,b_P\right) \left(4\,{a_P}^3\,{b_S}^4 - 12\,{a_P}^2\,a_S\,b_P\,{b_S}^3 + 12\,a_P\,{a_S}^2\,{b_P}^2\,{b_S}^2 - 4\,{a_S}^3\,{b_P}^3\,b_S \right)}{{b_P}^5} \\
& - \frac{\ln\left(a_P + h_2\,b_P\right) \left(4\,{a_P}^3\,{b_S}^4 - 12\,{a_P}^2\,a_S\,b_P\,{b_S}^3 + 12\,a_P\,{a_S}^2\,{b_P}^2\,{b_S}^2 - 4\,{a_S}^3\,{b_P}^3\,b_S \right)}{{b_P}^5} \\
& - \frac{{h_1}^3\,{b_S}^4}{3\,{b_P}^2} + \frac{{h_2}^3\,{b_S}^4}{3\,{b_P}^2} \\
& + \frac{{a_P}^4\,{b_S}^4 - 4\,{a_P}^3\,a_S\,b_P\,{b_S}^3 + 6\,{a_P}^2\,{a_S}^2\,{b_P}^2\,{b_S}^2 - 4\,a_P\,{a_S}^3\,{b_P}^3\,b_S + {a_S}^4\,{b_P}^4}{b_P \left(h_1\,{b_P}^5 + a_P\,{b_P}^4 \right)} \\
& - \frac{{a_P}^4\,{b_S}^4 - 4\,{a_P}^3\,a_S\,b_P\,{b_S}^3 + 6\,{a_P}^2\,{a_S}^2\,{b_P}^2\,{b_S}^2 - 4\,a_P\,{a_S}^3\,{b_P}^3\,b_S + {a_S}^4\,{b_P}^4}{b_P \left(h_2\,{b_P}^5 + a_P\,{b_P}^4 \right)}\,.
\end{aligned}
$$

We assume that with increasing depth, the measure of inhomogeneity changes equally for P- and S-waves, i.e.,

$$b_P = b_S = b.$$

As the values of a and b that are calculated in Section 5.4 are obtained from the least traveltime, we consider them as the values of a_P and b_P, respectively.

To calculate the values of $c^{\overline{\mathrm{TI}}}_{1111}$ and $c^{\overline{\mathrm{TI}}}_{3333}$, we assume that the level of anisotropy, from the $ab\chi$ model and $\chi_{\overline{\mathrm{TI}},b}$ are equal. As $c^{\overline{\mathrm{TI}}}_{3333}$ depends only on v_P, from the fact that $\chi_{\overline{\mathrm{TI}},b}$ is known, we calculate the value of $c^{\overline{\mathrm{TI}}}_{1111}$. Generally, parameter a is the representation of the velocity on the surface. Herein, we aim to find the parameter a_S to examine the ratio of $\frac{a_P}{a_S}$. From seismological properties, the ratio of P- and

S-velocities is approximately $\sqrt{3}$. With the assumptions that we made, we expect the value of a_S as $\sqrt{3}$ times smaller than the values of a_P.

For all calculation, we use the values from Section 5.4 for a single medium, where $a_P = 1343$, $b = 0.9$, and $\chi_{ab\chi} = 0.06$; $h_1 = 0\,\mathrm{m}$, $h_2 = 2013\,\mathrm{m}$.

With the assumptions of equal level of inhomogeneity and anisotropy for P- and S-waves, we simplify the equations (11.1)-(11.2), namely,

$$c_{3333}^{\overline{\mathrm{TI}}} = a_P\,(a_P + b\,h_2) \tag{11.3}$$

and

$$c_{1111}^{\overline{\mathrm{TI}}} = \left(1 - \frac{2\,I_1}{h_2}\right)^2 c_{3333}^{\overline{\mathrm{TI}}} + \frac{4\,I_2 - 4\,I_3}{h_2} - , \tag{11.4}$$

where

$$I_1 = h_2 + \frac{2\ln(a_P)\,(a_P - a_S)}{b} - \frac{2\ln(a_P + h_2\,b)\,(a_P - a_S)}{b} + \frac{(a_P - a_S)^2}{b\,a_P} - \frac{(a_P - a_S)^2}{b\,(h_2\,b + a_P)}\,,$$

$$I_2 = \frac{{h_2}^3\,b^2}{3} + {h_2}^2\,a_S\,b + h_2\,{a_S}^2\,,$$

$$I_3 = h_2\left(3a_P^2 - 8a_S\,a_P + 6a_S^2\right) - h_2^2\,(a_P\,b - 2\,a_S\,b) + \frac{4\ln(a_P)\,(a_P - a_S)^3}{b} - \frac{4\ln(a_P + h_2\,b)\,(a_P - a_S)^3}{b} + \frac{{h_2}^3\,b^2}{3} + \frac{(a_P - a_S)^4}{b\,a_P} - \frac{(a_P - a_S)^4}{b\,(h_2\,b + a_P)}\,.$$

As we assume that $\chi_{\overline{\mathrm{TI}},b} = \chi_{ab\chi} = 0.06$, we obtain $c_{1111}^{\overline{\mathrm{TI}}} = 4.74$ and $c_{3333}^{\overline{\mathrm{TI}}} = 4.23$. After

the calculations, we achieve $a_S = 1051$. The ratio:

$$\frac{a_P}{a_S} = \frac{1343}{1051} = 1.2781 < \sqrt{3}\,. \tag{11.5}$$

The value of the ratio from expression (11.5) is smaller than $\sqrt{3}$ which means that the assumptions that we made about anisotropy and inhomogeneity are not necessarily relevant. $\chi_{\overline{\mathrm{TI}},b}$ and $\chi_{ab\chi}$ represent a different medium and it is possible for the values to vary. Also, the values of b_P and b_S are not equivalent. Nevertheless, with such postulates, we can determine the values of two TI elasticity parameters and constrain the other three in the subsequent section.

Chapter 12

Constraints on field data

Mostly, we are not able to have all five parameters to describe the properties of the medium using TI tensor. We put fundamental constraints on the elastic parameters to estimate their values.

In Chapter 11 we obtain the values of $c_{1111} = 4.74\,[\text{GPa}]$ and $c_{3333} = 4.23\,[\text{GPa}]$, where GPa is gigapascal. We wish to find the constraints on the three parameters of a transversely isotropic elasticity tensor. With the stability conditions and common constraints from Section 9.2, we calculate the range of the values of the parameters. Firstly, we calculate the eigenvalues of the TI tensor which are:

$$\lambda_1 = \lambda_2 = 2c_{1212}\,, \qquad \lambda_3 = \lambda_4 = 2c_{2323}\,,$$

$$\lambda_5 = 6.85 - c_{1212} + \frac{1}{2}\sqrt{(2c_{1212} - 5.25)^2 + 8(c_{1133})^2}\,,$$

$$\lambda_6 = 6.85 - c_{1212} - \frac{1}{2}\sqrt{(2c_{1212} - 5.25)^2 + 8(c_{1133})^2}\,,$$

and its corresponding fundamental constraints from expression (9.4) are

$$0 < c_{1212} < 4.74\,, \qquad c_{2323} > 0\,, \qquad c_{1212} < 4.74 - \frac{(c_{1133})^2}{4.23}\,,$$

where $c_{1133} \in (-4.48\,,\, 4.48)$. Imposing the common constraints from expression (9.8), we obtain

$$c_{2323} < 4.23\,, \qquad \text{and} \qquad c_{1212} - c_{2323} > 0\,.$$

The effect of imposing the common constraints, as an additional restriction to the fundamental one, is illustrated in Figures 12.1a and 12.1b.

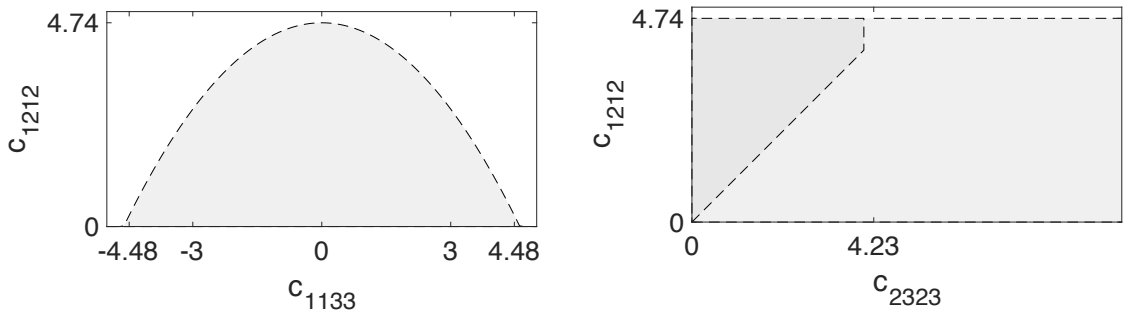

(a) no influence of common constraints **(b)** common constraints restrict the area

Figure 12.1: The area of all possible values of unknown elasticity parameters restricted by the fundamental constraints is shown by the light grey colour. The dark grey area is the intersection of both restricted areas that come from the common and from the fundamental constraints.

Chapter 13

Numerical examples with Green-river shale elasticity parameters

In this section, we study the fundamental and common constraints—shown in Section 9.2—imposed on four examples of a TI medium. In the first case, we examine a TI tensor with the known values of c_{1111} and c_{3333}. In the second case, the values of c_{2323} and c_{3333} are known, in the third, the values of c_{1111}, c_{2323}, and c_{1212}, and in the last one, the values of $c_{1111}, c_{3333}, c_{2323}$, and c_{1212}. The values of the elasticity parameters are based on the Green-river shale, as shown by Thomsen (1986) and exemplified by Slawinski (2015, Exercise 9.3). The values are following:

$$c_{1111} = 3.13\,[\text{GPa}],$$

$$c_{1133} = 0.34\,[\text{GPa}],$$

$$c_{3333} = 2.25\,[\text{GPa}],$$

$$c_{2323} = 0.65\,[\text{GPa}],$$

$$c_{1212} = 0.88\,[\text{GPa}].$$

From Section 10.1, we know that the condition of $c_{1111} \neq c_{2323}$ must be conserved, where the values from the Green-river shale obey the restriction.

13.1 TI tensor based on qP-wave information

Let us consider a TI tensor with given two elasticity parameters, $c_{1111} = 31.3\,[\text{GPa}]$ and $c_{3333} = 22.5\,[\text{GPa}]$. This case may be relevant to the studies of a TI medium based on qP-wave information. Its eigenvalues are

$$\lambda_1 = \lambda_2 = 2c_{1212}\,, \qquad \lambda_3 = \lambda_4 = 2c_{2323}\,,$$

$$\lambda_5 = 42.55 - c_{1212} + \frac{1}{2}\sqrt{(2c_{1212} - 40.1)^2 + 8(c_{1133})^2}\,,$$
$$\lambda_6 = 42.55 - c_{1212} - \frac{1}{2}\sqrt{(2c_{1212} - 40.1)^2 + 8(c_{1133})^2}\,,$$

and its corresponding fundamental constraints from expression (9.4) are

$$0 < c_{1212} < 31.3\,, \qquad c_{2323} > 0\,, \qquad 22.5 > 0\,, \qquad c_{1212} < 31.3 - \frac{(c_{1133})^2}{22.5}\,,$$

where $c_{1133} \in (-26.54\,,\, 26.54)$. Imposing the common constraints from expression (9.8), we obtain

$$8.8 > 0\,, \qquad c_{2323} < 22.5\,, \qquad \text{and} \qquad c_{1212} - c_{2323} > 0\,.$$

The effect of imposing the common constraints, as an additional restriction to the fundamental one, is illustrated in Figures 13.1a and 13.1b.

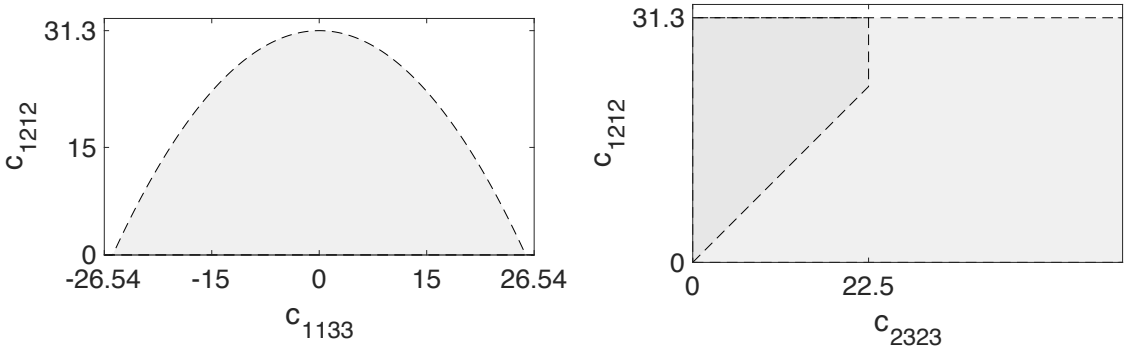

(a) no influence of common constraints

(b) common constraints restrict the area

Figure 13.1: The area of all possible values of unknown elasticity parameters restricted by the fundamental constraints is shown by the light grey colour. The dark grey area is the intersection of both restricted areas that come from the common and from the fundamental constraints.

The additional constraints significantly limit the possible values of the remaining three parameters.

13.2 TI tensor based on information along symmetry axis

Let us consider a TI tensor with given two elasticity parameters, $c_{2323} = 6.5\,[\text{GPa}]$ and $c_{3333} = 22.5\,[\text{GPa}]$. This case may be relevant to the studies of a TI medium based on measurements of qP and quasi-S waves along the symmetry axis. Its eigenvalues are

$$\lambda_1 = \lambda_2 = 13\,, \qquad \lambda_3 = \lambda_4 = 2c_{1212}\,,$$

$$\lambda_5 = c_{1111} - c_{1212} + 11.25 + \frac{1}{2}\sqrt{(2c_{1212} - 2c_{1111} + 22.5)^2 + 8(c_{1133})^2}$$

$$\lambda_6 = c_{1111} - c_{1212} + 11.25 - \frac{1}{2}\sqrt{(2c_{1212} - 2c_{1111} + 22.5)^2 + 8(c_{1133})^2}$$

and its corresponding fundamental constraints are

$$c_{1212} > 0\,, \qquad 6.5 > 0\,, \qquad 22.5 > 0\,, \qquad c_{1111} - c_{1212} > 0\,, \qquad (c_{1111} - c_{1212})22.5 > (c_{1133})^2\,.$$

Imposing the common constraints from expression (9.8), we obtain

$$c_{1111} > 22.5\,, \qquad 16 > 0\,, \qquad \text{and} \qquad c_{1212} > 6.5\,.$$

The effect of imposing the common constraints, as an additional restriction to the fundamental one, is illustrated in Figure 13.2.

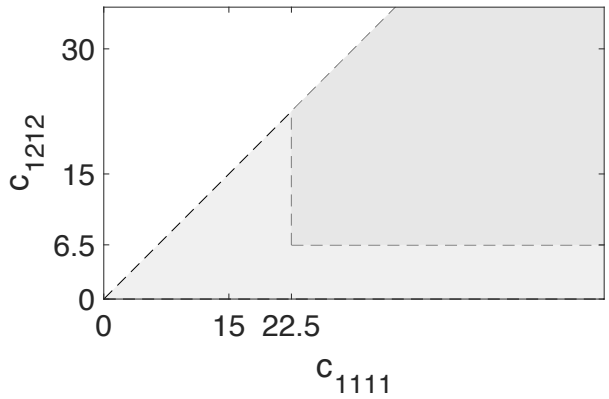

Figure 13.2: φ versus ϵ

13.3 TI tensor based on information along horizontal axis

Let us consider a TI tensor with given three elasticity parameters, $c_{1212} = 8.8\,[\text{GPa}]$, $c_{2323} = 6.5\,[\text{GPa}]$ and $c_{3333} = 22.5\,[\text{GPa}]$. This case may be relevant to the studies of a TI

medium based on measurements of qP, SV, and SH waves along the horizontal axis. Its eigenvalues are

$$\lambda_1 = \lambda_2 = 13\,, \qquad \lambda_3 = \lambda_4 = 17.6\,,$$

$$\lambda_5 = c_{1111} + 2.45 + \frac{1}{2}\sqrt{(40.1 - 2c_{1111})^2 + 8(c_{1133})^2}\,,$$

$$\lambda_6 = c_{1111} + 2.45 - \frac{1}{2}\sqrt{(40.1 - 2c_{1111})^2 + 8(c_{1133})^2}\,,$$

and its corresponding fundamental constraints are

$$8.8 > 0\,, \qquad 6.5 > 0\,, \qquad 22.5 > 0\,, \qquad c_{1111} > 8.8\,, \qquad (c_{1111} - 8.8)22.5 > (c_{1133})^2\,.$$

Imposing the common constraints from expression (9.8), we obtain

$$c_{1111} > 22.5\,, \qquad 16 > 0\,, \qquad \text{and} \qquad 2.3 > 0\,.$$

The effect of imposing the common constraints, as an additional restriction to the fundamental one, is illustrated in Figure 13.3.

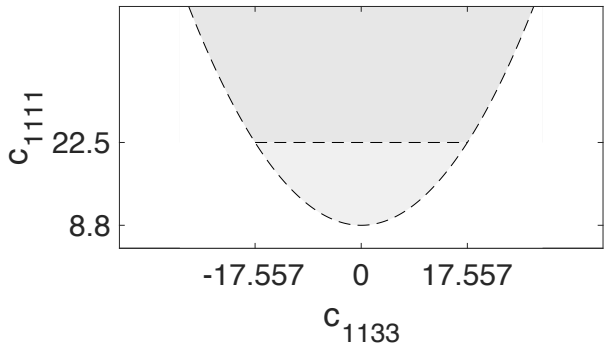

Figure 13.3: φ versus ϵ

13.4 TI tensor based on information along symmetry and horizontal axes

Let us consider a TI tensor with given four elasticity parameters, $c_{1212} = 8.8\,[\text{GPa}]$, $c_{2323} = 6.5\,[\text{GPa}]$, $c_{1111} = 31.3\,[\text{GPa}]$ and $c_{3333} = 22.5\,[\text{GPa}]$. This case may be relevant to the studies of a TI medium based on measurements of qP, SV, and SH waves along both the symmetry and horizontal axes. Its eigenvalues are

$$\lambda_1 = \lambda_2 = 13\,, \qquad \lambda_3 = \lambda_4 = 17.6\,,$$

$$\lambda_5 = 33.75 + \frac{1}{2}\sqrt{8(c_{1133})^2 + 506.25}\,,$$
$$\lambda_6 = 33.75 - \frac{1}{2}\sqrt{8(c_{1133})^2 + 506.25}\,,$$

and its corresponding fundamental constraints are

$$8.8 > 0\,, \qquad 6.5 > 0\,, \qquad 22.5 > 0\,, \qquad 22.5 > 0\,, \qquad 506.25 > (c_{1133})^2\,.$$

Imposing the common constraints from expression (9.8), we obtain

$$8.8 > 0\,, \qquad 16 > 0\,, \qquad \text{and} \qquad 2.3 > 0\,.$$

The common constraints do not additionally limit the possible values of c_{1133}. In this case, only the stability conditions are valuable.

In three out of four examples of a TI tensor, the common constraints limit the possible values of the unknown elasticity parameters of these tensors. That limitation occurs not to be entirely overlapping with the limitation caused by the fundamental

constraints, that is, by the stability conditions. Thus, the study of both the common and fundamental constraints is helpful, for example, in the prediction or estimation of the unknown parameters.

We notice that the fewer parameters of a TI tensor are known, the more useful the common constraints are.

The common constraints are the most useful if we know the values of c_{1111} and c_{3333}, than the values of c_{2323} and c_{3333}.

Chapter 14

Conclusions

Ray methods develop an essential theoretical platform for seismological investigations. They enable us to form problems by applying many mathematical tools. Nevertheless, given this being an approximate solution, we must be aware of its limitations.

By applying the assumption of linear inhomogeneity and elliptical anisotropy of the medium it results in the equations, thereby enabling us to achieve solutions with fewer unknowns.

Traveltimes from VSP surveys are essential for processing and velocity determination. The proposed two different methods of the inversion of traveltime with the velocity model of elliptical anisotropy and linear inhomogeneity, discussed in Chapter 2, allow us to obtain the required parameters.

We notice that in the Metropolis-Hastings method, the single-mode distributions of a, b, and χ allow us to infer that for a single medium, the local minimum is also the global minimum.

Section 5.3 presents the results from the *fminsearch* method. The method is error-laden because it numerically searches for the values that present the least-square

difference between the traveltimes. The minimization is local, which means that the results obtained after the optimization depend on the startup values. If the medium is divided into more layers, we obtain more unknowns in the target function. Since it is a mathematical curve fitting, the algorithm finds the best match, but the results do not necessarily represent the mechanical properties that describe the medium. We obtain unique results only in a single-medium model—however, a model of 2000 m depth with only three parameters is a significant generalization. For the two-, three-, and four-layer cases, we encounter the instability problem.

In Section 5.4, we confirm the accuracy of the results obtained from the Metropolis-Hastings algorithm by comparing them to the results acquired from the *fminsearch* method.

Furthermore, we examine Hookean solids that possess certain symmetries. The choice of the coordinate system of which axes coincide with the symmetry axes of materials is particularly useful. It allows us to represent these symmetries by an elasticity matrix in a simplified form having zero entries.

For thicknesses of individual layers that are much less than the wavelength, waves traveling through parallel isotropic layers behave as if they were traveling through a single transversely isotropic medium.

Backus average is a mathematical tool that allows us to obtain such transversely isotropic medium from parallel isotropic layers. In geological terms, the transversely isotropic medium may be a good analogy for thin sedimentary layers, unfractured shales or schists.

Let us emphasize that the analogy between the anisotropy and layers relies on the assumption that the thicknesses of parallel layers or the separations between parallel fractures are much smaller than the wavelength used for their examination.

We continue the work of Bos et al. (2017b) to investigate the sole mathematical approximation made by Backus (1962). The samples from Bormann (2012) result in $g > 0$, even if it is mathematically feasible to obtain a relative error of 100% for the Backus product approximation.

As the PREM describes the Earth at a regional scale, the potential issues with the approximation are unlikely to happen. However, it is possible to encounter such issues in the shallow-data acquisition, i.e., within the upper lithosphere. To verify the likeliness of the issue to occur, we require the wellbore data. Moreover, we suppose that the Backus average might encounter concerns when used on synthetic materials with, say, $\nu \approx 0$ or $\nu < 0$.

We use the derivation of an analytical relation between anisotropy parameter, $\chi_{\overline{\mathrm{TI}},b}$, of the Backus model, and linear inhomogeneity parameter, b, of the $ab\chi$ model for many layers by Sayed and Stanoev (2019). With the assumptions of the equal level of anisotropy from the $ab\chi$ model and $\chi_{\overline{\mathrm{TI}},b}$ and the same level of inhomogeneity from P- and S-waves, we obtain two elasticity parameters c_{1111} and c_{3333} and parameter a_S. Consequently, we find the more strict constraints on the other three elasticity parameters of the transversely isotropic tensor.

The concern with the common constraints investigated in this thesis is that, in some specific situations, they might be irrelevant to the actual behaviour of seismic waves. If it is not the case, it might be useful to impose the restrictions mentioned above along with the stability conditions to better estimate the unknown elasticity parameters of a TI tensor.

Bibliography

Adamus, F. and Kudela, I. (2019). On constraints imposed on a transversely isotropic elasticity tensor. *arXiv*, (arXiv:1904.01707v1 [physics.geo-ph]).

Adamus, F. P., Slawinski, M. A., and Stanoev, T. (2018). On effects of inhomogeneity on anisotropy in Backus average. *arXiv*, (arXiv:1802.04075v2 [physics.geo-ph]).

Backus, G. E. (1962). Long-wave elastic anisotropy produced by horizontal layering. *Journal of Geophysical Research*, 67(11):4427–4440.

Bona, A. and Slawinski, M. A. (2003). Fermat's principle for seismic rays in elastic media. *Journal of Applied Geophysics*, 54(3-4):445–451.

Bormann, P. (2012). *Global 1-D Earth models*, pages 1–11. New manual of seismological observatory practice 2 (NMSOP-2). Potsdam: Deutsches GeoForschungsZentrum GFZ.

Bos, L., Dalton, D. R., Slawinski, M. A., and Stanoev, T. (2017a). On Backus average for generally anisotropic layers. *J Elast*, 127(2):179–196.

Bos, L., Danek, T., Slawinski, M. A., and Stanoev, T. (2017b). Statistical and numerical considerations of Backus-average product approximation. *J Elast,* Advance online publication (doi:10.1007/s10659-017-9659-9).

Bos, L. P., Gibson, P. C., Kotchetov, M., and Slawinski, M. A. (2004). Classes of anisotropic media: a tutorial. *Studia geophysca and geodætica*, 48(1):265–287.

Danek, T. and Slawinski, M. A. (2012). Bayesian inversion of VSP traveltimes for linear inhomogeneity and elliptical anisotropy. *Geophysics*, 77(6):R239–R243.

Dziewoński, A. M. and Anderson, D. L. (1981). Preliminary Reference Earth Model. *Phys. Earth Planet. Inter.*, 25(4):297–356.

Epstein, M. and Slawinski, M. A. (1999). On raytracing in constant velocity–gradient media: Geometrical approach. *Canadian Journal of Exploration Geophysics*, 35(1/2):1–6.

Hastings, W. K. (1970). Monte Carlo sampling methods using Markov Chains and their applications. *Biometrika*, 57(1):97–109.

Helbig, K. (1994). *Foundations of anisotropy for exploration seismics*, volume 22. Pergamon, 1st edition.

Kaderali, A. (2009). Investigating anisotropy and inhomogeneity using tomographic inversion of VSP traveltimes: Validation of analytic expressions for linearly inhomogeneous elliptically anisotropic models. Master's thesis, Memorial University of Newfoundland.

Kaderali, A. and Kudela, I. (2019a). Inversion of traveltime for velocity parameters. (in preparation).

Kaderali, A. and Kudela, I. (2019b). On traveltime inverse in linearly inhomogeneous and elliptically anisotropic media. (in preparation).

Kudela, I. and Stanoev, T. (2018). On possible issues of Backus average. arXiv:1804.01917.

Lagarias, J. C., Reeds, J. A., Wright, M. H., and Wright, P. E. (1998). Convergence properties of the Nelder-Mead Simplex Method in low dimensions. *SIAM Journal of Optimization*, 9(1):112–147.

Mathews, J. H. and Frank, K. K. (2004). *Numerical methods using Matlab*. Pearson, 4th edition.

Metropolis, N. and Ulam, S. (1949). The Monte Carlo Method. *J. Am. Stat. Assoc.*, 44(247):335–341.

Postma, G. W. (1955). Wave propagation in a stratified medium. *Geophysics*, 20(4):780–806.

Raushan, Z. (2011). Metropolis-Hastings algorithms. Vienna University of Technology.

Rogister, Y. and Slawinski, M. A. (2005). Analytic solution of ray-tracing equations for a linearly inhomogeneous and elliptically anisotropic velocity model. *Geophysics*, 70(5):D37–D41.

Sayed, M. A. and Stanoev, T. (2019). Relation between anisotropy and inhomogeneity. arXiv:1906.10196.

Slawinski, M. A. (2015). *Waves and Rays in Elastic Continua*. World Scientific, 3rd edition.

Slawinski, M. A. (2018). *Waves and Rays in Seismology. Answers to Unasked Questions*. World Scientific, 3rd edition.

Slawinski, M. A., Wheaton, C. J., and Powojowski, M. (2004). VSP traveltime inversion for linear inhomogenity and elliptical anisotropy. *Geophysics*, 69(2):373–377.

Thomsen, L. (1986). Weak elastic aniostropy. *Geophysics*, 51(10):1954–1966.

Appendix A

Elliptical shape of wavefronts

To illustrate the kind of anisotropy that we use in this thesis in this section we explain the elliptical velocity in more details. The elliptical velocity dependence refers to the fact that the wavefronts generated by a point source are elliptical. In an elliptically anisotropic medium, if we change the direction of the propagation, the velocity varies in an elliptical fashion. In this section, we show the elliptical shape of the wavefront in the single medium using the values of a, b, and χ from Section 5.4.

We calculate v_v and v_h, which are the vertical and horizontal velocities, respectively,

$$v_v = a + bZ\,,$$

$$v_h = (a + bZ)\sqrt{2\chi + 1}\,.$$

In our velocity model, the wavefront velocity depends on the depth and the direction of propagation in a vertical plane but does not depend on the lateral location. The value of χ indicates the difference in the vertical and horizontal velocities. It is not

intuitive to try to conceptualize the anisotropy parameter χ with respect to the velocity anisotropy. However, χ can be used to calculate the percent difference between the horizontal and vertical ray velocities. The percent difference between the vertical and horizontal ray velocities can be expressed as:

$$\frac{v_h - v_v}{v_h} \times 100\% \,. \tag{A.1}$$

Using a numerical example to illustrate this, if χ is given a value of 0.0606 this implies that the difference between vertical and horizontal ray velocities 5.6%.

The resulting ellipses are shown in Figure A.1 are nearly circular because the anisotropy is weak. The velocities are the semi-axes of the ellipses.

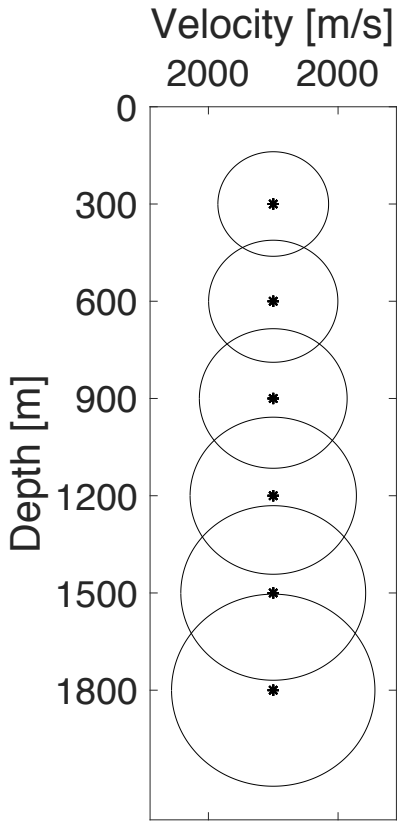

Figure A.1: Elliptical wavefronts in the interval of 300 m.

Appendix B

Example of code of Metropolis-Hastings algorithm

```
%% Data load
X1=xlsread('data','D10:D188');
X2=xlsread('data','I10:I188');
X3=xlsread('data','N10:N209');
X4=xlsread('data','S10:S209');
X5=xlsread('data','X10:X209'); %Offsets
Z1= 1973.923;
Z2= 1983.809;
Z3= 1993.699;
Z4= 2003.758;
Z5= 2013.927; % Depths of receivers
T1=0.001*xlsread('data','C10:C188');
T2=0.001*xlsread('data','H10:H188');
T3=0.001*xlsread('data','M10:M209');
```

```
15 T4=0.001*xlsread('data','R10:R209');
16 T5=0.001*xlsread('data','W10:W209'); % Traveltimes
17 T=[T1; T2 ; T3; T4; T5];
18 n=500000; % Number of iterations
19 k=0;
20 sigma =0.005; %Standard deviation
21
22 % Sample first accepted values
23 while 1
24 DATA=[randi([1000,2000]) , 0.001*randi([0,1500]) , 0.00001*
       randi([1000,5000]) ]; % Sample random nauber for each
       parameter
25 A=DATA(1,1);
26 B=DATA(1,2);
27 CHI=DATA(1,3);
28
29 time1= time_new(X1,Z1,A,B,CHI);
30 time2= time_new(X2,Z2,A,B,CHI);
31 time3= time_new(X3,Z3,A,B,CHI);
32 time4= time_new(X4,Z4,A,B,CHI);
33 time5= time_new(X5,Z5,A,B,CHI); % Calculate traveltime
34
35 time=[time1; time2 ;time3; time4; time5];
36
37 prob_prev=exp(-(norm((time-T)/sigma)).^2); %Compare
       traveltimes
```

```
38
39 if prob_prev>0 break; end
40 end
41
42 a(1)=DATA(1);
43 b(1)=DATA(2);
44 Chi(1)=DATA(3);
45
46 for i=2:n
47 DATA_next=[DATA(1)+10*randn, DATA(2)+0.01*randn, DATA(3)
       +0.001*randn]; % Sample next value for each parameter
48
49 A=DATA_next(1,1);
50 B=DATA_next(1,2);
51 CHI=DATA_next(1,3);
52
53 time1= time_new(X1,Z1,A,B,CHI);
54 time2= time_new(X2,Z2,A,B,CHI);
55 time3= time_new(X3,Z3,A,B,CHI);
56 time4= time_new(X4,Z4,A,B,CHI);
57 time5= time_new(X5,Z5,A,B,CHI);
58 time=[time1 ;time2 ;time3; time4 ; time5];
59
60 prob_next = exp(-(norm((time-T)/sigma)).^2);
61
62 %% Metropolis-Hastings condition
```

```
63              if rand < min(1,prob_next/prob_prev)
64                  k=k+1;
65                  a(i)=DATA_next(1);
66                  b(i)=DATA_next(2);
67                  Chi(i)=DATA_next(3);
68                  prob_prev = prob_next;
69                  DATA = DATA_next;
70              else
71 a(i)=a(i-1);
72 b(i)=b(i-1);
73 Chi(i)=Chi(i-1);
74              end
75
76 end
77 %% Display histograms
78
79          nbins=30;
80          cut=0.1*n;
81
82 histogram(a(cut:n),nbins),hold on
83 histogram(b(cut:n),nbins),hold on
84 histogram(Chi(cut:n),nbins),hold on

1
2
3
```

```
4  function time= time(X_source1,Z_rec,a1,b1,chi1)
5
6  p11=2.*(X_source1)./(sqrt(((X_source1).^2 + (1+2*chi1).*(
       Z_rec).^2).*((2*a1+b1.*(Z_rec)).^2.*(1+2*chi1)+b1.^2*(
       X_source1).^2)));
7
8  time=(1/b1).*(atanh(p11.*b1.*X_source1 - sqrt(1-(p11.^2 .*a1
       .^2 .* (1+2*chi1))))+atanh(sqrt(1-(p11.^2 .*a1.^2 .* (1+2*
       chi1)))));
9
10 end
```

Appendix C

Example of code of fminsearch algorithm for single medium

```
%% Data load
X1=xlsread('data','D10:D188');
X2=xlsread('data','I10:I188');
X3=xlsread('data','N10:N209');
X4=xlsread('data','S10:S209');
X5=xlsread('data','X10:X209'); % Offsets
Z1= 1973.923;
Z2= 1983.809;
Z3= 1993.699;
Z4= 2003.758;
Z5= 2013.927; % Depths of the receivers
T1=0.001*xlsread('data','C10:C188');
T2=0.001*xlsread('data','H10:H188');
T3=0.001*xlsread('data','M10:M209');
```

```
15 T4=0.001*xlsread('data','R10:R209');
16 T5=0.001*xlsread('data','W10:W209'); % Traveltimes
17
18 %% Initial values
19 a_prop=1300;
20 b_prop=0.9;
21 chi_prop=0.1;
22
23 %% Proper minimization
24
25 x0 = [a_prop,b_prop, chi_prop];
26
27 fun1 = @(X)mini1(X1,X2,X3,X4,X5,Z1,Z2,Z3,Z4,Z5,...
28     X(1),X(2),X(3),T1,T2,T3,T4,T5); %Target function
29
30 y= fminsearch(fun1,x0); % Minimize the function
31
32
33 %% Results
34 a=y(1);
35 b=y(2);
36 chi=y(3);

1
```

```
function [error]= mini1(X_source1,X_source2,X_source3,
    X_source4,X_source5,Z_rec1,Z_rec2,Z_rec3,Z_rec4,Z_rec5,a1,
    b1,chi1,T1,T2,T3,T4,T5)


p11=2.*(X_source1)./(sqrt(((X_source1).^2 + (1+2*chi1).*(
    Z_rec1).^2).*((2*a1+b1.*(Z_rec1)).^2.*(1+2*chi1)+b1.^2*(
    X_source1).^2)));
time11=(1/b1).*(atanh(p11.*b1.*X_source1 - sqrt(1-(p11.^2 .*
    a1.^2 .* (1+2*chi1))))+atanh(sqrt(1-(p11.^2 .*a1.^2 .*
    (1+2*chi1)))));

p22=2.*(X_source2)./(sqrt(((X_source2).^2 + (1+2*chi1).*(
    Z_rec2).^2).*((2*a1+b1.*(Z_rec2)).^2.*(1+2*chi1)+b1.^2*(
    X_source2).^2)));
time22=(1/b1).*(atanh(p22.*b1.*X_source2 - sqrt(1-(p22.^2 .*
    a1.^2 .* (1+2*chi1))))+atanh(sqrt(1-(p22.^2 .*a1.^2 .*
    (1+2*chi1)))));

p33=2.*(X_source3)./(sqrt(((X_source3).^2 + (1+2*chi1).*(
    Z_rec3).^2).*((2*a1+b1.*(Z_rec3)).^2.*(1+2*chi1)+b1.^2*(
    X_source3).^2)));
time33=(1/b1).*(atanh(p33.*b1.*X_source3 - sqrt(1-(p33.^2 .*
    a1.^2 .* (1+2*chi1))))+atanh(sqrt(1-(p33.^2 .*a1.^2 .*
    (1+2*chi1)))));

```

```
14 p44=2.*(X_source4)./(sqrt(((X_source4).^2 + (1+2*chi1).*(
       Z_rec4).^2).*((2*a1+b1.*(Z_rec4)).^2.*(1+2*chi1)+b1.^2*(
       X_source4).^2)));
15 time44=(1/b1).*(atanh(p44.*b1.*X_source4 - sqrt(1-(p44.^2 .*
       a1.^2 .* (1+2*chi1))))+atanh(sqrt(1-(p44.^2 .*a1.^2 .*
       (1+2*chi1)))));
16
17 p55=2.*(X_source5)./(sqrt(((X_source5).^2 + (1+2*chi1).*(
       Z_rec5).^2).*((2*a1+b1.*(Z_rec5)).^2.*(1+2*chi1)+b1.^2*(
       X_source5).^2)));
18 time55=(1/b1).*(atanh(p55.*b1.*X_source5 - sqrt(1-(p55.^2 .*
       a1.^2 .* (1+2*chi1))))+atanh(sqrt(1-(p55.^2 .*a1.^2 .*
       (1+2*chi1)))));
19
20 error1=abs(time11-T1).^2;
21 error2=abs(time22-T2).^2;
22 error3=abs(time33-T3).^2;
23 error4=abs(time44-T4).^2;
24 error5=abs(time55-T5).^2;
25
26
27 error=sum(error1)+sum(error2)+sum(error3)+sum(error4)+sum(
       error5);
28
29 end
```

Appendix D

Example of code of fminsearch algorithm for two layers

```
close all; clear all; clc
%% Data
n=179;
m=200;
X1=xlsread('data','D10:D188');
X2=xlsread('data','I10:I188');
X3=xlsread('data','N10:N209');
X4=xlsread('data','S10:S209');
X5=xlsread('data','X10:X209'); % Offsets
Z1= 1973.923;
Z2= 1983.809;
Z3= 1993.699;
Z4= 2003.758;
Z5= 2013.927; % Depths of the receivers
```

```
15 T1=0.001*xlsread('data','C10:C188');
16 T2=0.001*xlsread('data','H10:H188');
17 T3=0.001*xlsread('data','M10:M209');
18 T4=0.001*xlsread('data','R10:R209');
19 T5=0.001*xlsread('data','W10:W209'); % Traveltimes
20 Z_layer1=1000; % Depth of the layer
21 %% Initial values
22
23 a_prop1=1100;
24 b_prop1=1;
25 chi_prop1=0.01;
26
27 a_prop2=2400;
28 b_prop2=0.5;
29 chi_prop2=0.01;
30
31 %% Fermat's Principle ---- Finding the point where the ray
       crosses the boundary
32 tt=0.6;
33 LB = [0];
34 for i=1:n
35 fun = @(X)fermat2(X(1),X1(i),Z1,Z_layer1,a_prop1,b_prop1,
       chi_prop1,a_prop2,b_prop2,chi_prop2);
36 x0 = [X1(i)*tt];
37 UB = [X1(i)];
38 x1(:,i) = fminsearchbnd(fun,x0,LB,UB);
```

```
39 end
40 X_cross1=x1';
41 for i=1:n
42 fun = @(X)fermat2(X(1),X2(i),Z2,Z_layer1,a_prop1,b_prop1,
       chi_prop1,a_prop2,b_prop2,chi_prop2);
43 x0 = [X2(i)*tt];
44 UB = [X2(i)];
45 x2(:,i) = fminsearchbnd(fun,x0,LB,UB);
46 end
47 X_cross2=x2';
48 for i=1:m
49 fun = @(X)fermat2(X(1),X3(i),Z3,Z_layer1,a_prop1,b_prop1,
       chi_prop1,a_prop2,b_prop2,chi_prop2);
50 x0 = [X3(i)*tt];
51 UB = [X3(i)];
52 x3(:,i) = fminsearchbnd(fun,x0,LB,UB);
53 end
54 X_cross3=x3';
55 for i=1:m
56 fun = @(X)fermat2(X(1),X4(i),Z4,Z_layer1,a_prop1,b_prop1,
       chi_prop1,a_prop2,b_prop2,chi_prop2);
57 x0 = [X4(i)*tt];
58 UB = [X4(i)];
59 x4(:,i) = fminsearchbnd(fun,x0,LB,UB);
60 end
61 X_cross4=x4';
```

```
62 for i=1:m
63 fun = @(X)fermat2(X(1),X5(i),Z5,Z_layer1,a_prop1,b_prop1,
       chi_prop1,a_prop2,b_prop2,chi_prop2);
64 x0 = [X5(i)*tt];
65 UB = [X5(i)];
66 x5(:,i) = fminsearchbnd(fun,x0,LB,UB);
67 end
68 X_cross5=x5';
69
70
71 %% Proper minimization
72
73 x0 = [a_prop1,b_prop1, chi_prop1,a_prop2,b_prop2, chi_prop2];
74 fun1 = @(X)mini2(X_cross1,X_cross2,X_cross3,X_cross4,X_cross5
       ,...
75      X1,X2,X3,X4,X5,Z1,Z2,Z3,Z4,Z5,Z_layer1,...
76     X(1),X(2),X(3), X(4),X(5),X(6),T1,T2,T3,T4,T5); %Target
         function
77
78
79 y= fminsearch(fun1,x0); % Minimize the function
80
81 %% Results
82 a1=y(1);
83 b1=y(2);
84 chi1=y(3);
```

```
85 a2=y(4);
86 b2=y(5);
87 chi2=y(6);

1
2 function [error]= mini2(X_cross1,X_cross2,X_cross3,X_cross4,
      X_cross5,X_source1,X_source2,X_source3,X_source4,X_source5
      ,Z_rec1,Z_rec2,Z_rec3,Z_rec4,Z_rec5,Z1,a1,b1,chi1,a2,b2,
      chi2,T1,T2,T3,T4,T5)
3
4
5 p11=2.*(X_source1-X_cross1)./(sqrt(((X_source1-X_cross1).^2 +
      (1+2*chi1).*(Z1).^2).*((2*a1+b1.*(Z1)).^2.*(1+2*chi1)+b1
      .^2*(X_source1-X_cross1).^2)));
6 p21=2.*(X_cross1)./(sqrt(((X_cross1).^2 + (1+2*chi2).*(Z_rec1
      -Z1).^2).*((2*a2+b2.*(Z_rec1-Z1)).^2.*(1+2*chi2)+b2.^2*(
      X_cross1).^2)));
7
8 time11=(1/b1).*(atanh(p11.*b1.*(X_source1-X_cross1) - sqrt
      (1-(p11.^2 .*a1.^2 .* (1+2*chi1))))+atanh(sqrt(1-(p11.^2
      .*a1.^2 .* (1+2*chi1)))));
9 time21=(1/b2).*(atanh(p21.*b2.*X_cross1 - sqrt(1-(p21.^2 .*a2
      .^2 .* (1+2*chi2))))+atanh(sqrt(1-(p21.^2 .*a2.^2 .* (1+2*
      chi2)))));
10
```

```
11 p12=2.*(X_source2-X_cross2)./(sqrt(((X_source2-X_cross2).^2 +
       (1+2*chi1).*(Z1).^2).*((2*a1+b1.*(Z1)).^2.*(1+2*chi1)+b1
       .^2*(X_source2-X_cross2).^2)));
12 p22=2.*(X_cross2)./(sqrt(((X_cross2).^2 + (1+2*chi2).*(Z_rec2
       -Z1).^2).*((2*a2+b2.*(Z_rec2-Z1)).^2.*(1+2*chi2)+b2.^2*(
       X_cross2).^2)));
13
14 time12=(1/b1).*(atanh(p12.*b1.*(X_source2-X_cross2) - sqrt
       (1-(p12.^2 .*a1.^2 .* (1+2*chi1))))+atanh(sqrt(1-(p12.^2
       .*a1.^2 .* (1+2*chi1)))));
15 time22=(1/b2).*(atanh(p22.*b2.*X_cross2 - sqrt(1-(p22.^2 .*a2
       .^2 .* (1+2*chi2))))+atanh(sqrt(1-(p22.^2 .*a2.^2 .* (1+2*
       chi2)))));
16
17
18 p13=2.*(X_source3-X_cross3)./(sqrt(((X_source3-X_cross3).^2 +
       (1+2*chi1).*(Z1).^2).*((2*a1+b1.*(Z1)).^2.*(1+2*chi1)+b1
       .^2*(X_source3-X_cross3).^2)));
19 p23=2.*(X_cross3)./(sqrt(((X_cross3).^2 + (1+2*chi2).*(Z_rec3
       -Z1).^2).*((2*a2+b2.*(Z_rec3-Z1)).^2.*(1+2*chi2)+b2.^2*(
       X_cross3).^2)));
20
21 time13=(1/b1).*(atanh(p13.*b1.*(X_source3-X_cross3) - sqrt
       (1-(p13.^2 .*a1.^2 .* (1+2*chi1))))+atanh(sqrt(1-(p13.^2
       .*a1.^2 .* (1+2*chi1)))));
```

```
22 time23=(1/b2).*(atanh(p23.*b2.*X_cross3 - sqrt(1-(p23.^2 .*a2
       .^2 .* (1+2*chi2))))+atanh(sqrt(1-(p23.^2 .*a2.^2 .* (1+2*
       chi2)))));
23
24
25 p14=2.*(X_source4-X_cross4)./(sqrt(((X_source4-X_cross4).^2 +
       (1+2*chi1).*(Z1).^2).*((2*a1+b1.*(Z1)).^2.*(1+2*chi1)+b1
       .^2*(X_source4-X_cross4).^2)));
26 p24=2.*(X_cross4)./(sqrt(((X_cross4).^2 + (1+2*chi2).*(Z_rec4
       -Z1).^2).*((2*a2+b2.*(Z_rec4-Z1)).^2.*(1+2*chi2)+b2.^2*(
       X_cross4).^2)));
27
28 time14=(1/b1).*(atanh(p14.*b1.*(X_source4-X_cross4) - sqrt
       (1-(p14.^2 .*a1.^2 .* (1+2*chi1))))+atanh(sqrt(1-(p14.^2
       .*a1.^2 .* (1+2*chi1)))));
29 time24=(1/b2).*(atanh(p24.*b2.*X_cross4 - sqrt(1-(p24.^2 .*a2
       .^2 .* (1+2*chi2))))+atanh(sqrt(1-(p24.^2 .*a2.^2 .* (1+2*
       chi2)))));
30
31 p15=2.*(X_source5-X_cross5)./(sqrt(((X_source5-X_cross5).^2 +
       (1+2*chi1).*(Z1).^2).*((2*a1+b1.*(Z1)).^2.*(1+2*chi1)+b1
       .^2*(X_source5-X_cross5).^2)));
32 p25=2.*(X_cross5)./(sqrt(((X_cross5).^2 + (1+2*chi2).*(Z_rec5
       -Z1).^2).*((2*a2+b2.*(Z_rec5-Z1)).^2.*(1+2*chi2)+b2.^2*(
       X_cross5).^2)));
33
```

```
time15=(1/b1).*(atanh(p15.*b1.*(X_source5-X_cross5) - sqrt
    (1-(p15.^2 .*a1.^2 .* (1+2*chi1))))+atanh(sqrt(1-(p15.^2
    .*a1.^2 .* (1+2*chi1)))));
time25=(1/b2).*(atanh(p25.*b2.*X_cross5 - sqrt(1-(p25.^2 .*a2
    .^2 .* (1+2*chi2))))+atanh(sqrt(1-(p25.^2 .*a2.^2 .* (1+2*
    chi2)))));


T_calc1=time11+time21;
T_calc2=time12+time22;
T_calc3=time13+time23;
T_calc4=time14+time24;
T_calc5=time15+time25;


error1=abs(T_calc1-T1).^2;
error2=abs(T_calc2-T2).^2;
error3=abs(T_calc3-T3).^2;
error4=abs(T_calc4-T4).^2;
error5=abs(T_calc5-T5).^2;
error=sum(error1)+sum(error2)+sum(error3)+sum(error4)+sum(
    error5);

end
```

Appendix E

Table with values of Preliminary Reference Earth Model

Depth [km]	*Radius* [km]	V_p [km/s]	V_s [km/s]	*Density* [g/cm^3]	*Depth* [km]	*Radius* [km]	V_p [km/s]	V_s [km/s]	*Density* [g/cm^3]
0	63 71	1 45	0	1 . 2	2741	3630	13.68	7.27	5.49
3	6368	1.45	0	1.02	2771	3600	13.69	7.27	5.51
3	6368	5.8	3.2	2.6	2871	3500	13.71	7.26	5.56
15	6356	5.8	3.2	2.6	2891	3480	13.72	7.26	5.57
15	6356	6.8	3.9	2.9	2891	3480	8.06	0	9.9
24.4	6346 0.6	6.8	3.9	2.9	2971	3400	8.2	0	10.03
24.4	6346 0.6	8.11	4.49	3.38	3071	3300	8.36	0	10.18
71	6300	8.08	4.47	3.38	3171	3200	8.51	0	10.33
80	6291 0.9	8.08	4.47	3.37	3271	3100	8.66	0	10.47
80	6291	8.08	4.47	3.37	3371	3000	8.8	0	10.6
171	6200	8.02	4.44	3.36	3471	2900	8.93	0	10.73
220	6151	7.99	4.42	3.36	3571	2800	9.05	0	10.85
220	6151	8.56	4.62	3.44	3671	2700	9.17	0	10.97
271	6100	8.66	4.68	3.47	3771	2600	9.28	0	11.08
371	6000	8.85	4.75	3.53	3871	2500	9.38	0	11.19
400	5971	8.91	4.77	3.54	3971	2400	9.48	0	11.29
400	5971	9.13	4.93	3.72	4071	2300	9.58	0	11.39
471	5900	9.5	5.14	3.81	4171	2200	9.67	0	11.48
571	5800	10.01	5.43	3.94	4271	2100	9.75	0	11.57
600	5771	10.16	5.52	3.98	4371	2000	9.84	0	11.65
600	5771	10.16	5.52	3.98	4471	1900	9.91	0	11.73
670	5701	10.27	5.57	3.99	4571	1800	9.99	0	11.81
670	5701	10.75	5.95	4.38	4671	1700	10.06	0	11.88
771	5600	11.07	6.24	4.44	4771	1600	10.12	0	11.95
871	5500	11.24	6.31	4.5	4871	1500	10.19	0	12.01
971	5400	11.42	6.38	4.56	4971	1400	10.25	0	12.07
1071	5300	11.58	6.44	4.62	5071	1300	10.31	0	12.12
1171	5200	11.78	6.5	4.68	5149 0.5	122 1.5	10. 36	0	12.17
1271	5100	11.88	6.56	4.73	5149 0.5	122 1.5	11. 3	3.5	12.76
1371	5000	12.02	6.62	4.79	5171	1200	11.04	3.51	12.77

1471	4900	12.16	6.67	4.84	5271	1100	11.07	3.54	12.82
1571	4800	12.29	6.73	4.9	5371	1000	11.11	3.56	12.87
1671	4700	12.42	6.78	4.95	5471	900	11.14	3.58	12.91
1771	4600	12.54	6.83	5	5571	800	11.16	3.6	12.95
1871	4500	12.67	6.87	5.05	5671	700	11.19	3.61	12.98
1971	4400	12.78	6.92	5.11	5771	600	11.21	3.63	13.01
2071	4300	12.9	6.97	5.16	5871	500	11.22	3.64	13.03
2171	4200	13.02	7.01	5.21	5971	400	11.24	3.65	13.05
2271	4100	13.13	7.06	5.26	6071	300	11.25	3.66	13.07
2371	4000	13.25	7.1	5.31	6171	200	11.26	3.66	13.08
2471	3900	13.36	7.14	5.36	6271	100	11.26	3.67	13.09
2571	3800	13.48	7.19	5.41	6371	0	11.26	3.67	13.09

Appendix F

Table with traveltimes and offsets from VSP measurements

Data are obtained from Kaderali (2009).

Receiver 1973.923 m			Receiver 1983.809 m		
Source N.o.	Traveltime [ms]	Offset [m]	Source N.o.	Traveltime [ms]	Offset [m]
1	1036.432	1014.078	201	1038.840	1008.351
2	1031.409	989.797	202	1033.122	984.043
3	1027.439	966.288	203	1029.148	960.508
4	1023.055	941.466	204	1025.027	935.676
5	1018.204	915.969	205	1021.168	910.130
6	1014.435	889.718	206	1017.319	883.891
7	1010.473	864.303	207	1013.209	858.483
8	1005.947	841.107	208	1008.312	835.240
9	1002.145	816.118	209	1004.878	810.244
10	998.318	788.795	210	1001.203	782.892
11	994.844	765.793	211	997.567	759.852
12	991.292	740.308	212	994.381	734.346
13	987.772	716.162	213	990.638	710.170
14	985.218	694.514	214	988.177	688.527
15	980.535	663.944	215	983.886	657.899
16	977.875	642.565	216	981.287	636.545
17	975.246	617.231	217	977.982	611.188
18	971.165	591.674	218	974.139	585.598
19	968.847	568.580	219	971.586	562.487
20	966.045	538.050	220	968.724	531.796
21	963.125	515.799	221	966.093	509.525
22	960.062	489.340	222	963.084	483.059
23	958.225	469.040	223	961.095	462.703
24	955.686	444.262	224	958.631	437.891
25	953.700	418.215	225	956.849	411.844
26	951.439	394.946	226	954.877	388.454
27	949.506	373.059	227	953.134	366.440
28	948.215	344.072	228	951.426	337.400

29	946.461	324.116	229	949.415	317.048
30	944.746	297.101	230	947.845	289.835
31	943.693	275.418	231	946.987	267.858
32	941.976	246.708	232	945.197	239.050
33	940.090	225.285	233	943.625	217.478
34	938.334	201.211	234	942.345	193.088
35	937.775	182.634	235	941.309	174.105
36	937.281	151.037	236	940.727	142.494
37	936.890	136.395	237	940.937	126.875
38	936.139	119.615	238	939.762	109.503
39	935.931	94.406	239	939.623	83.743
40	935.126	82.931	240	938.903	71.966
41	935.534	76.916	241	939.149	66.459
42	935.336	74.741	242	939.227	66.310
43	935.707	84.530	243	939.528	78.328
44	935.612	93.234	244	939.563	89.803
45	936.244	112.705	245	940.394	111.608
46	936.110	130.648	246	940.091	130.642
47	937.377	152.613	247	941.688	153.154
48	938.209	176.332	248	942.350	177.687
49	939.183	200.664	249	943.109	202.354
50	940.566	222.033	250	944.924	224.320
51	941.458	244.406	251	945.205	247.111
52	942.481	270.447	252	946.367	273.339
53	944.033	293.032	253	947.988	296.045
54	945.562	317.805	254	949.649	321.033
55	947.720	343.415	255	952.137	346.827
56	949.464	369.719	256	953.549	373.160
57	952.038	393.092	257	955.886	396.718
58	953.379	417.457	258	957.665	421.107
59	956.346	443.392	259	960.745	447.157
60	958.015	465.151	260	962.260	469.001
61	960.078	493.184	261	964.153	497.013
62	963.346	515.711	262	967.471	519.641
63	965.572	541.511	263	969.745	545.499
64	968.150	566.218	264	972.201	570.228
65	971.846	594.084	265	975.986	598.156
66	974.437	616.525	266	978.617	620.641
67	977.709	640.390	267	981.874	644.580
68	980.848	666.096	268	985.060	670.325
69	983.892	686.674	269	988.157	691.031
70	987.625	714.131	270	991.753	718.482
71	990.735	734.065	271	994.879	738.482
72	994.462	763.765	272	998.693	768.171
73	998.943	790.341	273	1002.989	794.790
74	1002.359	818.537	274	1006.748	822.941
75	1006.107	838.613	275	1010.184	843.036
76	1009.904	864.183	276	1013.894	868.614
77	1015.459	889.644	277	1019.595	894.119
78	1018.333	916.870	278	1022.321	921.307
79	1022.636	938.114	279	1027.050	942.569
80	1028.093	967.871	280	1032.722	972.347
81	1032.088	984.094	281	1036.735	988.598
82	1035.925	1014.404	282	1040.235	1018.913
83	1041.995	1043.220	283	1045.885	1047.728
84	1046.384	1065.184	284	1050.348	1069.727
85	1050.471	1088.895	285	1054.671	1093.448
86	1055.210	1115.015	286	1059.151	1119.573
87	1060.235	1140.098	287	1064.439	1144.664
88	1065.256	1165.295	288	1069.724	1169.907
89	1070.389	1187.085	289	1074.964	1191.722
90	1075.694	1214.352	290	1080.203	1219.006
91	1080.502	1238.248	291	1084.769	1242.914
92	1085.769	1262.578	292	1090.486	1267.262
93	1092.119	1288.093	293	1096.443	1292.784

94	1097.591	1312.260	294	1101.800	1316.929
95	1102.887	1337.566	295	1107.092	1342.261
96	1110.075	1366.579	296	1113.786	1371.339
97	1113.877	1386.806	297	1118.027	1391.577
98	1120.171	1413.235	298	1124.079	1418.030
99	1125.078	1434.249	299	1129.362	1439.032
100	1129.865	1457.820	300	1134.666	1462.608
101	1136.798	1485.368	301	1140.644	1490.113
102	1143.508	1513.211	302	1147.233	1517.949
103	1149.417	1539.303	303	1153.155	1544.086
104	1154.933	1565.130	304	1158.895	1569.900
105	1160.874	1588.644	305	1164.270	1593.404
106	1167.062	1612.475	306	1170.602	1617.242
107	1173.549	1638.883	307	1177.444	1643.658
108	1178.955	1663.079	308	1182.653	1667.848
109	1185.425	1689.771	309	1189.136	1694.537
110	1191.324	1711.871	310	1194.793	1716.647
111	1197.521	1739.048	311	1201.199	1743.842
112	1203.817	1763.081	312	1207.696	1767.872
113	1210.837	1789.370	313	1214.073	1794.159
114	1217.784	1814.387	314	1220.868	1819.208
115	1223.474	1836.461	315	1226.550	1841.269
116	1231.080	1863.985	316	1233.862	1868.805
117	1235.614	1888.688	317	1240.130	1893.512
118	1242.405	1912.386	318	1246.604	1917.232
119	1250.340	1936.696	319	1253.548	1941.535
120	1255.989	1962.993	320	1259.847	1967.839
121	1262.363	1986.236	321	1265.565	1991.090
122	1269.025	2011.513	322	1273.312	2016.374
123	1276.389	2038.012	323	1280.025	2042.866
124	1281.452	2058.654	324	1285.407	2063.524
125	1291.095	2089.406	325	1294.071	2094.281
126	1297.340	2113.127	326	1299.952	2117.996
127	1304.095	2137.010	327	1307.700	2141.883
128	1308.005	2162.001	328	1310.301	2166.886
129	1318.307	2190.353	329	1323.274	2195.224
130	1324.103	2208.538	330	1327.841	2213.413
131	1332.692	2240.131	331	1336.037	2245.016
132	1340.505	2262.848	332	1343.859	2267.713
133	1346.629	2285.069	333	1348.996	2289.923
134	1354.231	2313.522	334	1357.301	2318.389
135	1361.689	2338.818	335	1365.345	2343.698
136	1368.898	2364.031	336	1372.069	2368.914
137	1376.166	2387.757	337	1379.635	2392.644
138	1384.134	2414.140	338	1386.817	2419.031
139	1389.482	2438.493	339	1392.626	2443.401
140	1396.500	2462.794	340	1400.358	2467.697
141	1404.673	2487.398	341	1408.040	2492.313
142	1412.021	2515.010	342	1415.364	2519.922
143	1420.411	2538.668	343	1422.726	2543.581
144	1425.506	2561.908	344	1429.279	2566.833
145	1432.678	2586.946	345	1436.051	2591.883
146	1439.409	2611.466	346	1443.447	2616.403
147	1447.930	2634.472	347	1451.370	2639.425
148	1457.009	2664.740	348	1459.092	2669.654
149	1465.913	2693.145	349	1468.384	2698.020
150	1471.688	2713.475	350	1472.716	2718.334
151	1478.316	2737.504	351	1481.698	2742.351
152	1486.156	2763.498	352	1489.435	2768.347
153	1492.776	2790.900	353	1496.836	2795.751
154	1501.544	2818.515	354	1504.003	2823.373
155	1509.010	2840.130	355	1510.775	2845.001
156	1516.612	2867.558	356	1517.430	2872.444
157	1522.475	2891.097	357	1527.097	2895.995
158	1527.969	2913.083	358	1531.993	2917.992

159	1537.739	2936.480	359	1540.569	2941.398
160	1544.497	2963.685	360	1546.735	2968.622
161	1551.710	2985.984	361	1553.385	2990.918
162	1560.112	3013.154	362	1561.528	3018.090
163	1566.471	3037.280	363	1568.398	3042.218
164	1575.806	3062.143	364	1576.207	3067.084
165	1582.710	3087.867	365	1585.550	3092.811
166	1587.800	3113.355	366	1590.731	3118.302
167	1597.852	3137.870	367	1600.101	3142.820
168	1605.218	3163.910	368	1608.303	3168.861
169	1614.170	3187.722	369	1615.857	3192.675
170	1620.041	3214.578	370	1622.663	3219.534
171	1627.195	3236.351	371	1631.572	3241.315
172	1634.435	3259.675	372	1638.071	3264.630
173	1645.422	3288.287	373	1647.669	3293.246
174	1651.273	3312.831	374	1653.441	3317.799
175	1660.710	3338.804	375	1662.421	3343.766
176	1665.429	3361.215	376	1667.257	3366.177
177	1674.863	3387.640	377	1675.520	3392.607
178	1681.033	3405.836	378	1681.964	3410.802
179	1690.683	3438.279	379	1691.929	3443.246
180	1698.660	3462.882	380	1710.587	3467.846
181	1706.745	3488.647	381	1709.635	3493.613
182	1712.753	3512.857	382	1713.031	3517.821
183	1720.417	3539.715	383	1722.879	3544.681
184	1742.573	3562.825	384	1741.318	3567.794
185	1738.627	3586.331	385	1736.081	3591.299
186	1743.987	3614.704	386	1747.966	3619.680
187	1750.378	3639.544	387	1752.301	3644.514
188	1773.884	3664.411	388	1778.166	3669.383
189	1767.780	3686.858	389	1770.612	3691.832
190	1773.923	3715.162	390	1775.954	3720.138
191	1782.683	3738.511	391	1783.222	3743.487
192	1802.645	3763.146	392	1791.143	3768.123
193	1796.954	3787.190	393	1802.154	3792.172
194	1807.817	3813.895	394	1808.063	3818.878
195	1825.078	3837.164	395	1812.050	3842.148
196	1823.494	3863.906	396	1834.522	3868.893
197	1820.780	3889.009	397	1832.293	3893.998
198	1833.245	3914.736	398	1841.510	3919.728
199	1860.562	3937.224	399	1849.791	3942.218
200	1870.558	3964.125	400	1856.989	3969.119

Receiver 1993.699 m			Receiver 2003.758 m		
Source N.o.	Traveltime [ms]	Offset [m]	Source N.o.	Traveltime [ms]	Offset [m]
401	1040.296	1002.711	601	1042.833	997.086
402	1034.723	978.378	602	1037.513	972.731
403	1031.448	954.820	603	1033.673	949.152
404	1027.611	929.979	604	1029.444	924.305
405	1023.126	904.386	605	1025.462	898.668
406	1019.032	878.162	606	1021.558	872.462
407	1015.012	852.764	607	1017.731	847.076
408	1010.589	829.477	608	1012.982	823.748
409	1007.059	804.476	609	1009.341	798.746
410	1003.557	777.100	610	1005.985	771.348
411	999.276	754.023	611	1002.028	748.238
412	996.141	728.501	612	999.005	722.703
413	992.892	704.297	613	995.761	698.475
414	990.319	682.665	614	993.036	676.858
415	986.067	651.983	615	988.844	646.129
416	982.786	630.660	616	985.924	624.840
417	980.150	605.282	617	983.380	599.449
418	976.420	579.666	618	979.481	573.811
419	974.146	556.544	619	977.140	550.684

420	971.431	525.697	620	974.557	519.689
421	968.550	503.412	621	971.818	497.397
422	965.518	476.947	622	969.121	470.942
423	963.432	456.543	623	966.698	450.496
424	961.216	431.704	624	964.633	425.642
425	959.313	405.669	625	962.887	399.631
426	957.363	382.167	626	960.981	376.026
427	955.795	360.032	627	959.268	353.782
428	953.984	330.958	628	957.854	324.691
429	952.081	310.206	629	955.870	303.545
430	950.759	282.808	630	954.239	275.979
431	949.642	260.541	631	953.240	253.431
432	948.256	231.657	632	952.059	224.502
433	946.459	209.954	633	950.595	202.690
434	945.197	185.259	634	949.141	177.711
435	944.430	165.862	635	948.403	157.906
436	943.874	134.304	636	948.019	126.487
437	943.475	117.607	637	947.600	108.628
438	942.953	99.571	638	947.095	89.868
439	942.483	73.169	639	946.545	62.742
440	941.891	61.000	640	945.980	50.086
441	942.147	56.197	641	946.538	46.358
442	942.353	58.722	642	946.447	52.469
443	942.618	73.252	643	946.954	69.671
444	942.868	87.620	644	947.101	86.893
445	943.735	111.582	645	947.711	112.734
446	943.171	131.554	646	947.722	133.464
447	945.169	154.473	647	949.129	156.651
448	945.881	179.703	648	949.660	182.453
449	946.732	204.619	649	950.746	207.535
450	948.627	227.115	650	952.851	230.490
451	949.125	250.268	651	953.203	253.949
452	950.369	276.636	652	954.468	280.412
453	952.101	299.430	653	956.100	303.261
454	953.662	324.600	654	957.547	328.581
455	955.781	350.549	655	959.877	354.657
456	957.374	376.889	656	961.524	380.983
457	960.273	400.611	657	964.467	404.849
458	961.745	425.009	658	965.664	429.240
459	964.632	451.156	659	968.875	455.469
460	966.243	473.074	660	970.314	477.448
461	968.510	501.052	661	972.350	505.381
462	971.570	523.771	662	975.954	528.180
463	973.782	549.677	663	977.649	554.124
464	976.722	574.419	664	980.507	578.871
465	980.039	602.401	665	984.222	606.897
466	982.692	624.922	666	987.011	629.448
467	985.882	648.928	667	990.246	653.514
468	988.900	674.706	668	993.458	679.317
469	992.308	695.534	669	996.693	700.261
470	995.547	722.973	670	1000.173	727.683
471	998.774	743.035	671	1003.167	747.801
472	1002.640	772.708	672	1006.854	777.454
473	1007.501	799.365	673	1011.369	804.143
474	1010.404	827.466	674	1015.020	832.193
475	1014.153	847.578	675	1018.689	852.318
476	1017.853	873.161	676	1022.437	877.902
477	1023.541	898.705	677	1027.936	903.481
478	1026.076	925.852	678	1030.703	930.585
479	1030.365	947.130	679	1035.000	951.877
480	1036.107	976.925	680	1040.677	981.685
481	1040.563	993.203	681	1045.077	997.988
482	1044.037	1023.519	682	1048.441	1028.302
483	1049.905	1052.331	683	1054.518	1057.108
484	1054.403	1074.363	684	1058.712	1079.172

485	1058.814	1098.092	685	1063.161	1102.905
486	1063.483	1124.219	686	1067.551	1129.033
487	1068.660	1149.317	687	1072.604	1154.135
488	1073.632	1174.603	688	1077.918	1179.462
489	1078.861	1196.443	689	1083.181	1201.324
490	1084.101	1223.741	690	1088.640	1228.635
491	1088.584	1247.658	691	1092.830	1252.559
492	1094.326	1272.022	692	1098.534	1276.939
493	1100.294	1297.550	693	1104.879	1302.470
494	1105.547	1321.672	694	1109.972	1326.568
495	1110.953	1347.028	695	1115.153	1351.947
496	1117.626	1376.170	696	1121.642	1381.150
497	1121.891	1396.418	697	1126.247	1401.407
498	1128.178	1422.895	698	1132.330	1427.905
499	1132.653	1443.884	699	1136.977	1448.880
500	1138.044	1467.463	700	1142.246	1472.461
501	1144.481	1494.924	701	1148.672	1499.879
502	1151.295	1522.751	702	1155.408	1527.695
503	1156.979	1548.932	703	1161.119	1553.918
504	1162.905	1574.732	704	1167.420	1579.704
505	1168.160	1598.225	705	1172.206	1603.186
506	1174.337	1622.070	706	1178.204	1627.036
507	1180.674	1648.491	707	1184.507	1653.462
508	1186.362	1672.676	708	1190.805	1677.641
509	1192.925	1699.359	709	1197.292	1704.318
510	1198.836	1721.478	710	1203.018	1726.445
511	1204.910	1748.692	711	1209.147	1753.676
512	1211.548	1772.717	712	1215.748	1777.695
513	1217.934	1799.002	713	1221.607	1803.977
514	1224.612	1824.082	714	1228.617	1829.087
515	1230.545	1846.130	715	1234.195	1851.122
516	1237.567	1873.676	716	1241.198	1878.678
517	1244.110	1898.386	717	1247.676	1903.390
518	1250.350	1922.128	718	1254.113	1927.153
519	1256.844	1946.425	719	1260.869	1951.442
520	1263.463	1972.733	720	1267.338	1977.755
521	1269.489	1995.992	721	1273.069	2001.021
522	1276.605	2021.284	722	1280.433	2026.319
523	1283.477	2047.768	723	1287.490	2052.794
524	1289.092	2068.441	724	1293.358	2073.482
525	1297.742	2099.202	725	1301.024	2104.247
526	1304.563	2122.910	726	1308.343	2127.948
527	1310.749	2146.801	727	1314.503	2151.842
528	1314.782	2171.815	728	1318.469	2176.867
529	1325.703	2200.140	729	1329.099	2205.177
530	1331.626	2218.331	730	1334.982	2223.370
531	1339.540	2249.944	731	1342.631	2254.993
532	1346.336	2272.620	732	1350.118	2277.647
533	1352.489	2294.818	733	1357.171	2299.834
534	1360.202	2323.298	734	1364.622	2328.326
535	1368.284	2348.619	735	1371.613	2353.659
536	1375.471	2373.838	736	1379.627	2378.880
537	1382.493	2397.572	737	1386.764	2402.618
538	1389.803	2423.962	738	1393.956	2429.010
539	1396.371	2448.348	739	1400.834	2453.412
540	1403.782	2472.638	740	1407.589	2477.697
541	1411.481	2497.266	741	1415.158	2502.335
542	1418.757	2524.872	742	1422.226	2529.938
543	1425.434	2548.532	743	1429.520	2553.598
544	1432.337	2571.795	744	1436.827	2576.873
545	1439.589	2596.858	745	1443.173	2601.946
546	1446.632	2621.377	746	1450.736	2626.465
547	1453.807	2644.413	747	1458.285	2649.516
548	1462.258	2674.605	748	1465.704	2679.669
549	1470.753	2702.929	749	1474.176	2707.953

550	1476.894	2723.228	750	1480.744	2728.236
551	1483.652	2747.233	751	1487.699	2752.229
552	1491.746	2773.232	752	1494.594	2778.230
553	1498.916	2800.637	753	1502.098	2805.637
554	1506.587	2828.265	754	1508.771	2833.270
555	1514.083	2849.906	755	1516.733	2854.923
556	1521.606	2877.363	756	1525.492	2882.394
557	1528.903	2900.926	757	1531.940	2905.969
558	1535.242	2922.933	758	1539.600	2927.986
559	1542.711	2946.349	759	1546.765	2951.411
560	1550.466	2973.590	760	1554.718	2978.669
561	1557.133	2995.885	761	1561.351	3000.961
562	1565.767	3023.058	762	1568.134	3028.136
563	1573.079	3047.187	763	1577.714	3052.265
564	1580.030	3072.056	764	1582.686	3077.138
565	1588.145	3097.786	765	1590.615	3102.869
566	1595.589	3123.280	766	1599.738	3128.367
567	1603.017	3147.799	767	1606.000	3152.887
568	1610.568	3173.841	768	1613.464	3178.930
569	1618.286	3197.658	769	1619.519	3202.748
570	1625.947	3224.520	770	1630.294	3229.613
571	1633.840	3246.308	771	1636.149	3251.407
572	1641.181	3269.615	772	1643.357	3274.706
573	1648.665	3298.234	773	1649.475	3303.329
574	1656.675	3322.795	774	1657.560	3327.898
575	1664.216	3348.757	775	1664.552	3353.854
576	1670.785	3371.168	776	1675.352	3376.264
577	1678.696	3397.601	777	1680.203	3402.702
578	1685.196	3415.795	778	1687.718	3420.895
579	1694.415	3448.241	779	1698.745	3453.340
580	1701.577	3472.837	780	1705.403	3477.933
581	1710.192	3498.606	781	1711.605	3503.704
582	1717.371	3522.813	782	1720.754	3527.909
583	1725.993	3549.675	783	1729.231	3554.773
584	1733.222	3572.790	784	1735.458	3577.890
585	1739.830	3596.293	785	1744.448	3601.391
586	1748.377	3624.682	786	1751.149	3629.788
587	1756.174	3649.510	787	1760.526	3654.610
588	1763.768	3674.382	788	1768.197	3679.484
589	1770.490	3696.833	789	1775.120	3701.937
590	1779.702	3725.141	790	1782.591	3730.246
591	1786.963	3748.488	791	1790.948	3753.592
592	1794.582	3773.125	792	1798.312	3778.230
593	1802.597	3797.180	793	1804.984	3802.290
594	1810.145	3823.886	794	1813.300	3828.996
595	1817.675	3847.157	795	1823.626	3852.268
596	1825.487	3873.904	796	1828.743	3879.018
597	1833.940	3899.011	797	1835.432	3904.126
598	1841.541	3924.745	798	1845.600	3929.863
599	1849.245	3947.236	799	1852.445	3952.356
600	1857.089	3974.137	800	1857.067	3979.256

Receiver 2013.927 m

Source N.o.	Traveltime [ms]	Offset [m]	Source N.o.	Traveltime [ms]	Offset [m]
801	1044.546	991.550	901	1152.406	1504.896
802	1039.433	967.175	902	1159.518	1532.702
803	1035.737	943.576	903	1164.752	1558.966
804	1031.620	918.726	904	1170.728	1584.736
805	1027.395	893.046	905	1176.191	1608.206
806	1023.883	866.861	906	1182.031	1632.059
807	1019.800	841.491	907	1188.399	1658.491
808	1015.300	818.125	908	1193.896	1682.662
809	1011.754	793.125	909	1200.831	1709.332
810	1008.324	765.709	910	1206.627	1731.466

811	1004.757	742.569	911	1212.206	1758.713
812	1001.513	717.025	912	1218.930	1782.727
813	998.272	692.777	913	1224.991	1809.004
814	995.647	671.179	914	1232.119	1834.144
815	991.688	640.407	915	1237.956	1856.165
816	988.858	619.158	916	1244.659	1883.729
817	986.490	593.758	917	1250.987	1908.443
818	982.274	568.106	918	1257.720	1932.226
819	980.074	544.979	919	1264.184	1956.508
820	977.187	513.842	920	1270.513	1982.824
821	974.652	491.551	921	1276.609	2006.097
822	971.956	465.116	922	1283.866	2031.400
823	970.103	444.635	923	1290.939	2057.867
824	967.793	419.775	924	1296.333	2078.568
825	966.024	393.803	925	1305.118	2109.336
826	963.975	370.105	926	1311.261	2133.030
827	962.375	347.762	927	1317.697	2156.926
828	960.815	318.675	928	1322.426	2181.962
829	959.260	297.136	929	1332.953	2210.257
830	957.826	269.418	930	1338.401	2228.452
831	956.764	246.599	931	1346.712	2260.084
832	955.323	217.658	932	1353.271	2282.716
833	953.803	195.765	933	1359.676	2304.890
834	952.296	170.528	934	1367.060	2333.394
835	951.830	150.322	935	1375.573	2358.739
836	951.246	119.158	936	1382.318	2383.962
837	951.140	100.035	937	1389.120	2407.702
838	950.595	80.477	938	1396.500	2434.097
839	950.060	52.512	939	1403.233	2458.515
840	949.748	39.174	940	1410.509	2482.793
841	949.931	37.125	941	1418.106	2507.442
842	949.852	47.917	942	1425.056	2535.041
843	950.437	67.679	943	1432.211	2558.701
844	950.647	87.531	944	1439.055	2581.986
845	951.544	114.917	945	1445.480	2607.071
846	951.374	136.226	946	1452.599	2631.588
847	953.025	159.548	947	1459.835	2654.653
848	953.865	185.804	948	1469.199	2684.768
849	954.950	210.975	949	1477.709	2713.012
850	956.605	234.325	950	1482.503	2733.279
851	957.373	258.040	951	1489.196	2757.260
852	958.386	284.557	952	1497.292	2783.262
853	960.111	307.433	953	1504.319	2810.670
854	961.630	332.872	954	1512.353	2838.309
855	963.944	359.049	955	1519.220	2859.972
856	965.418	385.343	956	1526.834	2887.458
857	968.447	409.334	957	1534.916	2911.043
858	969.921	433.705	958	1540.726	2933.070
859	972.838	460.001	959	1548.725	2956.504
860	974.457	482.029	960	1555.046	2983.778
861	976.609	509.907	961	1562.470	3006.069
862	979.967	532.777	962	1570.417	3033.245
863	981.933	558.748	963	1578.054	3057.374
864	985.107	583.493	964	1585.655	3082.250
865	988.531	611.554	965	1593.522	3107.982
866	991.086	634.129	966	1600.080	3133.483
867	994.422	658.248	967	1608.654	3158.005
868	997.434	684.072	968	1615.445	3184.048
869	1000.876	705.124	969	1623.756	3207.868
870	1004.018	732.526	970	1630.595	3234.734
871	1007.432	752.696	971	1639.147	3256.536
872	1011.254	782.323	972	1646.444	3279.827
873	1015.565	809.041	973	1654.579	3308.451
874	1019.073	837.034	974	1662.212	3333.029
875	1022.852	857.170	975	1669.892	3358.978

876	1026.294	882.753	976	1674.585	3381.389
877	1031.885	908.363	977	1683.330	3407.830
878	1034.363	935.422	978	1689.103	3426.021
879	1038.713	956.725	979	1699.251	3458.467
880	1044.700	986.543	980	1707.174	3483.057
881	1049.014	1002.868	981	1714.270	3508.829
882	1052.495	1033.179	982	1721.476	3533.031
883	1058.421	1061.975	983	1730.402	3559.898
884	1062.677	1084.068	984	1738.836	3583.016
885	1066.960	1107.805	985	1744.451	3606.516
886	1071.377	1133.931	986	1752.517	3634.919
887	1076.518	1159.036	987	1760.693	3659.735
888	1081.816	1184.402	988	1767.779	3684.612
889	1087.232	1206.284	989	1774.926	3707.066
890	1092.486	1233.606	990	1785.556	3735.376
891	1096.881	1257.536	991	1792.247	3758.721
892	1102.535	1281.929	992	1799.150	3783.360
893	1108.661	1307.463	993	1805.479	3807.424
894	1113.833	1331.536	994	1814.840	3834.131
895	1119.047	1356.935	995	1823.009	3857.404
896	1125.490	1386.199	996	1829.612	3884.155
897	1130.003	1406.463	997	1837.849	3909.264
898	1136.112	1432.981	998	1845.303	3935.005
899	1141.041	1453.941	999	1852.544	3957.499
900	1145.902	1477.524	1000	1860.716	3984.399